Theory of Scattering from Periodic Random Surfaces and Random Media

Lan Gao

December 1997

Abstract

This thesis studies a probabilistic theory of wave scattering from periodic random surfaces and random media. New concepts for analysis and several numerical results are described.

We assume a model such that a periodic random surface is generated by a periodic translation of a local surface boss; the height of each boss is modulated by a stationary random sequence. Mathematically, such a periodic random surface is a periodic stationary process that is a function of position and a sample point in the sample space. Its average and correlation function become periodic functions of position. A periodic stationary process is known to have a harmonic series representation, similar to the Fourier series, where "Fourier coefficients" are mutually correlated stationary processes rather than constants. Moreover, it is invariant under the two-dimensional translation which translates a sample function with a distance of the period and a sample point into another sample point. By the group theoretic translation of such a translation invariance, we first find that the scattered wave for an incident plane wave has a stochastic Floquet form, that is a product of a periodic stationary process and an exponential phase factor. This means that the coherent wave is diffracted into only discrete directions, because the average of a periodic stationary process is a periodic function. Furthermore, the scattering problem is mathematically reduced to finding out such a periodic stationary process, which is written by the harmonic series representation with stationary processes as the "Fourier coefficients". We represent such stationary processes in terms of functional expansions with unknown kernel functions, a set of equations for which is obtained from the boundary condition. Once kernel functions are determined, we reversely obtain the scattered wave field as a random function, from which any statistical properties of the scattering can be calculated.

First, we consider the case where the periodic random surface is generated by a Gaussian random sequence. For a TE plane incident wave, we approximately determine kernel functions. Then, we find that the incoherent scattering has ripples in angular distributions, because incoherent waves generated by coherently diffracted waves with different orders interfere. In the properties of the scattering and diffraction, we find several anomalies for a TM incident wave, which are caused by the guided surface waves propagating along the periodic random surface. When a coherently diffracted wave couples with the guided surface waves, Wood's anomaly appears as a rapid variation of the diffracted

power against the angle of incidence. Since the guided surface waves are excited by the surface randomness and diffracted again, strong anomalous peaks, which we call incoherent Wood's anomaly, appear in the angular distribution of the incoherent scattering. It is shown that the incoherent Wood's anomaly is independent of the angle of incidence but is determined by only period and wavelength. Further, because the guided surface waves are scattered and diffracted again, we find the enhanced backscattering and diffracted backscattering enhancement.

Second, we discuss the case where the height of the periodic surfaces is randomly deformed by a binary stationary sequence. Though the stochastic functional theory of the binary stationary sequence has been discussed, no mathematical formulas have given in explicit form. However, we first obtain several new explicit formulas. Then, we apply these formulas to diffraction and scattering problems, where periodic random surface is deformed by binary stationary sequence. We find that diffraction efficiencies are related with both the height of average periodic surface and the amplitude of random deformation, but the total diffraction power depends on only the amplitude of random deformation.

Finally, we discuss the scattering from a two-dimensional thin film with randomly fluctuating permittivity. For a Gaussian random fluctuation, the first order solution is derived explicitly by a probabilistic method. Using the solution, we calculate several statistical properties of the scattering. Then, we demonstrate that ripples appear in the angular distribution of the incoherent scattering. Moreover, the incoherent scattering can be enhanced in the directions of backscattering and specular reflection. We clarify that these phenomena occur from a combination of 'single-scattering' by the random thin film and multiple reflection between the top and bottom surfaces of the thin film.

Acknowledgment

I would like to take this opportunity to express my sincere gratitude to Professor Junichi Nakayama for his invaluable guidance, constant encouragement and generous support throughout this research.

I would like to thank Professor Makoto Tsutsumi and Professor Yasuo Yoshida for their helpful comments and suggestions for the thesis. I would like to specially thank Professor Hisanao Ogura, Kyoto University for his guidance and supervision.

Furthermore, I express my sincere gratitude to Mr. Yasuhiko Tamura for many fruitful help, discussions and valuable suggestions. I would like to thank all friends in the Nakayama laboratory who have been kind enough to assist in many ways during my study.

I would like to thank Mr. Kendou Tatsumi, my guarantor for his aid and care. In addition, acknowledgment is made to Rotary Yoneyama scholarship. I would like to thank all Rotarian, in particular, the Rotarian of Kyoto Sagano Rotary Club for their financial support and international service.

Contents

Chapter 1

Introduction

1.1 Research background

When a plane wave is incident on a smooth interface between two homogeneous media, the reflection and refraction take place. The reflected and refracted waves obey the law of reflection and Snell's law [1], respectively. The reflected and refracted directions are determined uniquely. When the interface is not planar, however, the diffraction and scattering occur. In a case of the periodic interfaces such as diffraction gratings, a plane wave is diffracted into discrete directions [2]. In another case of the irregular interfaces or inhomogeneous media, an incident wave is scattered into various directions [1]. Since many natural surfaces and media are often random in various degrees, the scattering problems from such random surfaces and random media have received much interest from theoretical and practical points of view. In fact, La Grone, Straition and Smith [1955] and Beard and Katz [1957] have investigated the relation between the rate of the rapid fluctuations of the received field and that of the deformation of the surface of the sea. In recent years, the problems of wave scattering from the earth's surface, the terrain and the sea surfaces have become increasing important; on the other hand, the problems of wave propagation in the atmosphere, the ocean and biological media have also received attention, particularly in the areas of communication, remote-sensing and detection [3]-[9]. These surfaces and media are, in general, randomly varying in time and space so that the amplitudes and phases of the waves may also fluctuate randomly in time and space. Communication engineers make use of the coherent scattering properties from ocean surfaces and atmosphere [3],[4]. In remote sensing, the scattering effects due to medium inhomogeneities and rough interfaces play a dominant role in the determination of brightness temperatures and radar backscattering coefficients [5],[6]. The detection of clear air turbulence by a scattering technique contributes significantly to safe navigation [7],[8]. In radio astronomy, the surface roughness of the Moon is estimated by studying the distortion of the radar pulse back-scattered from the Moon to the Earth [9].

(1) random surface

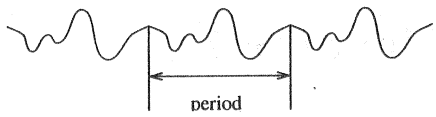

(2) periodic rough surface

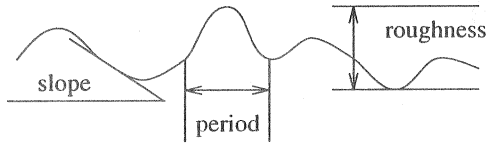

(3) periodic random surface

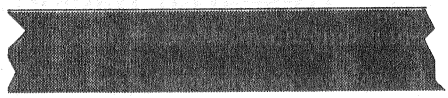

(4) random media with a flat interface

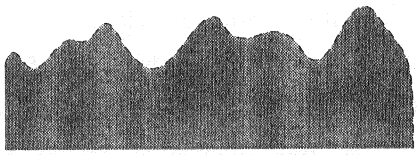

(5) random media with an irregular interface

Figure 1.1: Several types of random surfaces and random media.

We may classify random surfaces and random media into several types:

(1) random surfaces without any periodicity;

(2) periodic rough surfaces with an arbitrary profile;

(3) randomly deformed periodic surfaces;

(4) random media with a flat interface;

(5) random media with an irregular interface.

These types are shown in Fig.1.1. Many cases of the type (1) have been studied by many authors using several methods [10]-[12]. Type (2) is about a periodic structure, where the diffracted wave may be analyzed by use of the Fourier series [12]. The type (3) may include many kinds of structures. For example, the amplitude or the period is randomly deformed. In the thesis, however, we consider only such surfaces which we call

the periodic random surfaces. The periodic random surfaces have a periodic ensemble average and a periodic correlation function. Different from type (2), type (3) has not a periodic structure so that this kind of problem can not be solved by using the approach of the Fourier series. Because such surfaces show their periodic properties in the ensemble average and the correlation function, however, we can use harmonic series representation similar to Fourier series. The type (5) has little been studied theoretically because it is a much complex problem. In this thesis, we will study some cases of the types (3) and (4).

1.1.1 Periodic random surfaces

Periodic gratings such as lamellar grating and echelette grating are widely used in radiophysics, electronics and optics [13]. Ideal diffraction gratings without any deformation have been studied theoretically in detail. An incident plane wave may be diffracted into the discrete directions of the grating orders [14], which enjoy the relation

$$\sin\phi_n = \sin\theta + \frac{n\Lambda}{L}, \quad (n = 0, \pm 1, \pm 2, \cdots), \tag{1.1}$$

where Λ is wavelength, L is the period, θ is the angle of incidence and ϕ_n is the angle of diffraction with n-th order, shown in Fig.1.2. However, real diffraction gratings are never ideally periodic. Their deviation from periodicity comes from several factors such as inaccurate fabrication of the elements, inaccurate spacing, nonuniform heating of the system, and deformations, which are generally of random nature [15]. They cause the geometry of the array to become non-ideal and therefore the field scattered by such a grating differs from the field for an ideal grating [16]-[18].

Gratings are designed to have a distribution of diffracted energy among the orders. However, because one cannot manufacture an ideal grating, some of the energy is scattered into other directions rather than the desired one [14],[19]. Therefore, it is important to minimize the scattering for the use of diffraction gratings as optical components in a complex optical system. Thus, several researchers pay attention to the scattering problem from such randomly deformed periodic surfaces [20]. Experimental [21] and theoretical works [22]-[24] have reported some scattering properties.

Recently, on the other hand, wave scattering from irregular periodic surfaces deformed by a binary random sequence [25] becomes much important, because digital recording devices such as compact disks store binary random data by surface deformations called pits or bosses [26]. In disk memory devices, laser beam strikes on the pits in the disk

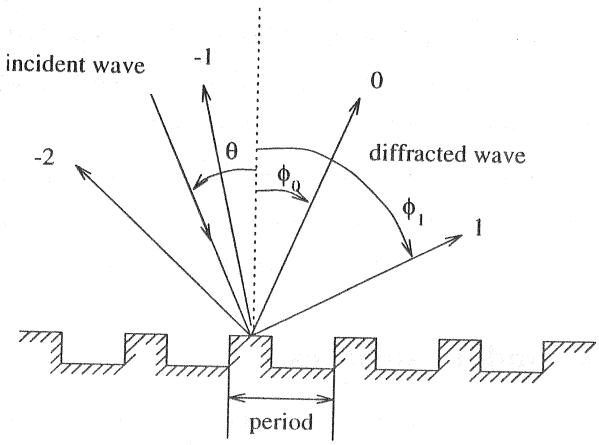

Figure 1.2: Diffraction grating. The incident wave is diffracted into discrete directions denoted by numbers.

base and the guide grooves which are used to control the tracking. Then, the scattering of laser beam from the pits is used to regenerate information. It is important for the high density recording to optimize the shapes of pit and guide groove [27]. Therefore, it is necessary to study the scattering of waves from such periodic random surfaces.

1.1.2 Random media

The wave propagation in random media has been studied extensively, because it is related with practical problems such as electromagnetic, optical and sonic wave propagation in turbulent air and in discrete random media such as fogs, rains and blood cells [28],[29]. Recently, however, the light scattering from a random thin film becomes much important as methods of non-destructive measurement and real time monitoring of thin film manufacturing process [30],[31]. This is because thin films often have volume disorder where permittivities are randomly fluctuated [31]-[33].

1.2 Anomalous scattering

All solid surfaces, even very carefully prepared ones, possess some degree of roughness. It becomes interest to examine the consequences of roughness for physical phenomena

associated with such surfaces. Vanishing of the amplitude of the wave, its retardation, and some anomalous phenomena have been observed [34]. Despite their different appearances, all these phenomena have a common origin. They all are connect with the excitation of the guided surface waves along the surface structure (see Fig.1.3). The propagation of surface waves along a rough surface has a particular interest, because the fields associated with such waves can be localized to the surface within a distance comparable with the lengths characterizing the surface roughness. The interaction between a surface wave and surface roughness can be very strong as a result [35].

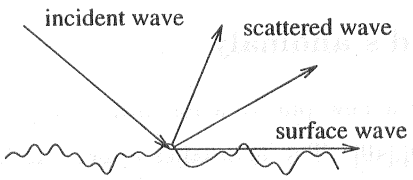

Figure 1.3: Surface wave propagates along the surface.

For example, when a surface wave propagates across a rough surface, it can be scattered by the hills and valleys on the surface into other surface wave. The surface wave is attenuated thereby, even if it is propagating on the surface of a lossless medium.

1.2.1 Wood's anomaly

Wood's anomalies (grating anomalies) are an effect observed in the spectrum of light resolved by diffraction grating. They were represented as an abrupt change in the intensity of the various diffracted spectral orders in certain narrow frequency bands. Such anomalies were first observed by Wood in 1902 in experiments on a reflection grating, and were termed anomalies because the effect could not be explained by ordinary grating theory at that time [34]. Anomalies are not caused by errors in the spacing of the gratings, they are caused by some type of resonant interaction between the light diffracted from gratings. Hessel and Oliner [1965] gave a new theory of Wood's anomalies on optical grating [36]. They showed that two different types of anomalies could exist: a Rayleigh wavelength type due to the emergence of a new spectral order at grazing angle, and a resonance type which is related to the guided complex waves supportable by the grating. Further, The Wood's anomalies are obtained for not only S polarization but also P polarization, but

P anomalies are found only on gratings with deep grooves.

Fano [1941] first suggested that anomalies could be associated with the excitation of surface waves along the grating. On the other hand, a separate approach was developed by people working on surface plasmons and solid state physics [37]. Starting from the plasmon resonance of a plane surface, they derived a perturbation treatment in which the groove profile is taken into account in the calculation of the surface plasmon excitation. The study of the anomalies of a metallic grating used in TM polarization was developed in a leaky wave (guided wave) viewpoint and studied with the electromagnetic theory [38].

1.2.2 Incoherent Wood's anomaly

Recently, we found theoretically a new phenomenon from the periodic random grating similar to Wood's anomalies [39],[40]. The anomalies appear as the rapid variations of incoherent scattering in the angular distribution, when a TM plane wave is incident on a periodic random surface with a small randomness. The scattering angles ϕ_{IW}^n of such anomalous peaks are determined only by the surface period L and wavelength Λ satisfying

$$\phi_{IW}^n = \sin^{-1}\left[\pm 1 - \frac{n\Lambda}{L}\right], \quad |n| \leq \frac{L}{\Lambda}, \quad n = 0, \pm 1, \pm 2, \cdots. \tag{1.2}$$

We call this anomalous phenomenon the incoherent Wood's anomaly. Note that Wood's anomalies depend on the angle of incidence, however, the incoherent Wood's anomalies are independent of the angle of the incidence. Due to the randomness of surface, an incoherent guided surface wave propagating along the surface is excited for any angle of incidence. Then, such a guided wave is diffracted again by the surface periodicity to yield the incoherent Wood's anomaly.

1.3 Multiple-scattering

When a random surface is slightly rough, the wave field can been expanded by the power series of the roughness parameter, and the first order expansion called single-scattering can well approximate the wave field. In some practical cases, however, this assumption and the single-scattering theory are no longer valid [41], and we need to take into account more than the first order expansions, such as the second and the third order expansion, representing multiple-scattering. Early studies on multiple-scattering include those by

Ryde, Cooper and Foldy et al. Those were extended by Twersky who obtained consistent sets of integral equations. Twersky's theory gives a clear physical picture of various processes of multiple-scattering.

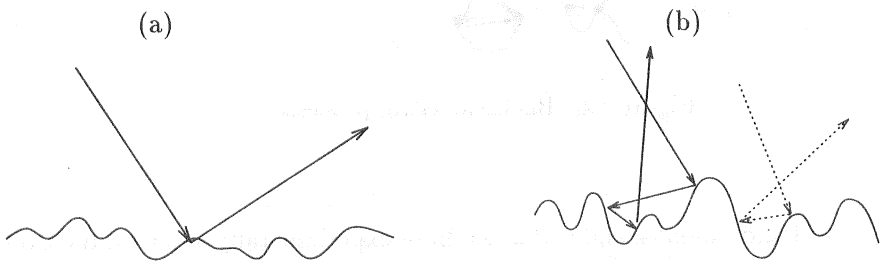

Figure 1.4: Scattering processes (a) single-scattering (b) multiple-scattering.

In recent years, there has been a renewed interest in the subjects of wave scattering by surfaces and by volume media. This is because that a number of measurements of light scattering from well characterized random rough surfaces have been reported: the light scattering from these surfaces involves multiple-scattering and exhibits the phenomenon on enhanced backscattering [42]-[44]. Further, the research on multiple-scattering phenomenon is extending into many fields such as metrology and astronomy [45]-[47].

1.3.1 Backscattering enhancement

Backscattering enhancement phenomena have been observed for many years. It has been sometimes called the "retroreflectance" or the "opposition effect". It is that the scattering in the backward direction of the incidence is relatively strong. An example is "glory" which appears around the shadow of an airplane cast on a cloud underneath the airplane.

Recently, more quantitative experimental and theoretical studies of enhanced backscattering from random rough surfaces or random media have been reported[48]-[50]. Watson noted that the backscattered intensity is twice the intensity calculated from single-scattering theory. Wolf showed that the backscattered intensity from turbulence is proportional to the fourth order moment and approximately twice the double-scattered intensity. Physically, the backscattering due to the double-scattering must be counted twice, where the same path is used twice to get the backscattering, but the backscattering due to the single-scattering should be counted only once.

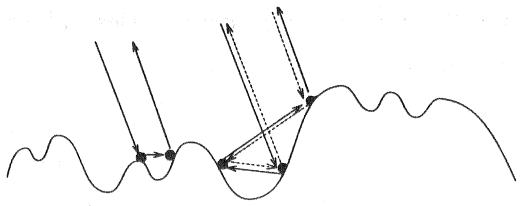

Figure 1.5: Backscattering processes.

On the other hand, Mendez and O'donnell have experimentally observed the backscattering enhancement from a randomly perturbed periodic grating [21], and several authors have given theoretical studies [39],[40].

1.3.2 Diffracted backscattering enhancement

As we were discussing the backscattering enhancement, we found a new enhanced scattering phenomenon in periodic random surfaces with a TM plane incidence [39]. We call this phenomenon the diffracted backscattering enhancement. Because of the interaction between double-scattering and diffraction, the enhanced backscattered wave is diffracted again by the periodic component of the surface. Due to this physical process, incoherent waves are slightly enhanced in the directions of diffraction of the backscattered wave.

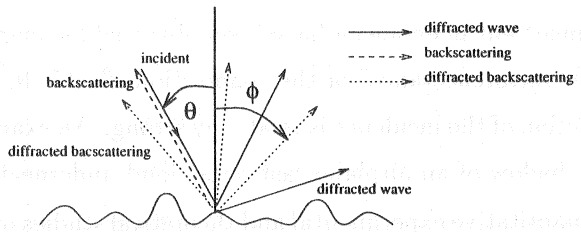

Figure 1.6: Diffracted backscattering.

The angle ϕ of the diffracted backscattering satisfies the relation:

$$\sin\phi = -\sin\theta + \frac{n\Lambda}{L}, \quad n = 0, \pm 1, \pm 2, \cdots, \tag{1.3}$$

where θ is the angle of incidence and $n \neq 0$ (when $n = 0$, (1.3) gives the backscattering

direction: $\phi = -\theta$). Note that the enhanced scattered angles are different from the diffracted angles determined by (1.1). Such an enhanced scattering phenomenon is only a theoretical result, so that the experiment observation is expected (see Fig.1.6).

1.4 Research purpose

The mathematical models of the problems discussed in this thesis are provided by stochastic partial differential equations and stochastic boundary value problems. In the case of wave propagation in continuous stochastic media, they are differential equations with random coefficients; in the case of wave scattering from stochastic surfaces, they have to do with boundary value problems for deterministic partial differential equations with boundary conditions defined on a stochastic surface. But, a complete mathematical theory of such stochastic problems has not yet been established, and so a theoretical analysis of stochastic waves has not exact probabilistic foundations; mathematically exact methods are of necessity limited to the simple models and problems. Nevertheless, the practical methods which are being developed have enormous importance for applications and also for mathematics itself, since they indicate possible problems and suggest ways of approach to the analysis of interesting new probabilistic questions.

On the other hand, several works have studied the backscattering from a random thin film by several different methods. Further, a multiple-scattering analysis was made by Frilikher and others [51],[52], where enhancement in backscattering was predicted. However, it seems that no systematic theories have been developed.

1.5 Research approaches

The modern theory of scattering is a statistical theory. The stochastic nature of real wave processes results from inhomogeneity and indeterminacy of the structure of most wave-transmitting media and the random irregularities of surfaces. The statistical methods provide the most natural tool for the description of waves, surfaces and media.

Scattering problems are commonly formulated as a mathematical boundary value problem of the wave equation with random boundary condition. In the single-scattering theories, well-known approaches such as the small perturbation method [53] and the Kirchhoff approximation [54],[55] are usually applied in order to obtain several statistical prop-

erties of the scattered wave. But these approaches are valid neither to a very rough surface nor to a slightly random surface with an infinite area. To overcome this point, the multiple-scattering theory by the diagrammatic technique was introduced to calculate the averaged intensities, the coherent scattering and the incoherent scattering [56]. This theory, however, has not been developed for any other statistical properties of the scattering. Different from these methods, a stochastic functional approach has been successfully applied to calculate any statistical properties of the scattering by Nakayama and Ogura et al [57]-[59]. Random surfaces or random media are first assumed to be a homogeneous random field in this approach. By use of the group theoretic consideration of the shift invariance property concerning the homogeneous random field, the stochastic wave solution with a plane wave incidence may be given by the stochastic Floquet form [60]: a product of an exponential phase factor and a homogeneous random process. Thus the problem is essentially reduced to finding such a homogeneous random field. Such a homogeneous random field is regarded as a stochastic functional of Gaussian random surfaces or Gaussian random media, and then is represented by Wiener expansion [61]-[64] with unknown kernel functions. Therefore, the problem is further reduced to finding such kernel functions. In this thesis, we will study the scattering problems from periodic random surfaces and random media by using the stochastic functional approach [61].

The stochastic functional approach was limited to Gaussian random media or surfaces. However, binary random cases become much important, recently. To represent the scattered wave from binary random surfaces systematically, we need a theory of a stochastic functional of a stationary binary sequence. Such a stochastic functional of a stationary binary sequence was introduced by Ogura [65] as a special case of a multi-valued stationary sequence. The Gram-Schmidt method constructing multi-variate orthogonal polynomials, mathematical definition of orthogonal stochastic functionals and completeness of orthogonal function series were discussed. A similar theory of a stochastic functional of binary and ternary random signals was discussed as a method of nonlinear system identification [66],[67]. However, it is difficult to apply these theories to the wave scattering theory, because formulas on the multi-variate orthogonal polynomials are not given in explicit form [65]-[67]. In the thesis, we will give some new formulas on multi-variate orthogonal polynomials in explicit form. We also illustrate examples of binary functional expansions.

1.6 Compositions of the thesis

This thesis consists of seven chapters and an appendix.

In chapter 2, we deal with the scattering of a TE plane wave from a periodic random surface, where the surface has the shape of periodic space-impulse series and the height of each impulse varies with Gaussian random sequence [68]. Because such a surface has a periodic average and a periodic correlation function, it becomes a periodic stationary process in the theory of stochastic processes. By the group theoretic consideration, such a periodic stationary process satisfies a shift invariance property, in terms of which a form of the scattered wave is determined. Then, it is shown that the scattered wave has a stochastic Floquet Form: a produce of a periodic stationary random function and an exponential phase factor. Due to the periodicity, such a periodic stationary random function may be written as a harmonic series representation [20], where the coefficient functions are mutually correlated stationary processes rather than constants. Due to the randomness, we may represent such stationary processes in terms of functional expansions with unknown Wiener kernel functions. When the surface has slight roughness and gentle slope, hierarchical equations of the kernel functions may be obtained from an approximate boundary condition. Determining the kernel functions, we then calculate several statistical properties, such as the coherent scattering, angular distributions of the incoherent scattering and the optical theorem. We find that the periodic random surface works as a periodic grating for the coherent wave, which is diffracted into discrete directions. These coherently diffracted waves are scattered into all the directions due to the randomness and diffracted again due to the periodicity. Moreover, the incoherent scattering has ripples in angular distributions due to inference between the coherently diffracted waves with different orders.

In chapter 3, we discuss the scattering of a TM plane wave from a periodic random surface [39]. When the average surface is flat and the TM plane incidence, the guided surface wave exists so that Wood's anomalies may be generated. Because of the existence of such anomalous scattering, it is difficult to obtain a convergent solution. Thus, we assume that the random surface has a periodic average with a small height. By the stochastic functional approach, we approximately obtain up to the second order Wiener kernels, in terms of which we calculate statistical quantities. The 0 order Wiener kernel describes the coherent diffraction amplitudes, which rapidly vary against the angle of incidence due to

Wood's anomalies. The 1st order Wiener kernel represents amplitudes of the incoherently scattered waves generated by a combination of single-scattering and diffraction. It yields the incoherent Wood's anomalies, which appear as strong and narrow peaks in the angular distribution of the incoherent scattering. The 2nd order kernel gives an interaction between double-scattering and diffraction. Even though the 2nd Wiener order kernel is relatively small in quantity for slightly rough case, it is important, because it gives the backscattering enhancement, which is a double-scattering effect on randomly rough surface. Furthermore, we find another enhancement, that is the "diffracted backscattering enhancement" of the incoherent scattering in the periodic random case.

As mentioned above, we discuss the scattering from periodic random surfaces with Gaussian random sequence by Wiener's functional theory. When the surfaces are randomly deformed by a binary sequence, however, we need a corresponding theory instead of Wiener's theory. Thus, in chapter 4, we discuss the theory concerning the orthogonal functionals of a stochastic binary sequence [69]-[71]. We give some new formulas such as the multi-variate orthogonal polynomials, recurrence formula and generating function in explicit form. We also discuss a simple example of a stochastic functional of the stationary binary sequence. These formulas may be applied to not only scattering problems but also various random problems in physics and engineering.

In chapter 5, we deal with the scattering from a periodic binary random surface, which is generated by a periodic translation of a local surface profile, of which height is modulated by a stationary binary sequence [72],[73]. Such a periodic random surface becomes mathematically a periodic stationary process. In chapter 2, we used Wiener expansion to represent wave function for the Gaussian random sequence. However, we will use the orthogonal functional expansion (binary expansion) to express the scattered wave for the stationary binary sequence. Binary kernels are approximately determined by matrix equations which are obtained from the boundary condition. Then, we calculate several statistical properties of the diffraction and scattering, such as the coherently diffracted power, the scattering cross section and the optical theorem. Even though diffraction efficiencies are related with both the height of average periodic surface and the amplitude of random deformation, it is concluded that the total diffraction power depends on only the amplitude of random deformation.

In chapter 6, we discuss a probabilistic theory of scattering from a two-dimensional thin film with randomly fluctuating permittivity [74]. For an Gaussian random disorder,

a first order solution is derived explicitly by a probabilistic method. Using the first order solution, we calculate several statistical properties of the scattering, such as the angular distribution of the incoherent scattering, optical theorem and the coherent scattering. Then, we demonstrate that ripples appear in the angular distribution of the incoherent scattering. Moreover, the incoherent scattering can be enhanced in the directions of backscattering and specular reflection. We clarify that these phenomena occur from a combination of 'single-scattering' by a random medium and multiple reflection between the top and bottom surfaces of the thin film.

Chapter 7 is the conclusion of our results in this thesis. We will give some problems which are to be resolved in future.

In chapters 2, 3 and 6, we have used some formulae on multi-variate Hermite polynomials and the Wiener expansion. In appendix A, we summarize several formulas on the Wiener expansion.

Chapter 2

Scattering of a TE plane wave from periodic random surfaces

2.1 Introduction

Scattering from periodic random surfaces is an important problem in practical applications such as active remote sensing of plowed fields and ocean surfaces. It is a theoretically interesting problem because the coherent wave is diffracted into discrete directions due to the periodicity, the incoherent wave is scattered into all directions due to the randomness, and the interactions occur between diffraction and scattering. Several authors have studied such problems by the small perturbation method [16],[17], the Kirchhoff approximation [17] and the integral equation method. In this chapter, we present another systematic formulation based on the stochastic functional approach [60],[75],[76].

We assume that a periodic random surface is generated by a periodic translation of a local surface profile, the amplitude of which is modulated by a stationary Gaussian sequence. In Sec.2.2, we show that the scattered wave has a stochastic Floquet form: a product of a periodic stationary random function and an exponential phase factor. In Sec.2.3, we represent such a periodic stationary random process by a harmonic series representation similar to a Fourier series, where the "Fourier coefficients" are not constants but mutually correlated stationary processes. As a stochastic functional of the Gaussian random amplitudes, such stationary processes are represented in terms of a Wiener expansion with unknown Wiener kernels; Wiener expansion formulae are summarized in Appendix A. In terms of the Wiener kernels, we get expressions of several statistical properties of the scattering, such as the coherent scattering, angular distributions of the incoherent scattering and optical theorem. Solving the approximate Dirichlet condition for the case of a slightly rough surface and TE wave incidence, we get an approximate result of low order Wiener kernels in Sec.2.5. Further, we illustrate the numerical results in Sec.2.6. Then, we find that the periodic random surface works as a periodic grating for the coherent wave, which is diffracted into discrete directions. Moreover, the incoherent waves scattered into all directions are generated from all coherently diffracted waves.

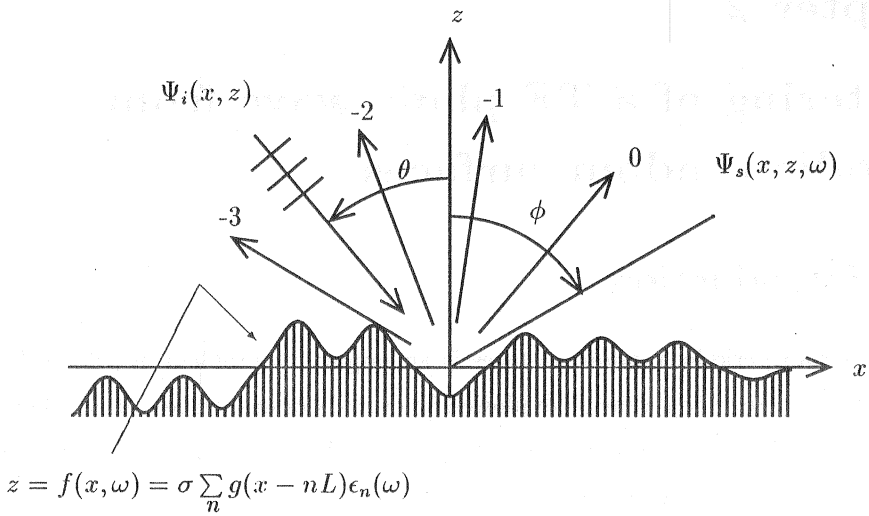

Figure 2.1: Scattering of a TE plane wave from a periodic random surface. L is the period, σ is a roughness parameter, θ is the angle of incidence and ϕ is a scattering angle. The coherent wave is diffracted into only discrete directions indicated by numbers.

2.2 Probabilistic formulation of the problem

Let us consider the periodic random surface, shown in Fig.2.1, where the surface deformation is expressed by a periodic stationary random process $f(x,\omega)$,

$$z = f(x,\omega) = \sigma \sum_{n=-\infty}^{\infty} g(x - nL)\epsilon_n(\omega), \tag{2.1}$$

where $g(x)$ is the local surface profile[1], L is the period, σ is a roughness parameter, and $\epsilon_n(\omega)$ is an independent Gaussian sequence with zero average and orthogonal correlation,

$$\langle \epsilon_n(\omega) \rangle = 0, \quad \langle \epsilon_n(\omega)\epsilon_m(\omega) \rangle = \delta(n,m), \tag{2.2}$$

where $\delta(n,m)$ is the Kronecker delta, ω is a probability parameter denoting a sample point in the sample space Ω, and the angle bracket is the ensemble average over Ω. From

[1]Here, without loss of generality, we may assume that $g(x)$ has the maximum value $g(0) = 1$ at $x = 0$ and rapidly vanishes as $|x| \to \infty$.

(2.1) and (2.2), $f(x,\omega)$ satisfies

$$\langle f(x,\omega)\rangle = 0, \tag{2.3}$$

$$R(x,x') = \left\langle f(x,\omega)f(x',\omega)\right\rangle = \sigma^2 \sum_{n=-\infty}^{\infty} g(x-nL)g(x'-nL) = R(x+L,x'+L). \tag{2.4}$$

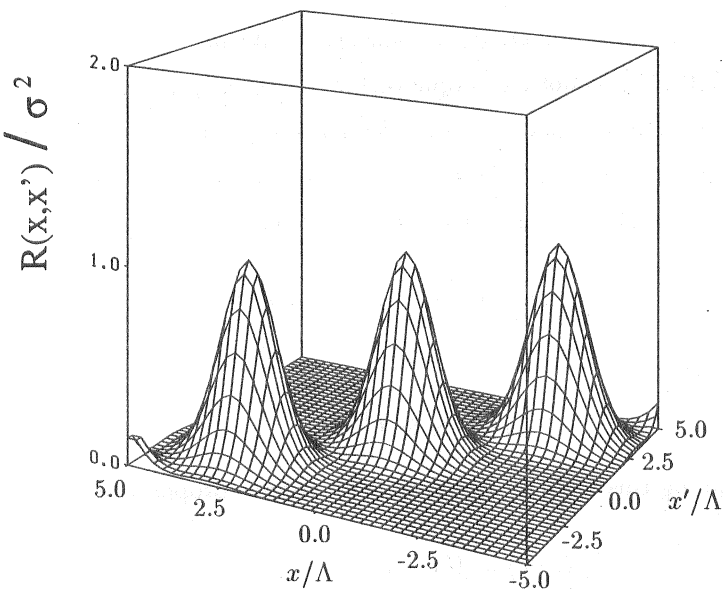

Figure 2.2: The correlation function $R(x,x')$, calculated by equations (2.4) and (2.63) with parameters $\kappa = 1.0\Lambda$ and $L = 3\Lambda$, where Λ is the wavelength. $R(x,x')$ is a periodic function of x or x' on the plane "$x - x'$ = constant" with period L.

Clearly, $f(x,\omega)$ has zero average, and the correlation function $R(x,x')$ is a periodic function of x or x' on the plane "$x-x'$ = constant" with period L. For understanding the periodicity, a numerical example is given in Fig.2.2. Note that there is no periodicity in a realization of our periodic random surface $f(x,\omega)$. However, it has a periodic correlation function so that the diffraction into discrete directions may take place. On the other hand, the scattering into all directions may exist due to the randomness .

For any periodic stationary process $f(x,\omega)$, it is convenient to introduce the norm $||\cdot||$

as

$$||f(x,\omega)||^2 = \frac{1}{L}\int_{-\frac{L}{2}}^{\frac{L}{2}} \langle |f(x,\omega)|^2 \rangle dx, \tag{2.5}$$

where $\langle |f(x,\omega)|^2 \rangle$ is a periodic function with the period L. Thus, the norm is proportional to the space average of $\langle |f(x,\omega)|^2 \rangle$ over one period.

We regard a probability parameter ω as an infinitely dimensional vector given by a sample sequence:

$$\omega = (\cdots, \omega_{-1}, \omega_0, \omega_1, \cdots), \quad \omega_n = \epsilon_n(\omega), \tag{2.6}$$

where ω_n is the n-th component of ω. By a translation with $m : \epsilon_n(\omega) \to \epsilon_{n+m}(\omega)$, such a sample vector ω is shifted into another sample vector $\omega' = (\cdots, \epsilon_{m-1}(\omega), \epsilon_m(\omega), \epsilon_{m+1}(\omega), \cdots)$, which is a shift in the sample space Ω and is formally represented as $\omega' = T^m\omega$ with a shift operator T. Since $\epsilon_n(\omega)$ is an independent stationary sequence, the shift T becomes a measure-preserving transformation[2] with group properties:

$$T^0 = 1(identity), \quad T^n T^m = T^{n+m}. \tag{2.7}$$

As a result, it holds that

$$\epsilon_m(\omega) = \epsilon_0(T^m\omega), \tag{2.8}$$

for almost all ω. Taking this fact, we find a shift invariance property of (2.1) as

$$f(x,\omega) = f(x + mL, T^{-m}\omega), \tag{2.9}$$

where m is any integer. Note that $f(x,\omega)$ is invariant under the two-dimensional shift which takes (x,ω) into $(x + mL, T^{-m}\omega)$. This property will be used later.

Let us denote the y component of the TE electric field by $\Psi(x,z,\omega)$, which satisfies the wave equation in free space,

$$\left[\frac{\partial^2}{\partial x^2} + \frac{\partial^2}{\partial z^2} + k^2\right]\Psi(x,z,\omega) = 0, \tag{2.10}$$

where real k is wave number. When the periodic random surface is perfectly conductive, the wave function satisfies the Dirichlet condition:

$$\Psi(x,z,\omega) = 0 \quad \text{for } z = f(x,\omega). \tag{2.11}$$

[2]A measure-preserving transformation T means that $P(\omega) = P(T^m\omega)$, where P is the probability, m is any integer and ω is any sample point.

The wave function $\Psi(x,z,\omega)$ may be written as a sum of the incident plane wave $\Psi_i(x,z)$ and the scattered wave $\Psi_s(x,z,\omega)$ which is a random function,

$$\Psi(x,z,\omega) = \Psi_i(x,z) + \Psi_s(x,z,\omega), \tag{2.12}$$

$$\Psi_i(x,z) = e^{ipx - i\beta_0(p)z}, \tag{2.13}$$

$$p = k\sin\theta, \quad \beta_n(\lambda) = \sqrt{k^2 - \left(\lambda + \frac{2\pi n}{L}\right)^2},$$

$$\mathrm{Im}[\beta_n(p)] \geq 0, \quad n = 0 \pm 1, \pm 2, \cdots, \tag{2.14}$$

where θ is the angle of incidence and 'Im' denotes the imaginary part. For determining a form of the scattered wave $\Psi_s(x,z,\omega)$, we introduce a translation operator D acting on the wave function $\Psi(x,z,\omega)$ by the relation:

$$D^m\Psi(x,z,\omega) = \Psi(x+mL, z, T^{-m}\omega), \quad (m = 0, \pm 1, \pm 2, \cdots). \tag{2.15}$$

As mentioned above, $f(x,\omega)$ is invariant under shift: $(x,\omega) \to (x+mL, T^{-m}\omega)$. Therefore, by the definition of the operator D, $f(x,\omega)$ is also invariant under the operator D, so that if $\Psi(x,z,\omega)$ is a solution satisfying wave equation (2.10) and boundary condition (2.11), $D^m\Psi(x,z,\omega)$ is a solution of the problem, too. Because the incident plane wave satisfies the relation

$$D^m\Psi_i(x,z) = e^{ipmL}\Psi_i(x,z), \tag{2.16}$$

and because the corresponding scattered wave is $D^m\Psi_s(x,z,\omega)$ and $e^{ipmL}\Psi_s(x,z,\omega)$, we get,

$$\Psi_s(x+mL, z, T^{-m}\omega) = D^m\Psi_s(x,z,\omega) = e^{ipmL}\Psi_s(x,z,\omega), \tag{2.17}$$

which indicates that the scattered wave does not satisfy the shift invariance property. If we put

$$U(x,z,\omega) = e^{-ipx}\Psi_s(x,z,\omega), \tag{2.18}$$

from (2.17) we find the shift invariance property

$$\begin{aligned} U(x+mL, z, T^{-m}\omega) &= e^{-ipx}e^{-ipmL}\Psi_s(x+L, z, T^{-m}\omega) \\ &= e^{-ipx}\Psi_s(x,z,\omega) \\ &= U(x,z,\omega). \end{aligned} \tag{2.19}$$

This means that a possible solution to this relation (2.17) is given by the stochastic Floquet form,

$$\Psi_s(x,z,\omega) = e^{ipx}U(x,z,\omega), \tag{2.20}$$

where $U(x,z,\omega)$ is a periodic stationary process of x with the period L, enjoying

$$\begin{aligned} \langle U(x+L,z,\omega)\rangle &= \langle U(x,z,T\omega)\rangle = \langle U(x,z,\omega)\rangle, \qquad (2.21)\\ R^U(x+L,x'+L,z) &= \langle U(x+L,z,\omega)U(x'+L,z,\omega)\rangle \\ &= \langle U(x,z,T\omega)U(x',z,T\omega)\rangle = R^U(x,x',z), \qquad (2.22)\end{aligned}$$

which are periodic average and periodic correlation function of x. Note that the form of solution (2.20) can be understood as a stochastic analogue to Floquet's solution

$$\Psi_s(x,z) = e^{ipx}U(x,z), \qquad (2.23)$$

which is the diffracted wave with an incident plane wave from a perfectly periodic surface. Here, $U(x,z)$ is reduced to a periodic function of x having the same period as the periodic surface does, and can be represented by Fourier series

$$U(x,z) = \sum_{n=-\infty}^{\infty} e^{\frac{i2\pi nx}{L}} V_n(z). \qquad (2.24)$$

where $V_n(z)$ is the Fourier coefficient.

We have seen that the problem is reduced to finding a periodic stationary process $U(x,z,\omega)$. In order to obtain the periodic stationary process, we employ a harmonic series representation for the periodic random surface and the periodic stationary process $U(x,z,\omega)$.

2.3 Representation for periodic stationary process

When the local surface profile $g(x)$ is a square integrable function, by use of the Fourier integral we may write

$$\begin{aligned} g(x) &= \int_{-\infty}^{\infty} e^{i\lambda x}G(\lambda)d\lambda = \sum_{q=-\infty}^{\infty} e^{\frac{i2\pi qx}{L}} \int_{-\frac{\pi}{L}}^{\frac{\pi}{L}} e^{i\lambda x}G^{(q)}(\lambda)d\lambda, \\ G^{(q)}(\lambda) &= G\left(\lambda + \frac{2\pi q}{L}\right), \quad G^{(q)*}(\lambda) = G^{(-q)}(-\lambda), \qquad (2.25)\end{aligned}$$

where the asterisk is the complex conjugate. Here, we have divided the wavenumber region into bands with equal bandwidth $2\pi/L$. Substituting (2.25) into (2.1), we obtain the harmonic series representation as

$$f(x,\omega) = \sum_{q=-\infty}^{\infty} e^{\frac{i2\pi qx}{L}} f^{(q)}(x,\omega), \qquad (2.26)$$

which is similar to Fourier series, but Fourier coefficient $f^{(q)}(x,\omega)$ is not a constant and is a complex valued stationary process:

$$\begin{aligned} f^{(q)}(x,\omega) &= \sigma \sum_{n=-\infty}^{\infty} \epsilon_n(\omega) \int_{-\frac{\pi}{L}}^{\frac{\pi}{L}} e^{i\lambda(x-nL)} G^{(q)}(\lambda) d\lambda, \\ f^{(q)*}(x,\omega) &= f^{(-q)}(x,\omega). \end{aligned} \tag{2.27}$$

Since $\epsilon_n(\omega)$ has zero average, $f^{(q)}(x,\omega)$ also has zero average

$$\langle f^{(q)}(x,\omega) \rangle = 0. \tag{2.28}$$

Let us calculate the mutual correlation function $R_{qq'}(x,x')$:

$$\begin{aligned} R_{qq'}(x,x') &= \left\langle f^{(q)}(x,\omega) f^{(q')*}(x',\omega) \right\rangle \\ &= \frac{2\pi\sigma^2}{L} \int_{-\frac{\pi}{L}}^{\frac{\pi}{L}} e^{i\lambda(x-x')} G^{(q)}(\lambda) G^{(q')*}(\lambda) d\lambda, \end{aligned} \tag{2.29}$$

which depends on only the difference $x - x'$. This means that $f^{(q)}(x,\omega)$ is a stationary process. Then, denoting $R_{qq'}(x,x') = R_{qq'}(x-x')$, we easily find

$$R^*_{qq'}(x) = R_{q'q}(-x), \quad R_{qq}(0) \geq 0. \tag{2.30}$$

Note that (2.29) is obtained from (2.27) and the relation:

$$\begin{aligned} \sum_{m=-\infty}^{\infty} e^{iLm(\lambda-\lambda')} &= 2\pi \sum_{m=-\infty}^{\infty} \delta(L\lambda - L\lambda' + 2\pi m) \\ &= \frac{2\pi}{L} \sum_{m=-\infty}^{\infty} \delta(\lambda - \lambda' + \frac{2\pi m}{L}). \end{aligned} \tag{2.31}$$

Next, let us consider a stochastic representation of the periodic stationary random process $U(x,z,\omega)$. Since $U(x,z,\omega)$ is a stochastic functional of the Gaussian sequence $\{\epsilon_n(\omega)\}$, it can be represented by a Wiener expansion (A.17) for each value of (x,z). Taking the fact that $U(x,z,\omega)$ is a periodic stationary process of x with period L and making a modification for such an expansion to satisfy (2.19), we write

$$\begin{aligned} U(x,z,\omega) = C_0(x,z) &+ \sum_{m=-\infty}^{\infty} C_1(x-mL,z) h^{(1)}[\epsilon_n] \\ &+ \sum_{m,n=-\infty}^{\infty} C_2(x-mL, x-nL, z) h^{(2)}[\epsilon_m, \epsilon_n] + \cdots, \end{aligned} \tag{2.32}$$

where $h^{(n)}[\cdot]$ is the multi-variate Hermite polynomial defined in Appendix A, $C_0(x,z)$, $C_1(x-mL,z)$, $\cdots$ are deterministic coefficient functions called Wiener kernels. From (2.19), (2.32) and the average relation (A.12) of $h^{(n)}[\cdot]$, we have

$$C_0(x+L,z) = \langle U(x+L,z,T\omega) \rangle = \langle U(x,z,\omega) \rangle = C_0(x,z). \tag{2.33}$$

Obviously, $\langle U(x,z,\omega)\rangle$ is periodic, and $C_0(x,z)$ becomes a periodic function of x. On one hand, representing the Wiener kernels by their Fourier integrals and dividing the wavenumber region into bands with equal band width $2\pi/L$, we can rewrite the periodic stationary process $U(x,z,\omega)$ in terms of a harmonic series representation. On the other hand, since $e^{ipx}U(x,z,\omega)$ satisfies the wave equation (2.10) and the radiation condition for $z\to\infty$, we can obtain the concrete form of the harmonic series representation

$$U(x,z,\omega)=\sum_{q=-\infty}^{\infty} e^{\frac{i2\pi qx}{L}}U^{(q)}(x,z,\omega), \tag{2.34}$$

which enjoys the shift invariance property

$$\begin{aligned}U^{(q)}(x,z,\omega) &= C_0^{(q)}(p)e^{i\beta_q(p)z}+\sum_{m=-\infty}^{\infty}h^{(1)}[\epsilon_m]\int_{-\frac{\pi}{L}}^{\frac{\pi}{L}}C_1^{(q)}(\lambda)e^{i\lambda(x-mL)+i\beta_q(p+\lambda)z}d\lambda\\ &+\sum_{m,n=-\infty}^{\infty}h^{(2)}[\epsilon_m,\epsilon_n]\int\int_{-\frac{\pi}{L}}^{\frac{\pi}{L}}C_2^{(q)}(\lambda_1,\lambda_2)e^{i\lambda_1(x-mL)+\lambda_2(x-nL)+i\beta_q(p+\lambda_1+\lambda_2)z}d\lambda_1 d\lambda_2\\ &+\cdots,\end{aligned} \tag{2.35}$$

$$U^{(q)}(x,z,\omega)=U^{(q)}(x+mL,z,T^{-m}\omega), \tag{2.36}$$

where $C_0^{(q)}(p)$, $C_1^{(q)}(\lambda)$, $C_2^{(q)}(\lambda_1,\lambda_2)$, $\cdots$ are deterministic Weiner kernels in the spectral domain. By the orthogonal property (A.11) of $h^{(n)}[\cdot]$, the identity (2.31) and (2.35), we have

$$\langle U^{(q)}(x,z,\omega)\rangle = C_0^{(q)}(p)e^{i\beta_q(p)z}, \tag{2.37}$$

which means that the average value of $U^{(q)}(x,z,\omega)$ is independent of x, and

$$\begin{aligned}R^U_{qq'}(x-x',z) &= \langle U^{(q)}(x,z,\omega)U^{(q')*}(x',z,\omega)\rangle\\ &= C_0^{(q)}(p)C_0^{(q')*}(p)e^{i\beta_q(p)z-i\beta_{q'}(p)z}\\ &\quad+\frac{2\pi}{L}\int_{-\frac{\pi}{L}}^{\frac{\pi}{L}}C_1^{(q)}(\lambda)C_1^{(q')*}(\lambda)e^{i\lambda(x-x')+i\beta_q(p+\lambda)z-i\beta_{q'}(p+\lambda)z}d\lambda\\ &\quad+\cdots,\end{aligned} \tag{2.38}$$

which indicates that the mutual correlation function $R^U_{qq'}(x-x',z)$ depends on only the difference $x-x'$, so that $U^{(q)}(x,z,\omega)$ becomes a stationary process of x. Using the relation (2.38), we obtain the correlation function $R^U(x,x',z)$ of $U(x,z,\omega)$

$$\begin{aligned}R^U(x,x',z) &= \langle U(x,z,\omega)U^*(x',z,\omega)\rangle\\ &= \sum_{q,q'=-\infty}^{\infty}\exp\left[\frac{i2\pi(qx-q'x')}{L}\right]R^U_{qq'}(x-x').\end{aligned} \tag{2.39}$$

As a result, a periodic stationary process of x satisfying the shift invariance property (2.19) has a harmonic series representation similar to Fourier series, where the "Fourier coefficients" are stationary processes having the averages independent of x and the mutual correlation functions which depend on only the difference of x. This conclusion will be used in section 2.5.

2.4 Coherent wave, optical theorem and incoherent scattering cross section

From the harmonic series representation (2.34), we complete a stochastic representation of the scattered wave field

$$\begin{aligned}\Psi_s(x,z,\omega) = \sum_{q=-\infty}^{\infty} e^{i(p+\frac{2\pi q}{L})x}\Bigg[&C_0^{(q)}(p)e^{i\beta_q(p)z} \\ &+ \sum_{m=-\infty}^{\infty} h^{(1)}[\epsilon_m]\int_{-\frac{\pi}{L}}^{\frac{\pi}{L}} C_1^{(q)}(\lambda)e^{i\lambda(x-)+i\beta_q(p+\lambda)z}d\lambda \\ &+ \sum_{m,n=-\infty}^{\infty} h^{(2)}[\epsilon_m,\epsilon_n]\int\int_{-\frac{\pi}{L}}^{\frac{\pi}{L}} C_2^{(q)}(\lambda_1,\lambda_2)e^{i\lambda_1(x-mL)+\lambda_2(x-nL)+i\beta_q(p+\lambda_1+\lambda_2)z}d\lambda_1 d\lambda_2 \\ &+\cdots\Bigg],\end{aligned} \tag{2.40}$$

which is physically represented only by out-going plane waves. Since $h^{(n)}[\cdot]$ has zero average when $n \geq 1$, we obtain from (2.12) and (2.40) the coherent wave (average wave)

$$\langle\Psi(x,z,\omega)\rangle = e^{ipx}\left[e^{-i\beta_0(p)z} + \sum_{q=-\infty}^{\infty} e^{\frac{i2\pi qx}{L}+i\beta_q(p)z}C_0^{(q)}(p)\right]. \tag{2.41}$$

This is exactly the Floquet's solution for a periodic grating. Thus, the periodic random surface works as a perfectly periodic surface for the coherent scattering. Here, $C_0^{(q)}(p)$ is the amplitude of the coherent wave diffracted into the direction $\phi_q(p)$, $C_1^{(q)}(\lambda)$ and $C_2^{(q)}(\lambda_1,\lambda_2)$ are amplitude factors of incoherent waves scattered into the directions $\phi_q(p+\lambda)$ and $\phi_q(p+\lambda_1+\lambda_2)$, respectively, where

$$\phi_q(p) = \sin^{-1}\frac{1}{k}\left(p+\frac{2\pi q}{L}\right), \quad q = 0,\pm1,\pm2,\cdots. \tag{2.42}$$

Note that the coherent wave is diffracted into only discrete directions but the incoherent wave is scattered into all directions, as shown in Fig.2.3.

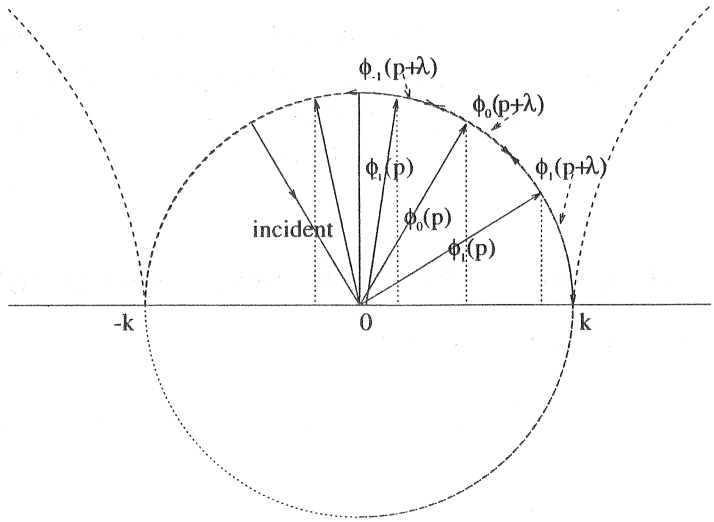

Figure 2.3: The coherent wave is diffracted into only discrete directions but the incoherent wave is scattered into all directions.

Next, we consider the optical theorem. From the wave equation (2.10), we obtain an identity:

$$\begin{aligned}\Psi^*\nabla^2\Psi - \Psi\nabla^2\Psi^* &= \nabla\cdot(\Psi^*\nabla\Psi - \Psi\nabla\Psi^*)\\ &= \mathrm{div}\Big[\mathrm{Im}\Big(\Psi^*\mathrm{grad}\Psi\Big)\Big] = 0,\end{aligned} \tag{2.43}$$

where ∇ is nabla operator, 'div' is the divergence and 'grad' denotes the gradient. In a loss-less case, we integrate the identity (2.43) over the area ABCDA (length: $2nL + L$; height: $z_0 > |f(x,\omega)|$) on the periodic random surface, shown in Fig.2.4. Note that we take a sufficiently large real number z_0 such that $z_0 > |f(x,w)|$ for any x and ω. Applying the Green theorem, we obtain another identity

$$\Big(\int_{\mathrm{AB}} dx + \int_{\mathrm{BC}} dz + \int_{\mathrm{CD}} dl + \int_{\mathrm{DA}} dz\Big)\,\mathrm{Im}\Big(\frac{\Psi^*}{k}\mathrm{grad}\Psi\Big) = 0, \tag{2.44}$$

where the third integral is the curvilinear integral along the periodic random surface. The integral over CD vanishes for the Dirichlet condition. Since the intervals BC and DA are finite, the integrals over BC and DA are physically expected to be finite. Dividing (2.44)

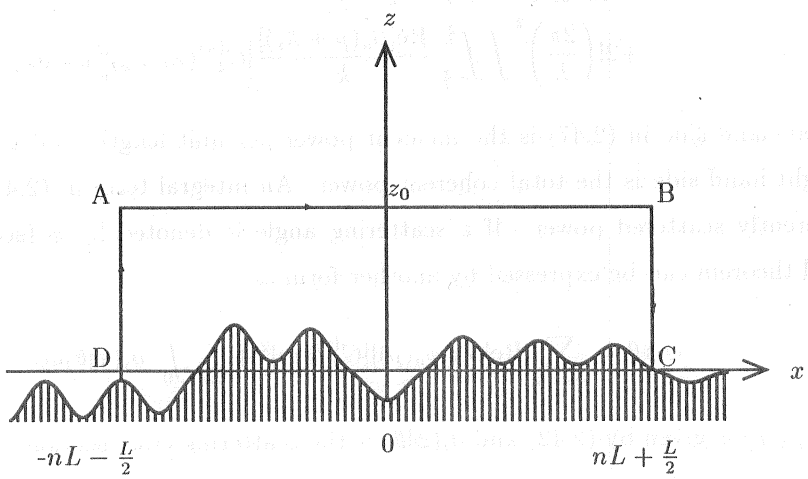

Figure 2.4: A box region ABCDA on the periodic random surface to derive the optical theorem.

by $2nL+L$ and letting $n\to\infty$, we have

$$\lim_{n\to\infty}\frac{1}{2nL+L}\int_{-nL-\frac{L}{2}}^{nL+\frac{L}{2}}\mathrm{Im}\left(\frac{\Psi^*}{k}\mathrm{grad}\Psi\right)\Big|_{z=z_0}dx$$
$$=\lim_{n\to\infty}\frac{1}{2nL+L}\sum_{k=-n}^{n}\int_{-kL-\frac{L}{2}}^{kL+\frac{L}{2}}\mathrm{Im}\left(\frac{\Psi^*}{k}\mathrm{grad}\Psi\right)\Big|_{z=z_0}dx=0. \tag{2.45}$$

Because of the stochastic Floquet form (2.20), $\Psi^*\mathrm{grad}\Psi$ is a periodic stationary process of x, and its integral over one period becomes a stationary sequence. Applying the ergodic theorem to such a stationary sequence, we get

$$\frac{1}{L}\int_{-\frac{L}{2}}^{\frac{L}{2}}\mathrm{Re}\left\langle\frac{\Psi^*}{ik}\frac{\partial\Psi}{\partial z}\Big|_{z=z_0}\right\rangle dx$$
$$=-\frac{\beta_0(p)}{k}+\frac{1}{L}\int_{-\frac{L}{2}}^{\frac{L}{2}}\mathrm{Re}\left\langle\frac{U^*}{ik}\frac{\partial U}{\partial z}\Big|_{z=z_0}\right\rangle dx=0, \tag{2.46}$$

where 'Re' denotes the real part. Substituting (2.34) and (2.35) into (2.46) and using the orthogonality relation (A.11), we obtain the optical theorem

$$\frac{\beta_0(p)}{k}=\sum_{n=-\infty}^{\infty}\frac{\mathrm{Re}[\beta_n(p)]}{k}\left|C_0^{(n)}(p)\right|^2$$

$$+\sum_{n=-\infty}^{\infty}\left\{1!\left(\frac{2\pi}{L}\right)\int_{-\frac{\pi}{L}}^{\frac{\pi}{L}}\frac{\mathrm{Re}[\beta_n(p+\lambda)]}{k}\left|C_1^{(n)}(\lambda)\right|^2 d\lambda\right.$$
$$\left.+2!\left(\frac{2\pi}{L}\right)^2\int\int_{-\frac{\pi}{L}}^{\frac{\pi}{L}}\frac{\mathrm{Re}[\beta_n(p+\lambda_1)]}{k}\left|C_2^{(n)}(\lambda_1,\lambda_2)\right|^2 d\lambda_1 d\lambda_2+\cdots\right\}. \quad (2.47)$$

The left-hand side in (2.47) is the incident power per unit length, and the first term of the right-hand side is the total coherent power. An integral term in (2.47) indicates an incoherently scattered power. If a scattering angle is denoted by ϕ (see Fig.2.1), the optical theorem can be expressed by another form as

$$\cos\theta=\sum_{n=-\infty}^{\infty}\mathrm{Re}[\cos\phi_n(p)]|C_0^{(n)}(p)|^2+\frac{1}{2\pi}\int_0^{\pi}\sigma_i(\phi|\theta)d\phi, \quad (2.48)$$

where $\phi_n(p)$ is given by (2.42) and $\sigma_i(\phi|\theta)$ is the scattering cross section per unit area,

$$\sigma_i(\phi|\theta)=2\pi k\cos^2\phi\sum_{n=-\infty}^{\infty}\left\{1!\left(\frac{2\pi}{L}\right)\left|C_1^{(n)}(\lambda_n)\right|^2 S(\lambda_n)\right.$$
$$\left.+2!\left(\frac{2\pi}{L}\right)^2\int_{-\frac{\pi}{L}}^{\frac{\pi}{L}}\left|C_2^{(n)}(\lambda_n-\lambda',\lambda')\right|^2 S(\lambda_n-\lambda')d\lambda'+\cdots\right\}, \quad (2.49)$$
$$\lambda_n=k(\sin\phi-\sin\theta)-\frac{2\pi n}{L},$$

where $S(\lambda)=1$ for $|\lambda|\le\pi/L$ and $S(\lambda)=0$ for $|\lambda|>\pi/L$. We will calculate numerically these quantities by use of zero order and first order Wiener kernels.

2.5 An approximate solution

Let us determine the Wiener kernel functions by using the boundary condition. For simplicity, however, we only consider the case that the random surface is slight roughness and gentle sloping. In this case, the boundary condition may be approximated by

$$\Psi(x,z,\omega)+f(x,\omega)\frac{\partial\Psi(x,z,\omega)}{\partial z}=0 \quad (z=0). \quad (2.50)$$

Because $f(x,\omega)$ is a periodic stationary process and $\Psi(x,z,\omega)$ is a product of a periodic stationary process and an exponential phase factor, the left-hand side of (2.50) becomes a product of an exponential phase factor and a periodic stationary process. As mentioned above, such a periodic stationary process can be expresses by a harmonic series representation, where the "Fourier coefficients" have the correlation functions depending on only the difference of variable x. Substituting (2.12), (2.20), (2.34) and (2.26) into (2.50), and

rewriting the left-hand side of (2.50), we have

$$\sum_{q=-\infty}^{\infty} e^{\frac{i2\pi qx}{L}} V^{(q)}(x,\omega) = 0, \tag{2.51}$$

$$V^{(q)}(x,\omega) = \delta(q,0) + U^{(q)}(x,0,\omega) - i\beta_0(p) f^{(q)}(x,\omega) + \sigma \sum_{m=-\infty}^{\infty} f^{(q-m)}(x,\omega) \left. \frac{\partial U^{(m)}(x,z,\omega)}{\partial z} \right|_{z=0,} \tag{2.52}$$

where $V^{(q)}(x,\omega)$ is a stationary process in the x direction, having a mean value independent of x and the mutual correlation function $R^V_{qq'}(x-x') = \langle V^{(q)}(x,\omega) V^{(q')*}(x',\omega) \rangle$ depending only the difference $x - x'$. Calculating (2.51) in the sense of the norm (2.5), we get

$$\begin{aligned} &|| \sum_{q=-\infty}^{\infty} e^{\frac{i2\pi qx}{L}} V^{(q)}(x,\omega) ||^2 \\ &= \sum_{q=-\infty}^{\infty} R^V_{qq}(0) = \sum_{q=-\infty}^{\infty} \left\langle \left| V^{(q)}(x,\omega) \right|^2 \right\rangle = 0, \end{aligned} \tag{2.53}$$

which implies

$$R^V_{qq}(0) = \left\langle \left| V^{(q)}(x,\omega) \right|^2 \right\rangle = 0, \quad \text{for any integer } q. \tag{2.54}$$

Substituting (2.35) and (2.52) into this, and using the orthogonality relation of $h^{(n)}[\cdot]$ in (2.54), we obtain hierarchical equations for the Wiener kernels. Some low order equations are

(0 order)

$$C_0^{(n)}(p) + \delta(n,0) + \frac{i2\pi\sigma}{L} \sum_{r=-\infty}^{\infty} \int_{-\frac{\pi}{L}}^{\frac{\pi}{L}} G^{(n-r)}(-\lambda) C_1^{(r)}(\lambda) \beta_r(p+\lambda) d\lambda = 0, \tag{2.55}$$

(1st order)

$$\begin{aligned} &C_1^{(n)}(\lambda) - i\sigma\beta_0(p) G^{(n)}(\lambda) + i\sigma \sum_{r=-\infty}^{\infty} G^{(n-r)}(\lambda) C_0^{(r)}(p) \beta_r(p) \\ &+ \frac{i4\pi\sigma}{L} \sum_{r=-\infty}^{\infty} \int_{-\frac{\pi}{L}}^{\frac{\pi}{L}} G^{(n-r)}(-\lambda') C_2^{(r)}(\lambda,\lambda') \beta_r(p+\lambda+\lambda') d\lambda' = 0, \end{aligned} \tag{2.56}$$

(2nd order)

$$\begin{aligned} &C_1^{(n)}(\lambda) - i\sigma\beta_0(p) G^{(n)}(\lambda) + i\sigma \sum_{r=-\infty}^{\infty} G^{(n-r)}(\lambda) C_0^{(r)}(p) \beta_r(p) \\ &+ \frac{i4\pi\sigma}{L} \sum_{r=-\infty}^{\infty} \int_{-\frac{\pi}{L}}^{\frac{\pi}{L}} G^{(n-r)}(-\lambda') C_2^{(r)}(\lambda,\lambda') \beta_r(p+\lambda+\lambda') d\lambda' = 0. \end{aligned} \tag{2.57}$$

Let us obtain a solution involving only $C_0^{(n)}(p)$ and $C_1^{(n)}(\lambda)$. Neglecting $C_2^{(r)}(\lambda,\lambda')$ in (2.56), we approximately get

$$C_1^{(n)}(\lambda) \approx i\sigma \sum_{r=-\infty}^{\infty} G^{(n-r)}(\lambda)\beta_r(p)\big[\delta(r,0) - C_0^{(r)}(p)\big]. \tag{2.58}$$

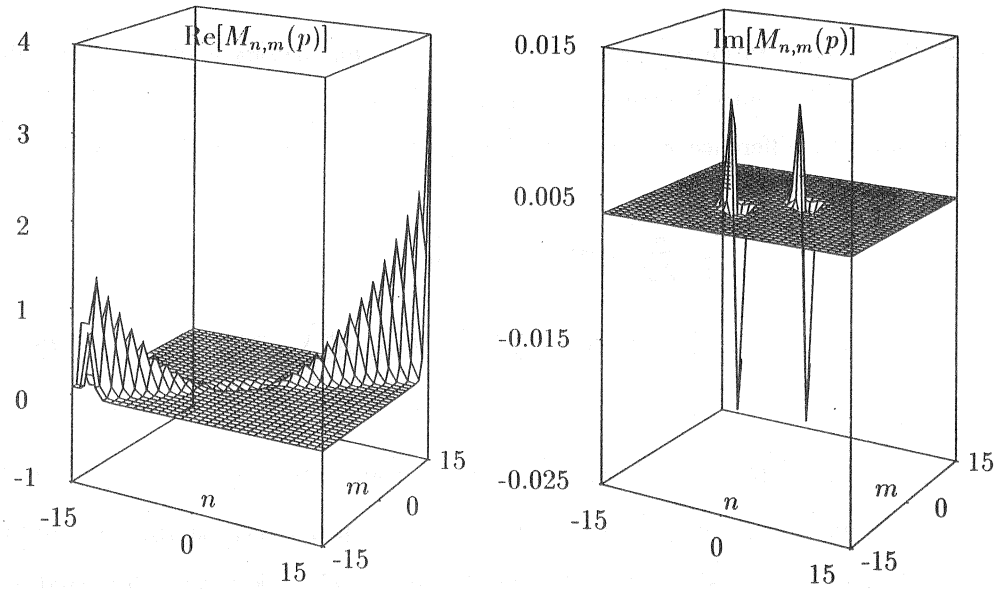

Figure 2.5: Real and imaginary parts of mass operator $M_{n,m}(p)$ for parameters $kL = 6\pi$, $\theta = 30°$, $k\kappa = 2\pi$ and $\sigma = 0.2\pi$. The real part becomes large as the diagonal value of $m = n$ gets large. The imaginary part is relatively small.

Since $C_1^{(n)}(\lambda)$ is an amplitude factor of an incoherent wave, this equation physically implies that incoherent scattered waves are generated by the incident plane wave and all order coherently diffracted waves. Substituting (2.58) into (2.55), we have an equation for $C_0^{(m)}(p)$,

$$\sum_{m=-\infty}^{\infty} \big[\delta(n,m) + M_{n,m}(p)\big]C_0^{(m)}(p) = -\delta(n,0) + M_{n,0}(p), \tag{2.59}$$

where $M_{n,m}(p)$ is the so-called mass operator

$$M_{n,m}(p) = \frac{2\pi\sigma^2}{L}\beta_m(p) \sum_{r=-\infty}^{\infty} \int_{-\frac{\pi}{L}}^{\frac{\pi}{L}} G^{(n-r)}(-\lambda)G^{(r-m)}(\lambda)\beta_r(p+\lambda)d\lambda, \tag{2.60}$$

which is proportional to σ^2. The real and imaginary parts are shown in Fig.2.5, where the $\mathrm{Re}[M_{n,m}(p)]$ is localized on the diagonal line with $n = m$ and the imaginary part is much small. It should be noted that $\mathrm{Re}[M_{n,m}(p)]$ increases on the diagonal line when $|m|(m = n)$ gets large. Since the mass operator describes a double-scattering effect, the solution $C_0^{(m)}(p)$ of (2.59) involves multiple-scattering effect. For a sufficiently small σ^2, we roughly estimate $C_0^{(m)}(p)$ from (2.59) as

$$C_0^{(0)}(p) \approx \frac{M_{0,0}(p) - 1}{M_{0,0}(p) + 1}, \quad C_0^{(m)}(p) \approx \frac{M_{0,0}(p) M_{m,0}(p)}{[M_{m,m}(p) + 1][M_{0,0}(p) + 1]} \quad (m \neq 0). \tag{2.61}$$

Since $C_0^{(0)}(p)$ is the reflection coefficient for the specularly reflected wave, $M_{0,0}(p)$ may be regarded as the equivalent surface impedance. The real part of $M_{0,0}(p)$ implies the energy dissipation of the specularly reflected wave due to diffraction and incoherent scattering, and the imaginary part suggests the stored energy due to evanescent waves propagating along the surface. $C_0^{(0)}(p)$ is of the order of σ^0, but the amplitude $C_0^{(m)}(p)$ becomes a small quantity proportional to σ^2 when $m \neq 0$. However, if we put $C_0^{(0)}(p) = -\delta(n, 0)$, then expression (2.58) is reduced to the first order perturbed solution involving only single-scattering. Such a solution involving multiple-scattering may be obtained by an alternative perturbation method [77] or by a smoothing method [78]. However, our approach has an advantage such that a solution involving multiple-scattering is obtained by simple algebraic calculations based on the orthogonality relation (A.11) and the recurrence formula (A.7).

Substituting (2.58) into (2.49), the incoherent scattering cross section $\sigma_i(\phi|\theta)$ is approximately expressed as

$$\sigma_i(\phi|\theta) \approx \frac{4\pi^2 k \sigma^2 \sin^2\phi}{L} \times \left| \sum_{r=-\infty}^{\infty} G(k\cos\phi - k\cos\theta - \frac{2\pi r}{L}) \beta_r(k\cos\theta) \left[\delta(r,0) - C_0^{(r)}(p)\right] \right|^2. \tag{2.62}$$

This means that $\sigma_i(\phi|\theta)$ is determined by the contributions from these coherently diffracted waves with amplitude $C_0^{(r)}(p)$. It is important to note that the summation is performed in complex amplitude in (2.62). In other words, incoherent waves generated by coherently diffracted waves with different order interfere each other, which causes ripples in the angular distribution of the incoherent scattering, as shown below. Note that such interference is physically expected, because each coherently diffracted wave is scattered by a single random surface when ω is fixed. Since coherently diffracted waves are generated by

the multiple-scattering, such ripples may disappear in case of the first order perturbation solution with $C_0^{(n)}(p) = -\delta(n,0)$. However, such ripples in the incoherent scattering were reported in case of a roughened sinusoid [17].

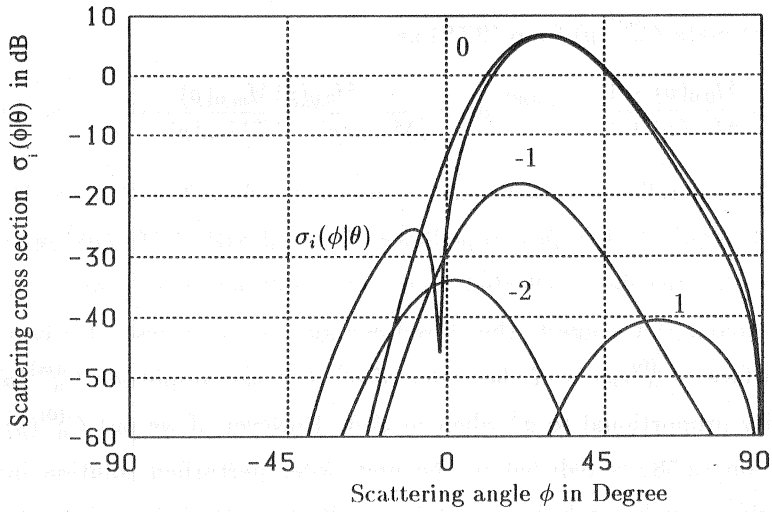

Figure 2.6: Scattering cross section $\sigma_i(\phi|\theta)$ and incoherent scattering generated by each coherently diffracted wave, the order of which is shown by a number. Here, parameters are $\theta = 30°$, $L = 3\Lambda$, $\kappa = 1\Lambda$ and $\sigma = 0.1\Lambda$. Due to the interference, the scattering cross section has a ripple.

2.6 Numerical examples

For numerical calculations, we assume the local surface profile function

$$g(x) = \exp\left(-\frac{x^2}{\kappa^2}\right), \quad G(\lambda) = \frac{\kappa}{2\sqrt{\pi}} \exp\left(-\frac{\kappa^2\lambda^2}{4}\right), \tag{2.63}$$

where κ is a constant determining the surface shape. Also, we approximate infinite summations in (2.58), (2.59), (2.60) and (2.62) by a finite sum from -15 to 15.

For the angle of incidence $\theta = 60°$, the period $L = 3\Lambda$, roughness parameter $\sigma = 0.1\Lambda$ and $\kappa = 1\Lambda$, Λ being wavelength, we calculated the scattering cross section $\sigma_i(\phi|\theta)$ in Figs.2.6-2.9. Figure 2.6 shows that the incoherent scattering is generated from each order

coherent diffracted wave. Due to the interference, there is a dip in the angular distribution of $\sigma_i(\phi|\theta)$. Figure 2.7 illustrates the scattering cross section for several angles of incidence. The incoherent scattering is relatively strong in the direction of specular reflection, i.e., $\phi_0(0)$ direction. We see ripples due to the interference. From (2.62), the scattering cross section is proportional to σ^2, as shown in Fig.2.8. As the period L becomes short, the incoherent scattering spreads widely, as illustrated in Fig.2.9. Figure 2.10 shows the backscattering cross section $\sigma_i(-\phi|\phi)$, which also has ripples due to the interference. The backscattering is relatively strong when the incident angle is 0°. When κ gets small, the backscattering cross section spreads widely in the scattering angle. This is because the surface slope increases for a small κ, as seen in (2.63).

Figure 2.11 illustrates the optical theorem as a function of the surface roughness parameter σ. When the surface becomes rough, the incoherent scattering and non-zero order coherent diffraction increase in power, but the zero order coherent diffraction and total coherent scattering, which includes all order coherent diffractions, decrease instead. However, non-zero order coherent diffractions are small, as is expected from (2.61). As a result, total power including all order coherent and incoherent scattering power becomes almost constant, approximately equal to the incident power that is normalized to unity. Figure 2.12 shows the optical theorem as a function of angle of incidence θ. Since $L = 3\Lambda$, the 1st and 2nd order coherent diffractions vanish when $\theta \leq 41.8°$ and $\theta \leq 19.5°$, respectively.

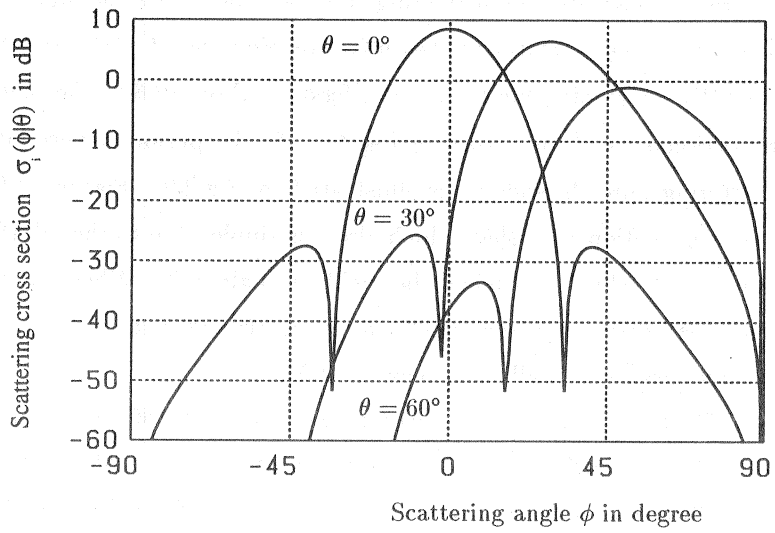

Figure 2.7: Scattering cross section $\sigma_i(\phi|\theta)$ for several angles of incidence θ with parameters $L = 3\Lambda$, $\kappa = 1\Lambda$ and $\sigma = 0.1\Lambda$. Incoherent scattering is relatively strong in the direction of specular reflection.

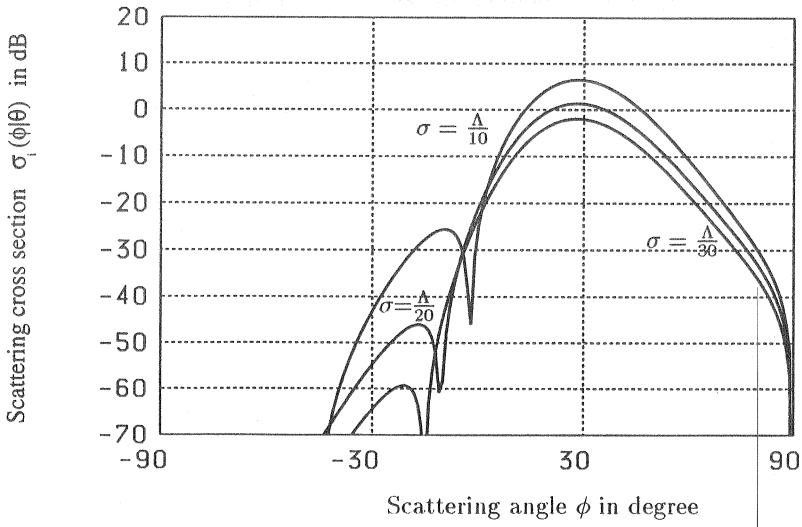

Figure 2.8: Scattering cross section $\sigma_i(\phi|\theta)$ for several values of roughness σ with parameters $\theta = 30°$, $L = 3\Lambda$ and $\kappa = 1\Lambda$. Scattering intensity is proportional to σ^2.

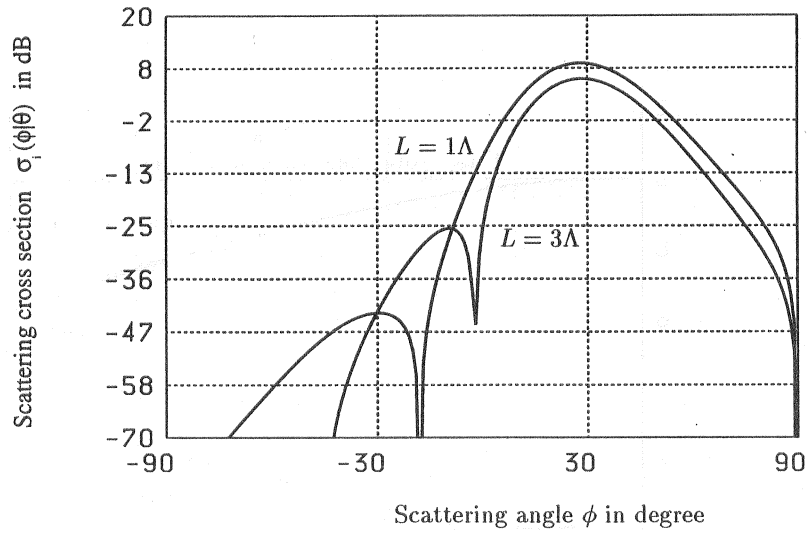

Figure 2.9: Scattering cross section for different period L with parameters $\theta = 30°$, $\sigma = 0.1\Lambda$ and $\kappa = 1\Lambda$. The incoherent scattering spreads widely as the period L gets short.

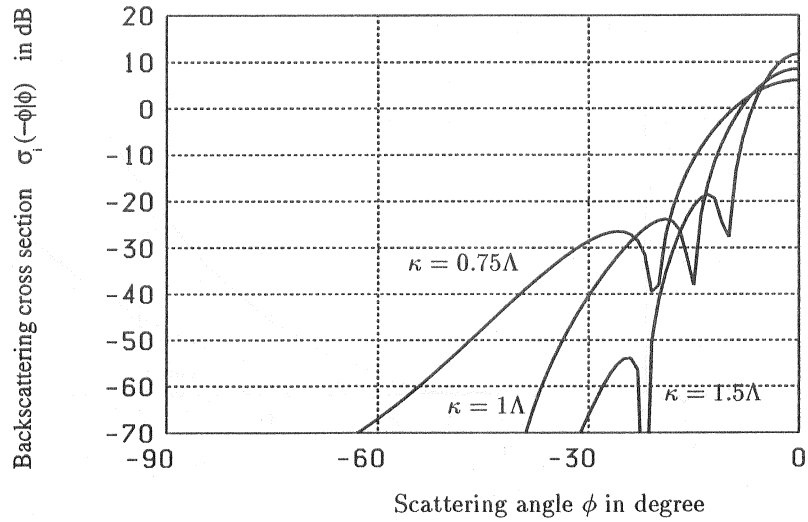

Figure 2.10: Backscattering cross section $\sigma_i(-\phi|\phi)$ with parameters $\sigma = 0.1\Lambda$ and $L = 3\Lambda$. Due to interference, there are some ripples in the backscattering cross section. The backscattering is relatively strong when the incident angle is 0°.

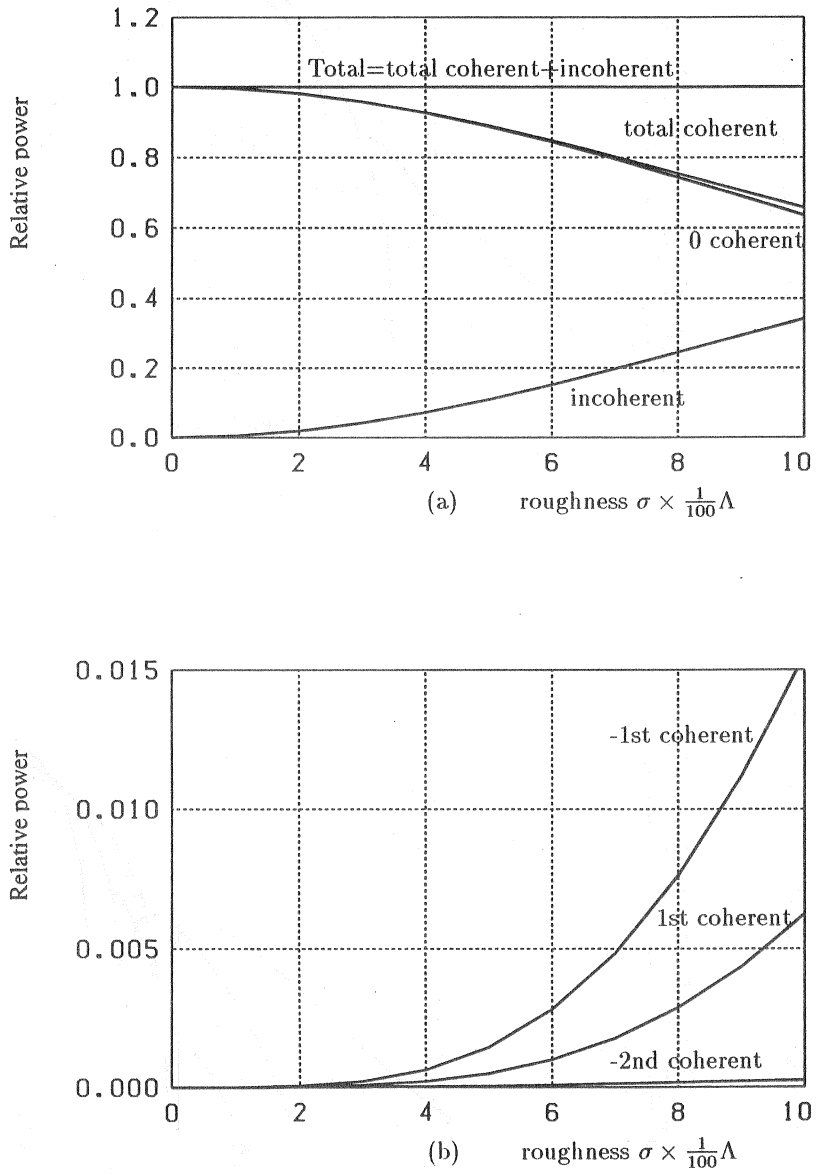

Figure 2.11: Relative power against roughness σ with parameters $L = 3\Lambda$, $\kappa = 1\Lambda$ and $\theta = 30°$. (a) Total power including incoherent and total coherent scattering power, total coherent power, the zero order coherently diffracted power (specularly reflected power), and incoherent scattering power. Total power is almost equal to the incident power that is normalized to unity. (b) Enlarged $\pm$1st order and 2nd order coherently diffracted power.

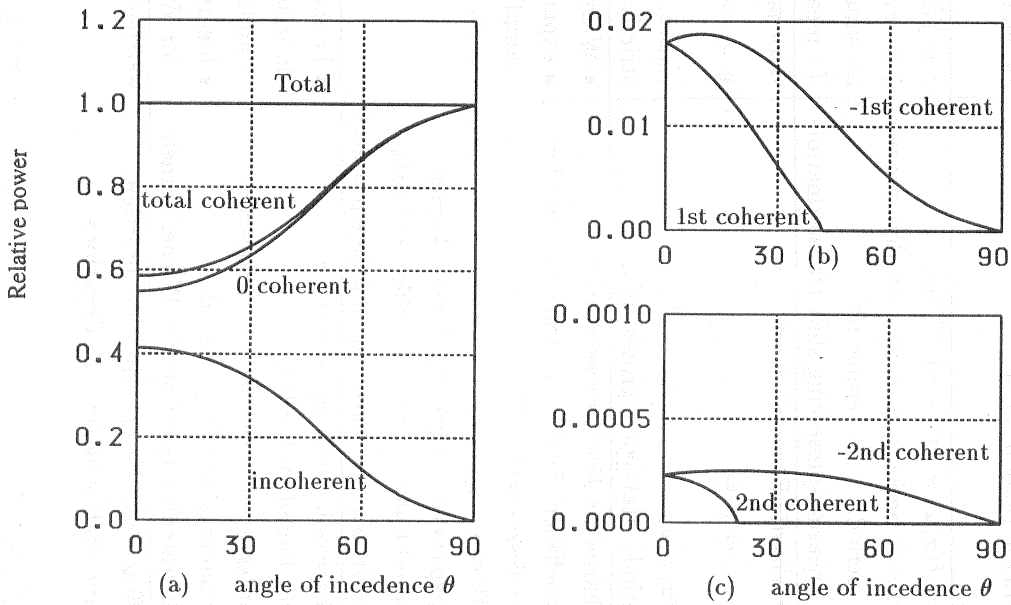

Figure 2.12: Optical theorem against the angle of incidence θ with parameters $L = 3\Lambda$, $\kappa = 1\Lambda$ and $\sigma = 0.1\Lambda$. (a) Total power including incoherent and total coherent power, total coherent power, the zero order coherently diffracted power (specularly reflected power), and incoherent power. Total power is almost equal to the incident power that is normalized as unity. (b) Enlarged $\pm$1st order coherently diffracted power, where the 1st order coherently diffracted power vanishes when $\theta \leq 41.8°$. (c) Enlarged $\pm$2nd order coherently diffracted power, where the 2nd order power becomes zero for $\theta \leq 19.5°$.

Table 2.1: Comparison of theory of diffraction gratings with scattering theory from periodic random surfaces and random surfaces

	periodic surface	periodic random surface	random surface
surface function (shift invariance)	$z = f(x) = f(x+L)$ $f(x)$: periodic function L: period	$z = f(x,\omega) = f(x+nL, T^{-n}\omega)$ $f(x,\omega)$: periodic stationary random process L: period; ω: sample point T: measure-preserving shift transformation	$z = f(x,\omega) = f(T^x\omega)$ $f(x,\omega)$: strictly stationary random process ω: sample point T: measure-preserving shift transformation
form of solution	(Floquet's form) $\Psi = e^{ipx}\left[e^{-i\beta_0(p)z} + U(x,z)\right]$ $U(x,z) = U(x+L,z)$: periodic function of x	(stochastic Floquet's form) $\Psi = e^{ipx}\left[e^{-i\beta_0(p)z} + U(x,z,\omega)\right]$ $U(x,z,\omega) = U(x+L,z,T^{-1}\omega)$: periodic stationary process of x	(stochastic Floquet's form) $\Psi = e^{ipx}\left[e^{-i\beta_0(p)z} + U(x,z,\omega)\right]$ $U(x,z,\omega) = U(z,T^x\omega)$: strictly stationary process of x
representation for U	(Rayleigh assumption) • Fourier series • Fourier coefficients (amplitudes of diffracted waves)	• harmonic series representation • coefficient functions : stationary random processes rather than constants • Wiener expansion • expansion coefficients (Wiener kernels) (amplitude of coherently diffracted wave or incoherent scattering in different order)	• Wiener expansion • expansion coefficients (Wiener kernels) (amplitude of coherent scattering or incoherent scattering)
solution of coefficients	• minimize the average of square boundary condition over a period	• harmonic series representation for boundary condition • integrating ensemble means square of boundary condition over all x • hierarchical equations for Wiener kernels	• boundary condition in ensemble mean square sense (random variables of a point x) • hierarchical equations for Wiener kernels
angular distribution	diffraction (into only discrete directions)	diffraction (into only discrete directions) and scattering (into all directions)	scattering (into all directions)
optical theorem	$\frac{1}{L}\int_0^L \mathrm{Im}\left[\frac{\psi^*}{k}\frac{\partial}{\partial z}\Psi\right]dx = 0$	$\frac{1}{L}\int_{-\frac{L}{2}}^{\frac{L}{2}} \mathrm{Im}\left\langle\frac{\psi^*}{k}\frac{\partial}{\partial z}\Psi\right\rangle dx = 0$	$\lim_{n\to\infty}\frac{1}{2n}\int_{-n}^{n} \mathrm{Im}\left\langle\frac{\psi^*}{k}\frac{\partial}{\partial z}\Psi\right\rangle dx = 0$

2.7 Conclusion

We have proposed a probabilistic theory of scattering from periodic random surfaces. Assuming that the periodic random surface is mathematically modeled by a periodic stationary process, we first point out that the scattered wave has a stochastic Floquet form. We prove that coherent wave has the Floquet form, which means that the random surface works as a periodic grating for the coherent scattering. Further, we find that incoherent waves are generated by coherently diffracted waves with different order and interfere each other to cause ripples in the angular distribution of the incoherent scattering.

Also, our probabilistic approach can be applied to other periodic random surfaces such as a randomly roughened sinusoid and an array of randomly rough strips, because such surfaces are modeled by a periodic stationary process.

In table 2.1, we compare the theory of diffraction gratings with the scattering theory from periodic random surfaces and random surfaces.

In this chapter, however, we only discussed periodic random surfaces with zero average. In fact, there is no difficulty to study periodic random surfaces which has a nonzero periodic average. On the other hand, we have calculated statistical properties of the scattering only by the zero order and first order kernels, neglecting higher order kernels. To get accurate statistical properties, we should consider the second order kernels. It seems that no problem in theory to determine high order kernels.

Further, there are some problems to be considered. They are

(i) the roughness parameter is relatively large,

(ii) the case of two-dimensional surface.

It is quite difficult to treat the problem (i) of scattering from very rough surfaces analytically, and few analytical theories have been proposed for such surfaces.

To resolve the problem (ii), some formulas of orthogonal functionals on two-dimensional Gaussian sequence have to be first developed. The orthogonal relation formulas of the Hermite polynomials in Appendix A are easily extended for the two-dimensional case.

Chapter 3

Scattering of a TM plane wave from periodic random surfaces

3.1 Introduction

In the previous chapter, we have discussed the statistical properties of scattering from periodic random surfaces by the stochastic functional theory, where the boundary condition was given by the Dirichlet condition. In this chapter, we will study the case of Neumann condition by use of the stochastic functional theory,

Enhanced backscattering from random rough surfaces has been studied in several cases, for example, by Ishimaru and Chen for a very rough surface using Kirchhoff approximation [79], Ogura et al for a slightly random surface [43] and for a dielectric waveguide with a rough boundary [80] based on stochastic functional approach. On the other hand, Mendez and O'donnell have experimentally observed the enhanced backscattering from a randomly perturbed periodic grating [21]. In this chapter, theoretical study is developed for the enhanced backscattering from a randomly deformed periodic grating.

Scattering problem of Neumann condition is quite complicated, because a guided surface wave propagates along the surface and is excited by an incident wave. The perturbation method gives a wave field where the guided surface wave has an infinitely large amplitude. As a result, the coherent wave and the incoherent wave by the perturbation method diverge unphysically. However, our stochastic functional theory yields a finite wave field, in terms of which any statistical properties of the scattering and diffraction can be obtained. In this chapter, we assume that the periodic random surface has a periodic average with a relatively small height. We express the scattered wave as the harmonic series representation with coefficient functions represented by Wiener expansions. In Sec.3.3, we represent the reciprocal theorem of Wiener kernels and the incoherent scattering cross section. From an approximate Neumann boundary condition, we obtain the zero, first and second order Wiener kernels, which are expressed in matrix form and satisfy reciprocal relations.

In Sec.3.5, we discuss the 0 order kernels, which describe the coherent diffraction

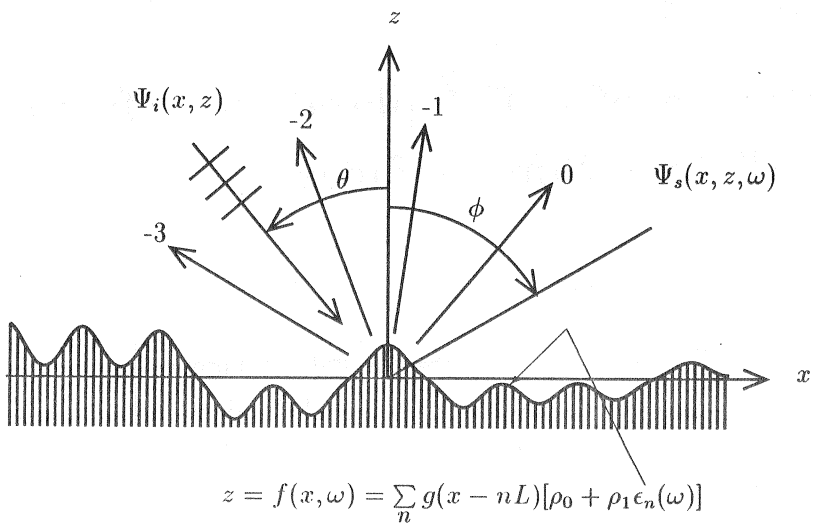

Figure 3.1: Scattering of a TM plane wave from a randomly deformed periodic surface. L is the period. ρ_0 and ρ_1 are height parameters. θ is the angle of incidence and ϕ is a scattering angle. The coherent wave is diffracted into only discrete directions indicated by numbers.

amplitudes. We see that Wood's anomalies appear as rapid variations in the diffracted amplitudes against the angle of incidence. In Sec.3.6, we consider the first order kernels, which are generated by a combination of single-scattering and diffraction. Because an incoherent guided surface wave propagating along the surface is excited for any angle of incidence, there is anomalous scattering that appears as strong and narrow peaks in angular distribution of incoherent scattering. We call this anomalous phenomenon the incoherent Wood's anomaly. The scattering angles of such peaks are determined by the surface period and wavelength, but they are independent of the angle of incidence. In Sec.3.7, we analyze the 2nd order kernels, which involve two double-scattering and diffraction processes. Even though the 2nd order kernel is small in quantity for slightly rough case, it is important, because it gives the backscattering enhancement. As is well-known [81], the backscattering enhancement is a double-scattering effect on randomly rough surfaces. Furthermore, we find another enhancement phenomenon of the incoher-

ent scattering, which we call the diffracted backscattering enhancement. Because of the interaction between double-scattering and diffraction, however, the enhanced backscattering wave is diffracted again by the periodic component of the surface. Due to this physical process, the incoherent wave is slightly enhanced in the directions of diffraction of the backscattered wave.

3.2 Probabilistic formulation of the problem

Let us consider a periodic random surface, shown in Fig.3.1, where the surface deformation is expressed by a periodic stationary random process $f(x,\omega)$,

$$z = f(x,\omega) = \sum_{n=-\infty}^{\infty} g(x-nL)[\rho_0 + \rho_1 \epsilon_n(\omega)], \tag{3.1}$$

where $g(x)$ is the local surface profile, L is the period, $\rho_0 + \rho_1\epsilon_n(\omega)$ is the amplitude of the local surface at $x = nL$, and $\epsilon_n(\omega)$ is an independent Gaussian sequence with zero average and orthogonal correlation satisfying (2.2). From (3.1) and (2.2), $f(x,\omega)$ satisfies

$$\langle f(x,\omega)\rangle = \rho_0 \sum_{n=-\infty}^{\infty} g(x-nL) = \langle f(x+L,\omega)\rangle, \tag{3.2}$$

$$\begin{aligned} R(x,x') &= \Big\langle [f(x,\omega) - \langle f(x,\omega)\rangle] \cdot [f(x',\omega) - \langle f(x',\omega)\rangle] \Big\rangle \\ &= \rho_1^2 \sum_{n=-\infty}^{\infty} g(x-nL)g(x'-nL) = R(x+L,x'+L). \end{aligned} \tag{3.3}$$

Clearly, $f(x,\omega)$ has periodic average and periodic correlation. Note that the periodic random surface consists of periodic component (average part) with the height parameter ρ_0 and random component with the amplitude parameter ρ_1.

As discussed in chapter 2, a periodic stationary random function is known to have a harmonic series representation, whose coefficient functions are stationary random processes. We obtain from (3.1) the harmonic series representation for $f(x,\omega)$ as

$$f(x,\omega) = \sum_{q=-\infty}^{\infty} e^{\frac{i2\pi qx}{L}} f^{(q)}(x,\omega), \tag{3.4}$$

$$f^{(q)}(x,\omega) = \frac{2\pi\rho_0}{L} G^{(q)}(0) + \rho_1 \sum_{n=-\infty}^{\infty} h^{(1)}[\epsilon_n] \int_{-\frac{\pi}{L}}^{\frac{\pi}{L}} e^{i\lambda(x-nL)} G^{(q)}(\lambda) d\lambda,$$

$$f^{(q)*}(x,\omega) = f^{(-q)}(x,\omega), \tag{3.5}$$

where $G^{(q)}(\lambda)$ is obtained from the Fourier integral of the local profile $g(x)$ defined by (2.25). Here, $f^{(q)}(x,\omega)$ is a complex stationary random process with a constant average

and mutual correlation function $R_{qq'}(x)$:

$$\langle f^{(q)}(x,\omega)\rangle = \frac{2\pi\rho_0}{L}G^{(q)}(0), \tag{3.6}$$

$$R_{qq'}(x'-x'') = \left\langle \left[f^{(q)}(x',\omega) - \langle f^{(q)}(x',\omega)\rangle\right]\left[f^{(q)}(x'',\omega) - \langle f^{(q)}(x'',\omega)\rangle\right]\right\rangle$$

$$= \frac{2\pi\rho_1^2}{L}\int_{-\frac{\pi}{L}}^{\frac{\pi}{L}} e^{i\lambda(x'-x'')}G^{(q)}(\lambda)G^{(q')*}(\lambda)d\lambda, \tag{3.7}$$

$$R^*_{qq'}(x) = R_{q'q}(-x), \qquad R_{qq}(0) \geq 0.$$

Let us denote the y component of the TM magnetic field by $\Psi(x,z,\omega|\lambda_0)$, which is a sum of the incident plane wave $\Psi_i(x,z|\lambda_0)$ and the scattered field $\Psi_s(x,z,\omega|\lambda_0)$ that is a random function, and these fields satisfy

$$\left[\frac{\partial^2}{\partial x^2} + \frac{\partial^2}{\partial z^2} + k^2\right]\Psi(x,z,\omega|\lambda_0) = 0, \tag{3.8}$$

$$\Psi(x,z,\omega|\lambda_0) = \Psi_i(x,z|\lambda_0) + \Psi_s(x,z,\omega|\lambda_0), \tag{3.9}$$

$$\Psi_i(x,z|\lambda_0) = e^{i\lambda_0 x - i\beta_0(\lambda_0)z}, \tag{3.10}$$

$$\lambda_0 = k\sin\theta, \quad \beta_n(\lambda) = \sqrt{k^2 - \left(\lambda + \frac{2\pi n}{L}\right)^2},$$

$$\mathrm{Im}[\beta_n(\lambda_0)] \geq 0, \quad \beta_n(\lambda_0) = \beta_{-n}(-\lambda_0), \quad n = 0 \pm 1, \pm 2, \cdots,$$

[1] where θ is the angle of incidence. When the random surface is perfectly conductive, the wave function satisfies the Neumann condition:

$$\frac{\partial\Psi(x,z,\omega|\lambda_0)}{\partial n} = 0 \quad \text{for } z = f(x,\omega), \tag{3.11}$$

where $\frac{\partial}{\partial n}$ is derivative normal to the random surface. As discussed in chapter 2, a stochastic Floquet form of the scattered wave may be determined from the shift invariance property as

$$\Psi_s(x,z|\lambda_0) = e^{i\lambda_0 x}U(x,z,\omega|\lambda_0), \tag{3.12}$$

where $U(x,z,\omega|\lambda_0)$ is a periodic stationary process of x with the period L satisfying the shift invariate property (2.19). It is also written by the harmonic series representation

$$U(x,z,\omega|\lambda_0) = \sum_{q=-\infty}^{\infty} e^{\frac{i2\pi qx}{L}}U^{(q)}(x,z,\omega|\lambda_0), \tag{3.13}$$

$$U^{(q)}(x,z,\omega|\lambda_0) = C_0^{(q)}(\lambda_0)e^{i\beta_q(\lambda_0)z}$$

[1] Here, notations are slightly modified. The x component of the incident wave vector was denoted as $p = k\sin\theta$ in chapter 2. But it is $\lambda_0 = k\sin\theta$ in this chapter.

$$+\sum_{m=-\infty}^{\infty} h^{(1)}[\epsilon_m]\int_{-\frac{\pi}{L}}^{\frac{\pi}{L}} C_1^{(q)}(\lambda|\lambda_0)e^{i\lambda(x-mL)+i\beta_q(\lambda_0+\lambda)z}d\lambda$$
$$+\sum_{m,n=-\infty}^{\infty} h^{(2)}[\epsilon_m,\epsilon_n]\int\int_{-\frac{\pi}{L}}^{\frac{\pi}{L}} C_2^{(q)}(\lambda_1,\lambda_2|\lambda_0)e^{i\lambda_1(x-mL)+i\lambda_2(x-nL)+i\beta_q(\lambda_0+\lambda_1+\lambda_2)z}d\lambda_1 d\lambda_2$$
$$+\cdots, \tag{3.14}$$

where $U^{(q)}(x,z,\omega|\lambda_0)$ is a stationary process of x, and $C_0^{(q)}(\lambda_0)$, $C_1^{(q)}(\lambda|\lambda_0)$, $C_2^{(q)}(\lambda_1,\lambda_2|\lambda_0)$, $\cdots$ are deterministic Weiner kernels.

3.3 Reciprocal theorem and scattering cross section

Assuming that Ψ_1 and Ψ_2 are wave functions for two different incident waves. By the wave equation (3.8), an identity holds

$$\begin{aligned}&\Psi_1\cdot\nabla^2\Psi_2-\Psi_2\cdot\nabla^2\Psi_1\\&=\nabla\cdot(\Psi_1\cdot\nabla\Psi_2-\Psi_2\cdot\nabla\Psi_1)=0.\end{aligned} \tag{3.15}$$

Integrating the identity (3.15) over an area ABCDA on the periodic random surface, shown in Fig.2.5, and using the Gauss formula (the Stokes formula), we get

$$\left(\int_{\mathrm{AB}}dx+\int_{\mathrm{BC}}dz+\int_{\mathrm{CD}}dl+\int_{\mathrm{DA}}dz\right)\left[\Psi_1\frac{\partial\Psi_2}{\partial n}-\Psi_2\frac{\partial\Psi_1}{\partial n}\right]=0, \tag{3.16}$$

where the third integral is the curvilinear integral along the periodic random surface. The integral over CD vanishes for the Neumann condition. Because the wave functions are expected to be finite for any value (x,z), the second and fourth integrals are finite. Dividing (3.16) by $2nL$ and letting n infinitely large, the second and fourth integrals become zero and the identity (3.16) becomes

$$\lim_{n\to\infty}\frac{1}{2nL}\int_{-nL}^{nL}\left[\Psi_1\frac{\partial\Psi_2}{\partial z}-\Psi_2\frac{\partial\Psi_1}{\partial z}\right]\Bigg|_{z=z_0}dx=0. \tag{3.17}$$

Representing the wave functions Ψ_1 and Ψ_2 by their harmonic series representations (3.9), (3.12) and (3.13) with Wiener expansion coefficient functions (3.14), and substituting them into (3.17), we have

$$\lim_{n\to\infty}\frac{1}{2nL}\int_{-nL}^{nL}\left\{\left[\Psi_1\right]_{n_1}\left[\frac{\partial\Psi_2}{\partial z}\right]_{n_2}-\left[\Psi_2\right]_{n_2}\left[\frac{\partial\Psi_1}{\partial z}\right]_{n_1}\right\}\Bigg|_{z=z_0}dx=0, \tag{3.18}$$
$$n_1,n_2=1,2,\cdots,$$

which is true for any positive integers n_1 and n_2. Here, $[\cdot]_n$ denotes the component of n-dimensional Hermite polynomial in the Wiener expansion. To understand the expression $[\cdot]_n$ well, we write two concrete examples on the wave function $\Psi(x,z,\omega|\lambda_0)$ in (3.9),

$$[\Psi]_0 = e^{i\lambda_0 x}\left[e^{-i\beta_0(\lambda_0)z} + \sum_{q=-\infty}^{\infty} e^{\frac{i2\pi qx}{L}} C_0^{(q)}(\lambda_0) e^{i\beta_q(\lambda_0)z}\right], \tag{3.19}$$

$$[\Psi]_1 = e^{i\lambda_0 x}\sum_{q=-\infty}^{\infty} e^{\frac{i2\pi qx}{L}} \sum_{m=-\infty}^{\infty} h^{(1)}[\epsilon_m] \int_{-\frac{\pi}{L}}^{\frac{\pi}{L}} C_1^{(q)}(\lambda|\lambda_0) e^{i\lambda(x-mL)+i\beta_q(\lambda_0+\lambda)z} d\lambda. \tag{3.20}$$

To obtain the result (3.18), we have used the relation:

$$\lim_{n\to\infty}\frac{1}{2nL}\int_{-nL}^{nL} e^{i\lambda x}dx = \delta(\lambda,0) = \begin{cases} 1 & (\lambda = 0) \\ 0 & (\lambda \neq 0) \end{cases}. \tag{3.21}$$

Using the relation (3.18), the $[\cdot]_0$ component of (3.17) becomes

$$\lim_{n\to\infty}\frac{1}{2nL}\int_{-nL}^{nL}\left\{\left[\Psi_1\right]_0\left[\frac{\partial\Psi_2}{\partial z}\right]_0 - \left[\Psi_2\right]_0\left[\frac{\partial\Psi_1}{\partial z}\right]_0\right\}\Bigg|_{z=z_0} dx = 0, \tag{3.22}$$

and the $[\cdot]_m$ component of (3.17) becomes

$$\lim_{n\to\infty}\frac{1}{2nL}\int_{-nL}^{nL}\left\{\left[\Psi_1\right]_0\left[\frac{\partial\Psi_2}{\partial z}\right]_m - \left[\Psi_2\right]_m\left[\frac{\partial\Psi_1}{\partial z}\right]_0 + \left[\Psi_1\right]_m\left[\frac{\partial\Psi_2}{\partial z}\right]_0 - \left[\Psi_2\right]_0\left[\frac{\partial\Psi_1}{\partial z}\right]_m\right\}\Bigg|_{z=z_0} dx = 0. \tag{3.23}$$

From (3.22), the reciprocal relation of the 0 order Wiener kernel is given by

$$\begin{aligned} &\frac{C_0^{(q)}(\lambda_0)}{\beta_0(\lambda_0)} = \frac{C_0^{(q)}(\lambda)}{\beta_0(\lambda)}, \\ &-\lambda = \lambda_0 + \frac{2\pi q}{L}, \quad q = 0, \pm1, \pm2, \cdots. \end{aligned} \tag{3.24}$$

Using the orthogonality of Hermite polynomials and the relation (3.21) in (3.23), the reciprocal relation of n-th order Wiener kernels is obtained [2]

$$\begin{aligned} &\frac{C_n^{(q)}(\lambda_1,\lambda_2,\cdots|\lambda_0)}{\beta_0(\lambda_0)} = \frac{C_n^{(q)}(\lambda_1,\lambda_2,\cdots,\lambda_n|\lambda)}{\beta_0(\lambda)}, \\ &-\lambda = \lambda_0 + \lambda_1 + \lambda_2 + \cdots + \lambda_n + \frac{2\pi q}{L}, \\ &q = 0, \pm1, \pm2, \cdots, \quad n \geq 1. \end{aligned} \tag{3.25}$$

[2]Note that the mathematical deduction to obtain the reciprocal relation (3.25) from (3.23) is not exact. However, the result (3.25) seems to be correct physically. How to deduce the relation exactly is an open problem to be solved.

The reciprocal relations (3.24) and (3.25) can be interpreted in terms of power. When $\beta_0(\lambda_0) = \beta_0(-\lambda_0)$ and $\beta_0(-\lambda) = \beta_0(\lambda)$ are real numbers, we get

$$\frac{\beta_0(\lambda)}{\beta_0(\lambda_0)}|C_0^{(q)}(\lambda_0)|^2 = \frac{\beta_0(-\lambda_0)}{\beta_0(-\lambda)}|C_0^{(q)}(\lambda)|^2, \tag{3.26}$$

$$\frac{\beta_0(\lambda)}{\beta_0(\lambda_0)}|C_n^{(q)}(\lambda_1,\cdots,\lambda_n|\lambda_0)|^2 = \frac{\beta_0(-\lambda_0)}{\beta_0(-\lambda)}|C_n^{(q)}(\lambda_1,\cdots,\lambda_n|-\lambda)|^2. \tag{3.27}$$

Since $\beta_0(\lambda)|C_n^{(q)}(\lambda_1,\cdots,\lambda_n|\lambda_0)|^2$ is the power scattered into $\phi_0(\lambda)$ and $\beta_0(\lambda_0)$ is the incident power, the left-hand sides are the efficiencies diffracted into $\phi_0(\lambda)$ direction for the incident direction of $\phi_0(\lambda_0) = \theta$. On the other hand, the right-hand sides are the efficiencies diffracted into $\phi_0(-\lambda_0) = -\theta$ direction for the incident direction of $\phi_0(-\lambda) = -\phi_0(\lambda)$.

In particular, it holds that $-\lambda = \lambda_0$ for $q = 0$ in (3.26). In this case, the efficiency in the zero order doesn't change when the periodic random surface is rotated by 180° about z axis . It must be emphasized that the invariance holds even if the surface is not symmetrical with respect to the z axis.

In loss-less case, we have obtained the optical theorem for the Dirichlet condition (2.11) in Sec.2.4. Replacing the Dirichlet condition (2.11) by the Neumann condition (3.11), we obtain the optical theorem (2.47) and the scattering cross section (2.49) again. Here, let $\sigma(\phi|\theta)$ represent the scattering cross section for the incoherent wave, we write

$$\sigma(\phi|\theta) = \sigma_1(\phi|\theta) + \sigma_2(\phi|\theta) + \cdots, \tag{3.28}$$

where σ_1 is the contribution from the first order Wiener kernels

$$\sigma_1(\phi|\theta) = \frac{4\pi^2 k\cos^2\phi}{L}\sum_{n=-\infty}^{\infty}\left|C_1^{(n)}(\lambda_n|\lambda_0)\right|^2 S(\lambda_n), \tag{3.29}$$

and σ_2 is the contribution from the second order Wiener kernels

$$\sigma_2(\phi|\theta) = \frac{16\pi^3 k\cos^2\phi}{L^2}\sum_{n=-\infty}^{\infty}\int_{-\frac{\pi}{L}}^{\frac{\pi}{L}}\left|C_2^{(n)}(\lambda_n-\lambda',\lambda'|\lambda_0)\right|^2 S(\lambda_n-\lambda')d\lambda', \tag{3.30}$$

where

$$S(\lambda) = \begin{cases} 1 & |\lambda| \le \frac{\pi}{L} \\ 0 & |\lambda| > \frac{\pi}{L} \end{cases}, \quad \lambda_n = \lambda_s - \lambda_0 - \frac{2\pi n}{L}, \quad \lambda_s = k\sin\phi, \tag{3.31}$$

and ϕ is a scattering angle shown in Fig.3.1. We will calculate numerically these quantities by use of approximate Wiener kernels.

3.4 An approximate solution

Let us determine the kernel functions by using the Neumann condition. For simplicity, however, we only consider the case that the random surface has slight roughness and gentle slope. In this case, the boundary condition may be approximated by

$$-\frac{df}{dx}\frac{\partial\Psi}{\partial x}+\frac{\partial\Psi}{\partial z}+f\frac{\partial^2\Psi}{\partial z^2}=0 \quad (z=0). \tag{3.32}$$

Substituting (3.9), (3.12), (3.13) and (3.4) into (3.32) and using the orthogonality relation of $h^{(n)}[\cdot]$, we obtain hierarchical equations for the kernels. Some low order equations are : the zero order equation

$$\sum_{r=-\infty}^{\infty}\left[i\beta_n(\lambda_0)\delta(n,r)+\frac{2\pi\rho_0}{L}d_{n,r}(0,\lambda_0)\right]C_0^{(r)}(\lambda_0)+\frac{2\pi\rho_0}{L}d_{n,0}(0,\lambda_0)-i\beta_0(\lambda_0)\delta(n,0)$$
$$+\frac{i2\pi\rho_1}{L}\sum_{r=-\infty}^{\infty}\int_{-\frac{\pi}{L}}^{\frac{\pi}{L}}d_{n,r}(-\lambda,\lambda_0+\lambda)C_1^{(r)}(\lambda|\lambda_0)d\lambda=0, \tag{3.33}$$

the first order equation

$$\sum_{r=-\infty}^{\infty}\left[i\beta_n(\lambda_0+\lambda)\delta(n,r)+\frac{2\pi\rho_0}{L}d_{n,r}(0,\lambda_0+\lambda)\right]C_1^{(r)}(\lambda|\lambda_0)$$
$$+\rho_1\sum_{r=-\infty}^{\infty}d_{n,r}(\lambda,\lambda_0)\left[\delta(r,0)+C_0^{(r)}(\lambda_0)\right]$$
$$+\frac{4\pi\rho_1}{L}\sum_{r=-\infty}^{\infty}\int_{-\frac{\pi}{L}}^{\frac{\pi}{L}}d_{n,r}(-\lambda',\lambda_0+\lambda+\lambda')C_2^{(r)}(\lambda,\lambda'|\lambda_0)d\lambda'=0, \tag{3.34}$$

the second order equation

$$\sum_{r=-\infty}^{\infty}\left[i\beta_n(\lambda_0+\lambda_1+\lambda_2)\delta(n,r)+\frac{2\pi\rho_0}{L}d_{n,r}(0,\lambda_0+\lambda_1+\lambda_2)\right]C_2^{(r)}(\lambda_1,\lambda_2|\lambda_0)$$
$$+\frac{\rho_1}{2}\sum_{r=-\infty}^{\infty}\left[d_{n,r}(\lambda_2,\lambda_0+\lambda_1)C_1^{(r)}(\lambda_1|\lambda_0)+d_{n,r}(\lambda_1,\lambda_0+\lambda_2)C_1^{(r)}(\lambda_2|\lambda_0)\right]$$
$$+\frac{6\pi\rho_1}{L}\sum_{r=-\infty}^{\infty}\int_{-\frac{\pi}{L}}^{\frac{\pi}{L}}d_{n,r}(-\lambda',\lambda_0+\lambda_1+\lambda_2+\lambda')C_3^{(r)}(\lambda_1,\lambda_2,\lambda'|\lambda_0)d\lambda'=0, \tag{3.35}$$

where

$$d_{n,r}(\lambda_1,\lambda_2)=\left[\left(\frac{2\pi}{L}(n-r)+\lambda_1\right)\left(\frac{2\pi r}{L}+\lambda_2\right)-\beta_r^2(\lambda_2)\right]G^{(n-r)}(\lambda_1). \tag{3.36}$$

Neglecting the integral terms in these equations, we get approximate equations for $C_0^{(r)}(\lambda_0)$, $C_1^{(r)}(\lambda)$ and $C_2^{(r)}(\lambda_1,\lambda_2)$, which satisfy reciprocal relations (3.24) and (3.25), and are represented in vector form

$$\boldsymbol{\Delta}(\lambda_0)\mathbf{C}_0(\lambda_0) = \left[\mathbf{B}(\lambda_0)-\frac{2\pi\rho_0}{L}\mathbf{D}(0,\lambda_0)\right]\mathbf{I}^0, \tag{3.37}$$

$$\mathbf{\Delta}(\lambda_0+\lambda)\mathbf{C}_1(\lambda|\lambda_0) = -\rho_1\mathbf{D}(\lambda,\lambda_0)\left[\mathbf{I}^0+\mathbf{C}_0(\lambda_0)\right], \tag{3.38}$$

$$\mathbf{\Delta}(\lambda_0+\lambda_1+\lambda_2)\mathbf{C}_2(\lambda_1,\lambda_2|\lambda_0) = -\frac{\rho_1}{2}\mathbf{D}(\lambda_2,\lambda_0+\lambda_1)\mathbf{C}_1(\lambda_1|\lambda_0) - \frac{\rho_1}{2}\mathbf{D}(\lambda_1,\lambda_0+\lambda_2)\mathbf{C}_1(\lambda_2|\lambda_0), \tag{3.39}$$

where we have put

$$\begin{aligned}
\mathbf{I}^0 &= (\cdots,\delta(n,0),\cdots)^t,\\
\mathbf{C}_0(\lambda_0) &= \left(\cdots,C_0^{(-1)}(\lambda_0),C_0^{(0)}(\lambda_0),C_0^{(1)}(\lambda_0),\cdots\right)^t,\\
\mathbf{C}_1(\lambda|\lambda_0) &= \left(\cdots,C_1^{(-1)}(\lambda|\lambda_0),C_1^{(0)}(\lambda|\lambda_0),C_1^{(1)}(\lambda|\lambda_0),\cdots\right)^t,\\
\mathbf{C}_2(\lambda_1,\lambda_2|\lambda_0) &= \left(\cdots,C_2^{(-1)}(\lambda_1,\lambda_2|\lambda_0),C_2^{(0)}(\lambda_1,\lambda_2|\lambda_0),C_2^{(1)}(\lambda_1,\lambda_2|\lambda_0),\cdots\right)^t.
\end{aligned} \tag{3.40}$$

$\mathbf{B}(\lambda_0)$, $\mathbf{D}(\lambda_1,\lambda_2)$ and $\mathbf{\Delta}(\lambda_0+\lambda)$ are infinitely dimensional matrixes

$$\mathbf{B}(\lambda_0) = \begin{pmatrix} \cdots & \cdots & \cdots & \cdots & \cdots \\ \cdots & i\beta_{-1}(\lambda_0) & 0 & 0 & \cdots \\ \cdots & 0 & i\beta_0(\lambda_0) & 0 & \cdots \\ \cdots & 0 & 0 & i\beta_1(\lambda_0) & \cdots \\ \cdots & \cdots & \cdots & \cdots & \cdots \end{pmatrix}, \tag{3.41}$$

$$\mathbf{D}(\lambda_1,\lambda_2) = \begin{pmatrix} \cdots & \cdots & \cdots & \cdots & \cdots \\ \cdots & d_{-1,-1}(\lambda_1,\lambda_2) & d_{-1,0}(\lambda_1,\lambda_2) & d_{-1,1}(\lambda_1,\lambda_2) & \cdots \\ \cdots & d_{0,-1}(\lambda_1,\lambda_2) & d_{0,0}(\lambda_1,\lambda_2) & d_{0,1}(\lambda_1,\lambda_2) & \cdots \\ \cdots & d_{1,-1}(\lambda_1,\lambda_2) & d_{1,0}(\lambda_1,\lambda_2) & d_{1,1}(\lambda_1,\lambda_2) & \cdots \\ \cdots & \cdots & \cdots & \cdots & \cdots \end{pmatrix}, \tag{3.42}$$

$$\mathbf{\Delta}(\lambda_0+\lambda) = -i\mathbf{B}(\lambda_0+\lambda)+\frac{2\pi\rho_0}{L}\mathbf{D}(0,\lambda_0+\lambda), \tag{3.43}$$

where subscripts n and r denote the (n,r) element of matrix. The matrixes $\mathbf{D}$ and $\mathbf{\Delta}$ satisfy relations:

$$\mathbf{D}^S(\lambda_1,\lambda_2) = \mathbf{D}(-\lambda_1,-\lambda_2), \qquad \mathbf{\Delta}^S(\lambda_0) = \mathbf{\Delta}(-\lambda_0), \tag{3.44}$$

$$\mathbf{D}^t(\lambda_1,\lambda_2) = \mathbf{D}(-\lambda_1,\lambda_1+\lambda_2), \qquad \mathbf{\Delta}^t(\lambda_0) = \mathbf{\Delta}(\lambda_0), \tag{3.45}$$

where the superscript t implies transposed matrix and the superscript S indicates the centrally symmetrical operation in matrix:

$$(a_{n,r})^S = (a_{-n,-r}). \tag{3.46}$$

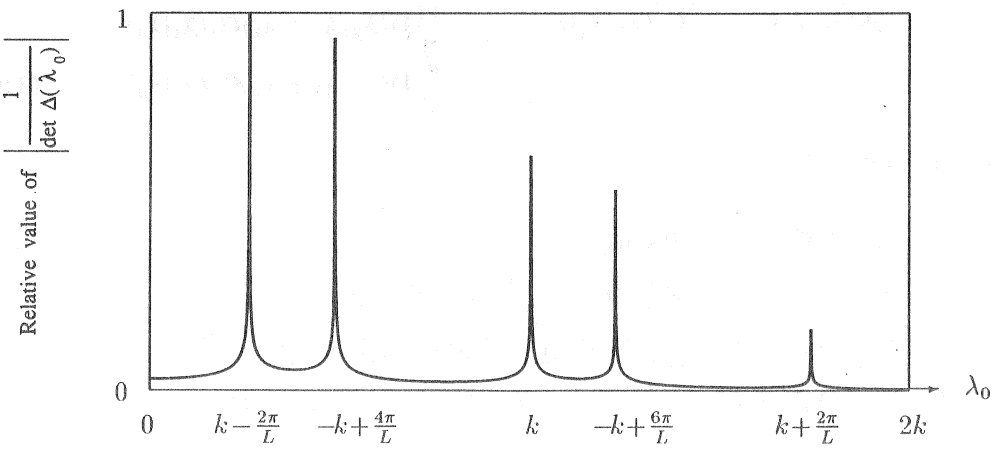

Figure 3.2: Relative value of $\left|\frac{1}{\det\Delta(\lambda_0)}\right|$ with parameters $k\rho_0 = 0.1\pi$, $k\kappa = 0.4\pi$ and $kL = 2.7\pi$. There are anomalous peaks at Rayleigh wavelengths $\lambda_0 = \pm k - \frac{2\pi n}{L}$, $(n = 0, \pm 1, \pm 2, \cdots)$. Here, $\mathbf{\Delta}(\lambda_0)$ is approximately calculates by a 7×7 matrix.

3.5 Wood's anomaly

If $\rho_0 \neq 0$ (this means that the periodic random surface has a periodic average with non-zero height ρ_0), the inverse of $\mathbf{\Delta}(\lambda_0)$ exists for any real λ_0, and amplitude of the coherent diffraction is given from (3.37) as

$$\mathbf{C}_0(\lambda_0) = \mathbf{\Delta}^{-1}(\lambda_0)\left[\mathbf{B}(\lambda_0) - \frac{2\pi\rho_0}{L}\mathbf{D}(0,\lambda_0)\right]\mathbf{I}^0 \tag{3.47}$$

$$= 2\mathbf{\Delta}^{-1}(\lambda_0)\mathbf{B}(\lambda_0)\mathbf{I}^0 - \mathbf{I}^0, \tag{3.48}$$

where the resonance factor $\mathbf{\Delta}^{-1}(\lambda_0)$ describes the diffraction process due to surface periodicity. When a diagonal element of the matrix $\mathbf{\Delta}(\lambda_0)$ vanishes at the so-called Rayleigh wavenumber

$$\beta_m(\lambda_0) = 0, \quad \lambda_0 = \pm k - \frac{2\pi m}{L}, \quad m = 0, \pm 1, \pm 2, \cdots, \tag{3.49}$$

however, $|1/\det\mathbf{\Delta}(\lambda_0)|$ has large peaks shown in Fig.3.2. Physically, such a peak suggests the existence of the guided surface waves propagating along the surface. Then,

such a guided surface wave is excited by a wave with Rayleigh wavenumber and causes well-known Wood's anomaly that appears as a rapid variation of the amplitude of the coherent diffraction (see Fig.3.3) and the diffracted power (see Fig.3.7) against the angle of incidence.

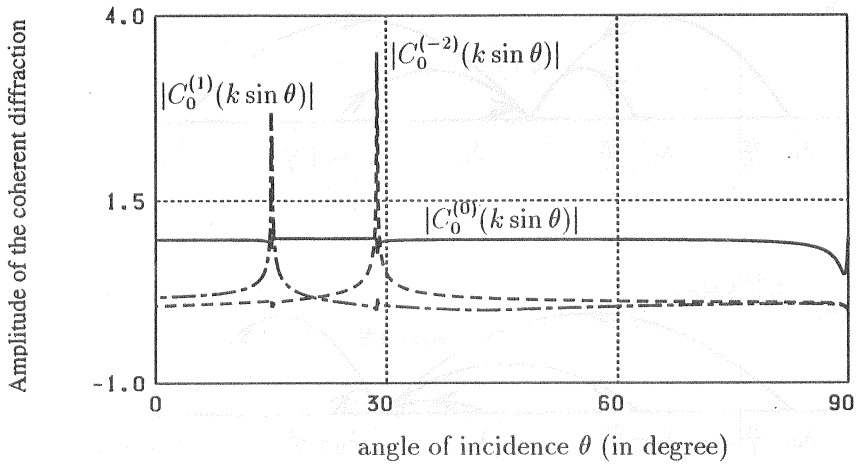

Figure 3.3: Amplitude of coherent diffraction against the angle of incidence with parameter $kL = 2.7\pi$. There exist resonance anomalies appearing at some angles of incidence, which relate with the Rayleigh wavelength.

3.6 Incoherent Wood's anomaly

From (3.38) and (3.48), we introduce a new representation for the first order kernel vector,

$$\mathbf{C}_1(\lambda|\lambda_0) = -\rho_1\mathbf{H}(\lambda_0+\lambda|\lambda_0)\left[\mathbf{I}^0 + \mathbf{C}_0(\lambda_0)\right] \tag{3.50}$$

$$= -2\rho_1\mathbf{\Delta}^{-1}(\lambda_0+\lambda)\mathbf{D}(\lambda,\lambda_0)\mathbf{\Delta}^{-1}(\lambda_0)\mathbf{B}(\lambda_0), \tag{3.51}$$

$$\mathbf{H}(\Lambda_1+\Lambda_2|\Lambda_1) = \mathbf{\Delta}^{-1}(\Lambda_1+\Lambda_2)\mathbf{D}(\Lambda_2,\Lambda_1) \tag{3.52}$$

$$= [H_{n,r}(\Lambda_1+\Lambda_2|\Lambda_1)], \tag{3.53}$$

where $\mathbf{H}(\Lambda_1+\Lambda_2|\Lambda_1)$ describes the single-scattering diffraction process. The coefficient $H_{n,r}(\Lambda_1+\Lambda_2|\Lambda_1)$ converts a plane wave with $\Lambda_1+\frac{2\pi r}{L}$ into a plane wave with $\Lambda_1+\Lambda_2+\frac{2\pi n}{L}$, where $\Lambda_1+\frac{2\pi r}{L}$ and $\Lambda_1+\Lambda_2+\frac{2\pi n}{L}$ are x components of their wave vectors. The n-th

component of the first order kernel is given by

$$C_1^{(n)}(\lambda|\lambda_0) = -\rho_1 \sum_{r=-\infty}^{\infty} H_{n,r}(\lambda_0+\lambda|\lambda_0)\left[\delta(r,0) + C_0^{(r)}(\lambda_0)\right], \tag{3.54}$$

which illustrates a scattering-diffraction process shown in Fig.3.4.

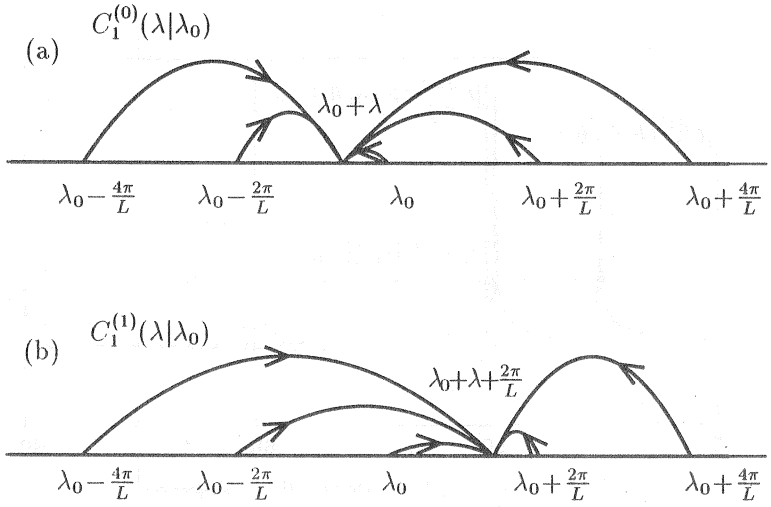

Figure 3.4: The single-scattering diffraction process described by $C_1^{(n)}(\lambda|\lambda_0)$ for $-3 < r < 3$. (a) $n = 0$ and (b) $n = 1$.

The incident plane wave with λ_0, which is the x component of wave vector, is first transformed by the periodic component of the surface into the coherent diffracted wave with amplitude $C_0^{(r)}(\lambda_0)$ and wave number $\lambda_0 + \frac{2\pi r}{L}$. From such a diffracted wave, an incoherent wave propagating with wavenumber $\lambda_0 + \lambda + \frac{2\pi n}{L}$ and amplitude $C_1^{(n)}(\lambda|\lambda_0)$ is generated by a single-scattering diffraction. Because $\mathbf{H}(\lambda_0+\lambda|\lambda_0)$ involves the resonance factor $\mathbf{\Delta}(\lambda_0+\lambda)^{-1}$, the amplitude $|C_1^{(n)}(\lambda|\lambda_0)|$ could have anomalous peaks (see Fig.3.5) for λ enjoying

$$\lambda = \pm k - \lambda_0 - \frac{2\pi m}{L}, \quad |\lambda| \le \frac{\pi}{L}, \quad m = 0, \pm 1, \pm 2, \cdots, \tag{3.55}$$

where m is an integer making $|\lambda| \le \frac{\pi}{L}$. Thus, an anomalous peak, which we call the incoherent Wood's anomaly, appears at a scattering angle:

$$\phi_{IW}^m = \sin^{-1}\left(\pm 1 - \frac{2\pi m}{kL}\right), \quad m = \pm 1, \pm 2, \cdots. \tag{3.56}$$

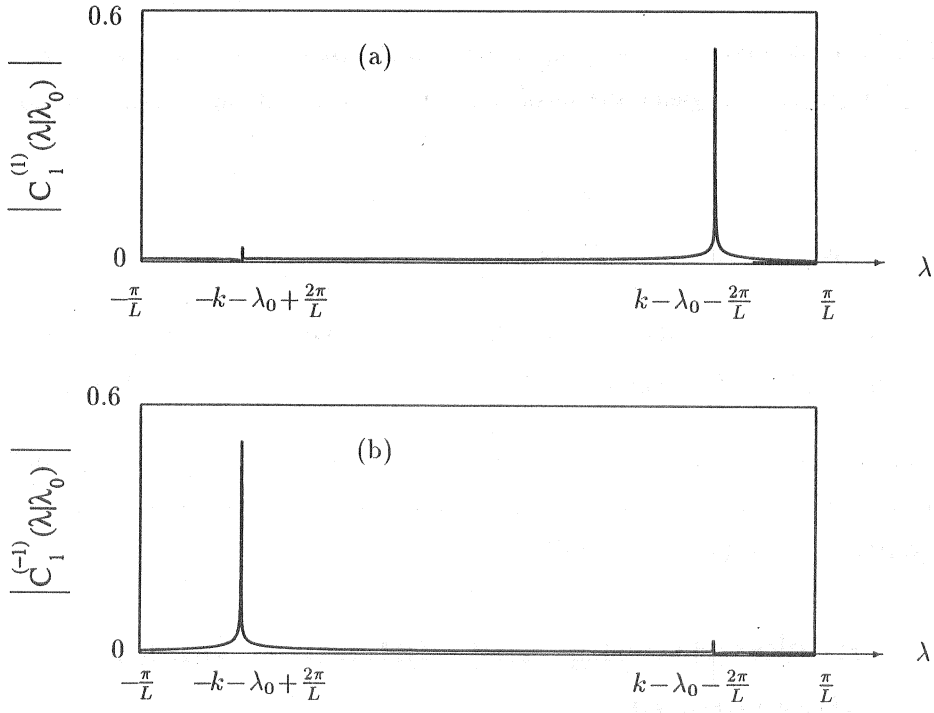

Figure 3.5: Anomalies occur in amplitude $|C_1^{(n)}(\lambda|\lambda_0)|$, where $k\rho = k\rho_1 = 0.1\pi$, $k\kappa = 0.4\pi$ and $kL = 2.7\pi$. (a) $n = 1$ and (b) $n = -1$.

Since the surface has continuous spectrum, an incoherent guided surface wave propagating along the surface is excited for any angle of incidence. Such a guided wave is diffracted again by the surface periodicity to yield a strong incoherent wave into the direction ϕ_{IW}^m. It should be noted that the incoherent Wood's anomaly may occur for any angle of incidence, whereas Wood's anomaly takes place for an incident angle determined by the period and wavelength.

We also obtain the second order kernel from (3.39), (3.51) and (3.52)

$$\begin{aligned}\mathbf{C}_2(\lambda_1,\lambda_2|\lambda_0) &= -\frac{\rho_1}{2}\mathbf{H}(\lambda_0+\lambda_1+\lambda_2|\lambda_0+\lambda_1)\mathbf{C}_1(\lambda_1|\lambda_0)\\ &\quad -\frac{\rho_1}{2}\mathbf{H}(\lambda_0+\lambda_1+\lambda_2|\lambda_0+\lambda_2)\mathbf{C}_1(\lambda_2|\lambda_0) \qquad (3.57)\\ &= \rho_1^2\boldsymbol{\Delta}^{-1}(\lambda_0+\lambda_1+\lambda_2)\left[\mathbf{D}(\lambda_2,\lambda_0+\lambda_1)\boldsymbol{\Delta}^{-1}(\lambda_0+\lambda_1)\mathbf{D}(\lambda_1,\lambda_0)\right.\end{aligned}$$

$$+ \mathbf{D}(\lambda_1, \lambda_0 + \lambda_2)\mathbf{\Delta}^{-1}(\lambda_0 + \lambda_2)\mathbf{D}(\lambda_2, \lambda_0)\Big]\, \mathbf{\Delta}^{-1}(\lambda_0)\mathbf{B}(\lambda_0)\mathbf{I}^0, \quad (3.58)$$

which involves double-scattering proportional to ρ_1^2. Due to resonance factor $\mathbf{\Delta}^{-1}(\lambda_0 + \lambda_1 + \lambda_2)$, $\mathbf{C}_2(\lambda_1, \lambda_2|\lambda_0)$ yields the incoherent Wood's anomaly also. Here, we note that when

$$\lambda_0 + \lambda_1 = -(\lambda_0 + \lambda_2), \quad (3.59)$$

the two double-scattering processes of (3.58) have a same vector value

$$\begin{aligned} &\mathbf{\Delta}^{-1}(\lambda_0 + \lambda_1 + \lambda_2)\mathbf{D}(\lambda_2, \lambda_0 + \lambda_1)\mathbf{\Delta}^{-1}(\lambda_0 + \lambda_1)\mathbf{D}(\lambda_1, \lambda_0)\mathbf{\Delta}^{-1}(\lambda_0)\mathbf{B}(\lambda_0)\mathbf{I}^0 \\ &= \mathbf{\Delta}^{-1}(\lambda_0 + \lambda_1 + \lambda_2)\mathbf{D}(\lambda_1, \lambda_0 + \lambda_2)\mathbf{\Delta}^{-1}(\lambda_0 + \lambda_2)\mathbf{D}(\lambda_2, \lambda_0)\mathbf{\Delta}^{-1}(\lambda_0)\mathbf{B}(\lambda_0)\mathbf{I}^0, \quad (3.60) \end{aligned}$$

which means that $\mathbf{C}_2(\lambda_1, \lambda_2|\lambda_0)$ yields the backscattering enhancement and the diffracted backscattering enhancement, as is discussed later. To obtain the result (3.60), we have used relations (3.58), (3.44) and (3.45).

3.7 Backscattering and diffracted backscattering enhancement

As shown in the next section, there are enhanced peaks in angular distribution of the incoherent scattering in the backscattering direction and diffracted backscattering directions. These peaks are shown to come from the contribution σ_2 of (3.28) given by the sum of integrals of the second order kernel $C_2^{(n)}(\lambda_n - \lambda', \lambda'|\lambda_0)$,

$$\begin{aligned} &C_2^{(n)}(\lambda_n - \lambda', \lambda'|\lambda_0) \\ &= \rho_1^2 \sum_{r,m=-\infty}^{\infty} \Big\{ H_{n,-r}(\lambda_s|\lambda_0 + \lambda_n - \lambda')H_{-r,m}(\lambda_0 + \lambda_n - \lambda'|\lambda_0) \\ &\quad + H_{n,r}(\lambda_s|\lambda_0 + \lambda')H_{r,m}(\lambda_0 + \lambda'|\lambda_0)\Big\}\Big[\delta(m,0) + C_0^{(m)}(\lambda_0)\Big] \quad (3.61) \\ &= \rho_1^2 \mathbf{\Delta}_n^{-1}(\lambda_0 + \lambda_n)\Big[\mathbf{D}(\lambda', \lambda_0 + \lambda_n - \lambda')\mathbf{\Delta}^{-1}(\lambda_0 + \lambda_n - \lambda')\mathbf{D}(\lambda_n - \lambda', \lambda_0) \\ &\quad + \mathbf{D}(\lambda_n - \lambda', \lambda_0 + \lambda')\mathbf{\Delta}^{-1}(\lambda_0 + \lambda')\mathbf{D}(\lambda', \lambda_0)\Big]\, \mathbf{\Delta}^{-1}(\lambda_0)\mathbf{B}(\lambda_0)\mathbf{I}^0, \quad (3.62) \\ &\lambda_n = \lambda_s - \lambda_0 - \frac{2\pi n}{L}, \qquad \lambda_s = k\sin\phi, \end{aligned}$$

which involves two double-scattering processes. Here, $\mathbf{\Delta}_n^{-1}(\lambda_0 + \lambda_n)$ denotes the n-th row vector of matrix $\mathbf{\Delta}^{-1}(\lambda_0 + \lambda_n)$. As is shown in Fig.3.6, these double-scattering processes commonly start from $\lambda_0 + \frac{2\pi m}{L}$ to λ_s, where $\lambda_0 + \lambda_n - \lambda' - \frac{2\pi r}{L}$ and $\lambda_0 + \lambda' + \frac{2\pi r}{L}$ are two

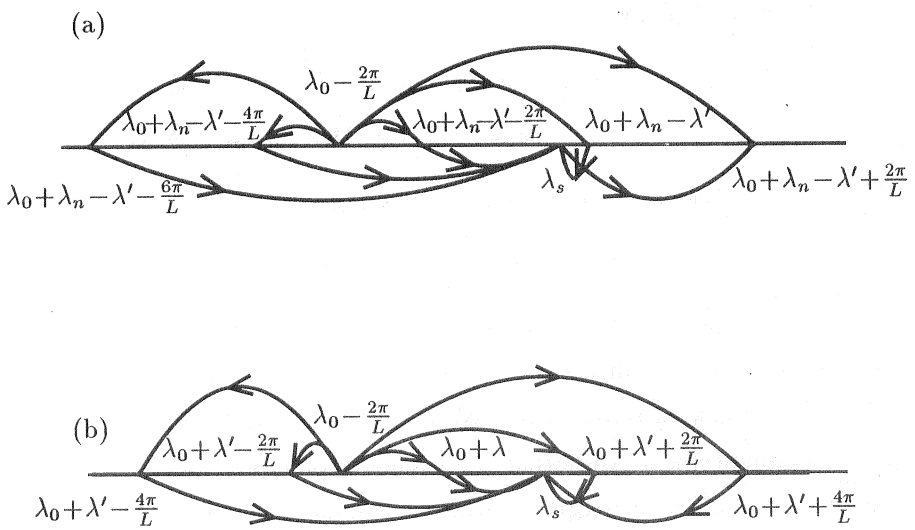

Figure 3.6: The double-scattering diffraction process described by $C_2^{(n)}(\lambda_n - \lambda', \lambda'|\lambda_0)$ for $n = -1$ and some $\lambda' \in \left[-\frac{\pi}{L}, \frac{\pi}{L}\right]$. (a) $\left\{\lambda_0 + \frac{2\pi n}{L} \to \lambda_0 + \lambda_n - \lambda' + \frac{2\pi r}{L} \to \lambda_s\right\}$, where $-4 < r < 2$, and (b) $\left\{\lambda_0 + \frac{2\pi n}{L} \to \lambda_0 + \lambda' + \frac{2\pi r}{L} \to \lambda_s\right\}$, where $-3 < r < 3$.

different intermediate states (n and r are any integers). These processes are weak in general. However, when the intermediate states enjoy the resonance condition at which $C_1^{(n)}(\lambda|\lambda_0)$ has peaks as shown in Fig.3.5 and incoherent Wood's anomalies take place, these double-scattering processes may become slightly strong and yield an enhancement in the incoherent scattering. The resonance conditions of the intermediate states are

$$\lambda_0 + \lambda' + \frac{2\pi r}{L} = \pm k \quad \text{or} \quad \lambda_0 + \lambda_n - \lambda' - \frac{2\pi r}{L} = \mp k, \qquad r, n = 0, \pm 1, \pm 2, \cdots. \tag{3.63}$$

On the other hand, when

$$2\lambda_0 + \lambda_n = \lambda_0 + \lambda_s - \frac{2\pi n}{L} = 0, \quad n = 0, \pm 1, \pm 2, \cdots, \tag{3.64}$$

holds, (3.60) implies the contributions from the two double-scattering processes become equal in amplitude and phase

$$C_2^{(n)}(\lambda_n - \lambda', \lambda'|\lambda_0) = 2\rho_1^2 \mathbf{\Delta}_n^{-1}(\lambda_0 + \lambda_n)\mathbf{D}(\lambda_n - \lambda', \lambda_0 + \lambda') \times \mathbf{\Delta}^{-1}(\lambda_0 + \lambda')\mathbf{D}(\lambda', \lambda_0)\mathbf{\Delta}^{-1}(\lambda_0)\mathbf{B}(\lambda_0)\mathbf{I}^0. \quad (3.65)$$

Hence, the scattering is enhanced in such a scattering angle ϕ

$$\sin\phi = -\sin\theta + \frac{2\pi n}{kL}, \quad n = 0, \pm 1, \pm 2, \cdots. \quad (3.66)$$

When $n = 0$, (3.66) gives the backscattering direction: $\phi = -\theta$. For $n \neq 0$, it determines the scattering angle of the diffracted backscattering, that is exactly same as the diffraction angle for the backscattered wave. We call the enhanced scattering the diffracted backscattering enhancement. Note that the phenomenon of enhanced backscattering has been found in many kinds of irregular surfaces including such periodic random surfaces, however, the phenomenon of diffracted backscattering enhancement is first found by the authors [39].

3.8 Numerical examples

For numerical calculations, we use the Gaussian local surface (2.63) and we approximate (3.37), (3.38) and (3.39) by 7×7 matrices and 7 dimensional vectors.

Let us first see Fig.3.7, which shows the variation of coherent power as a function of incident angle. Only the 0, $\pm$ 1st and -2nd order coherently diffracted waves may become propagating. For angles of incidence less than $\sin^{-1}\left(1 - \frac{2}{kL}\right) \approx 28.7°$, the -2nd order coherently diffracted wave is non-propagating; $\theta \approx 28.7°$ corresponds to a Rayleigh wavelength, at which resonance anomalies exist. Similarly, for angles of incidence greater than $\sin^{-1}\left(-1 + \frac{1}{kL}\right) \approx 15°$, the 1st order coherently diffracted wave is non-propagating; $\theta \approx 15°$, therefore, corresponds to a Rayleigh wavelength, at which resonance anomalies also exist. When the the -2nd and 1st order coherent power have a maximum, the 0 order coherent power possesses a minimum. Further, the total coherent power is unity. The physical interpretation is obvious: the incident energy is equal to the total diffracted energy. The power conservation holds for only coherently diffracted energy with the approximate solution $C_0^{(q)}(\lambda_0)$.

Figure 3.8 shows the scattering cross sections: $\sigma_1(\theta|\phi)$, $\sigma_2(\phi|\theta)$ and $\sigma(\phi|\theta) = \sigma_1(\phi|\theta) + \sigma_2(\phi|\theta)$, for the incident angle $\theta = 10°$, $k\rho_0 = k\rho_1 = 0.1\pi$, $kL = 2.7\pi$ and $k\kappa = 0.4\pi$.

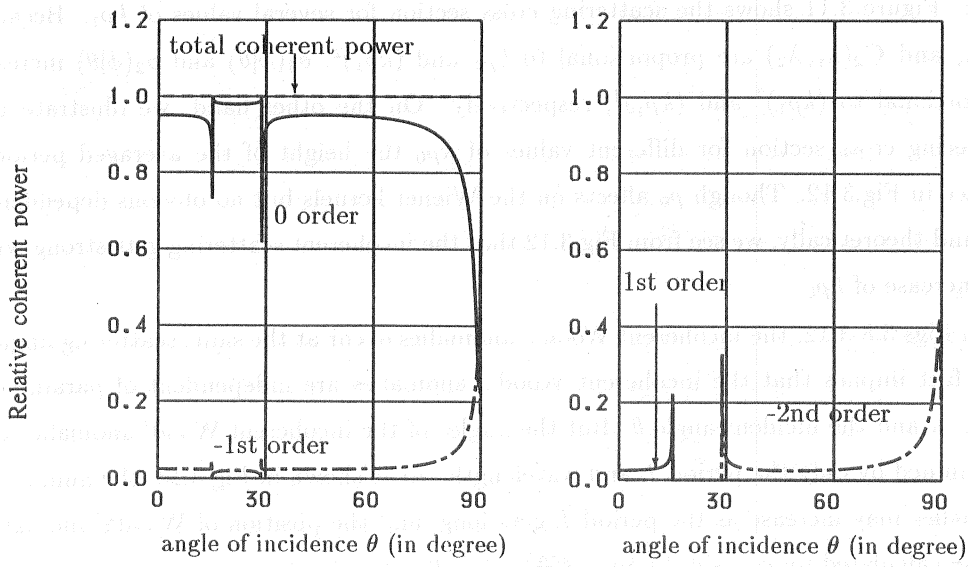

Figure 3.7: Relative coherent power against the angle of incidence with parameters $kL = 2.7\pi$, $k\rho_0 = k\rho_1 = 0.1\pi$ and $k\kappa = 0.4\pi$. Only the 0, $\pm$ 1st and -2nd order coherently diffracted waves may become propagating. For angles of incidence less than 28.7° and greater than 15°, the -2nd and 1st order coherently diffracted waves are non-propagating, respectively. There are anomalies exist at 28.7° and 15°, which correspond to the Rayleigh wavelength, respectively. When the -2nd and 1st order coherent power have a maximum, the 0 order coherent power becomes a minimum. We find that the optical theorem is satisfied by only coherent power.

In Figs.3.8(a), 3.8(b) and 3.8(c), we see four resonance peaks, which are the incoherent Wood's anomalies. In addition, there are not only enhanced backscattering but also enhanced diffracted backscattering peaks from the contribution σ_2 in $\sigma(\phi|\theta)$. These enhanced peaks are much weaker than the contribution $\sigma_1(\phi|\theta)$, so that enlarged figures are illustrated in Figs.3.8(d), 3.8(e) and 3.8(f). These angles of enhanced scattering are $\phi = -66.1°$, $-10°$ and 34.5°, which agree with theoretical values computed from (3.66). In order to compare with Fig.3.8, we display the case of incident angle $\theta = 45°$ in Fig.3.9, in which the enhanced scattering appears at scattering angles $-45°$, 1.9° and 50.7°.

The scattering cross section for different values of $k\kappa$ is illustrated in Fig.3.10. As $k\kappa$

increases, the scattering intensities increase but the effect of enhanced scattering becomes weak. Figure 3.11 shows the scattering cross section for several values of $k\rho_1$. Because $C_1(\lambda)$ and $C_2(\lambda_1, \lambda_2)$ are proportional to $k\rho_1$ and $(k\rho_1)^2$, $\sigma_1(\phi|\theta)$ and $\sigma_2(\phi|\theta)$ increase proportional to $(k\rho_1)^2$ and $(k\rho_1)^4$, respectively. On the other hand, we illustrate the scattering cross section for different values of $k\rho_0$ the height of the averaged periodic surface in Fig.3.12. Though ρ_0 affects on the Wiener kernels but no obvious dependence is found theoretically, we see from Fig.3.12 that the incoherent scattering gets strong with the increase of $k\rho_0$.

In Figs 3.8-3.12, the incoherent Wood's anomalies occur at the same scattering angles. This fact implies that the incoherent Wood's anomalies are independent of parameters ρ_0, ρ_1, κ and the incident angle θ. But the angles of the incoherent Wood' anomalies are determined by only the period L and wavelength. As is shown in Fig.3.13, the number of anomalies may increase as the period L gets long, and the position of Wood's anomalies can be calculated by $\phi = \sin^{-1}\left(\pm 1 - \frac{2\pi n}{kL}\right)$, $(n = 0, \pm 1, \pm 2, \cdots)$.

3.9 Conclusion

We have studied the scattering of a TM plane wave from periodic surfaces randomly deformed by a Gaussian sequence. By means of the stochastic functional approach, the scattered field is expressed in terms of a harmonic series representation, of which coefficients are homogeneous random functions and are written by Wiener expansions. Approximate Wiener kernels which satisfies reciprocal relations are obtained up to the second order in vector form. By physical combinations of scattering due to surface randomness and diffraction due to surface periodicity, it is then found that several phenomena appear in the angular distributions of the incoherent scattering. These phenomena are

(a) incoherent Wood's anomalies;

(b) enhanced backscattering;

(c) diffracted backscattering enhancement.

The incoherent Wood's anomalies and enhanced backscattering are also found theoretically in other paper [40]. Besides, Mendez and O'donnell have experimentally observed the backscattering enhancement from a periodic random silver surface, but no experimental report has been given for the incoherent Wood's anomaly. The phenomenon of diffracted backscattering enhancement is first found theoretically by the authors. However, no other

researchers have reported such a result in theory or experiment. Maybe, the existence of diffracted backscattering enhancement is weak; this means that it is difficult to obtain the phenomenon, if our conditions are not satisfied.

In this chapter, we have assumed that the averaged periodic surface has non-zero height. When the periodic random surface has a flat average surface, the solution by means of the method of this chapter is divergent. In such a case, we have to take the mass operator involving multiple-scattering effects into consideration. Though the mass operator can be calculated numerically, it will take a lot of computation time and hence it is left for future study.

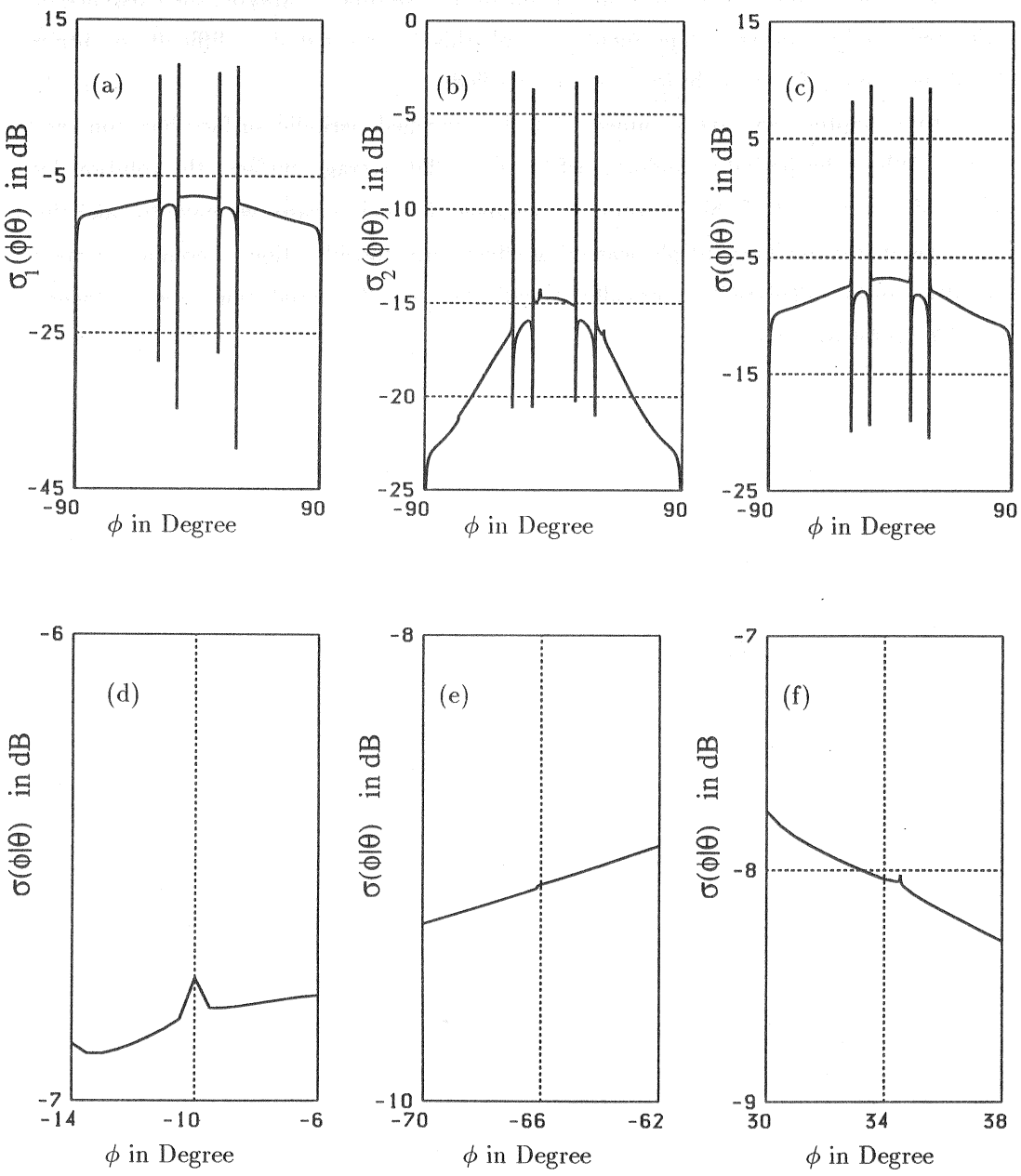

Figure 3.8: The scattering cross section for the incident angle $\theta = 10°$, $k\rho_0 = k\rho_1 = 0.1\pi$, $kL = 2.7\pi$ and $k\kappa = 0.4\pi$. The Wood's anomalies, enhanced backscattering and diffracted backscattering enhancement occur. (a) $\sigma_1(\phi|\theta)$, (b) $\sigma_2(\phi|\theta)$, (c) the scattering cross section $\sigma_1(\phi|\theta)+\sigma_2(\phi|\theta)$, (d) the backscattering peak at $\phi = -10°$, (e) the diffracted backscattering peak at $\phi = -66.1°$ and (f) the diffracted backscattering peak at $\phi = 34.5°$.

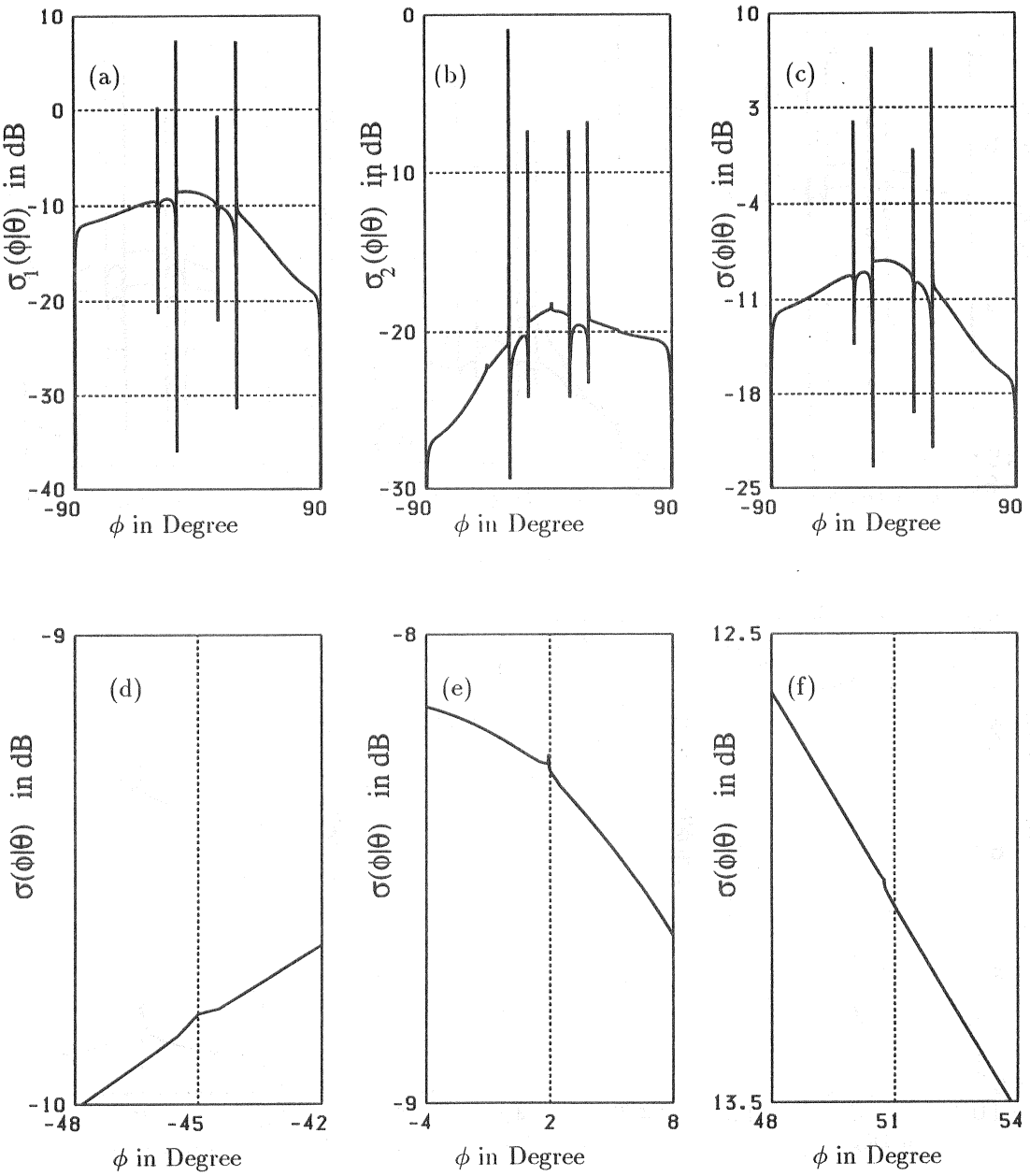

Figure 3.9: Same as Fig.3.8 for the incident angle $\theta = 45°$. (a) $\sigma_1(\phi|\theta)$, (b) $\sigma_2(\phi|\theta)$, (c) the total $\sigma_1(\phi|\theta) + \sigma_2(\phi|\theta)$, (d) the backscattering peak at $\phi = -45°$, (e) the diffracted backscattering peak at $\phi = 1.9°$ and (f) the diffracted backscattering peak at $\phi = 50.7°$.

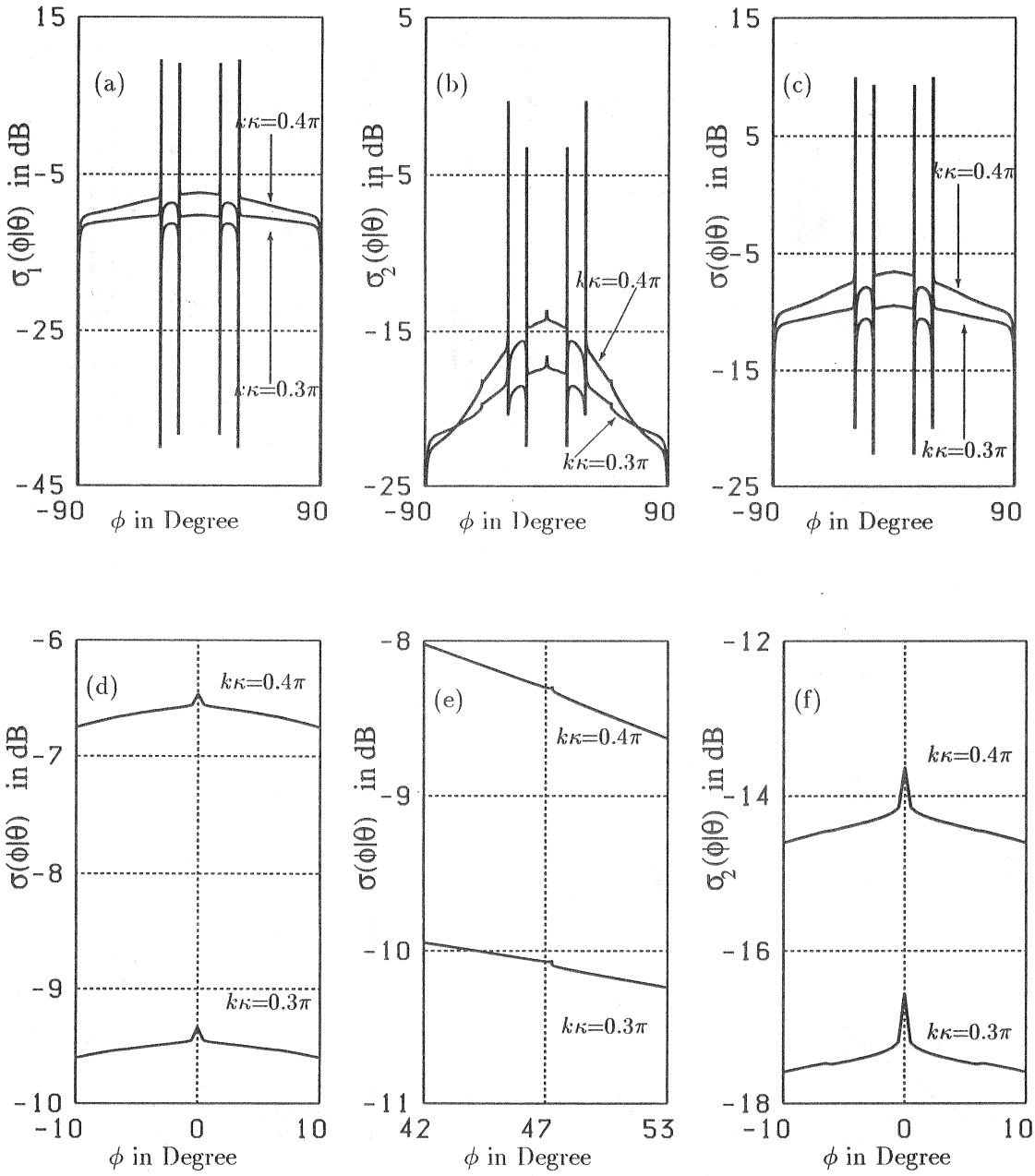

Figure 3.10: The scattering cross section with parameters $k\rho_0 = k\rho_1 = 0.1\pi$, $kL = 2.7\pi$ and $\theta = 0°$ for different values of $k\kappa$. As $k\kappa$ increases, the scattering intensities increase but the effect of enhanced scattering becomes weak. (a) $\sigma_1(\phi|\theta)$, (b) $\sigma_2(\phi|\theta)$, (c) the total $\sigma_1(\phi|\theta) + \sigma_2(\phi|\theta)$, (d) the backscattering peak at $\phi = 0°$ in the $\sigma(\phi|\theta)$, (e) the diffracted backscattering peak at $\phi = 47.8°$ and (f) the backscattering peak at $\phi = 0°$ in $\sigma_2(\phi|\theta)$.

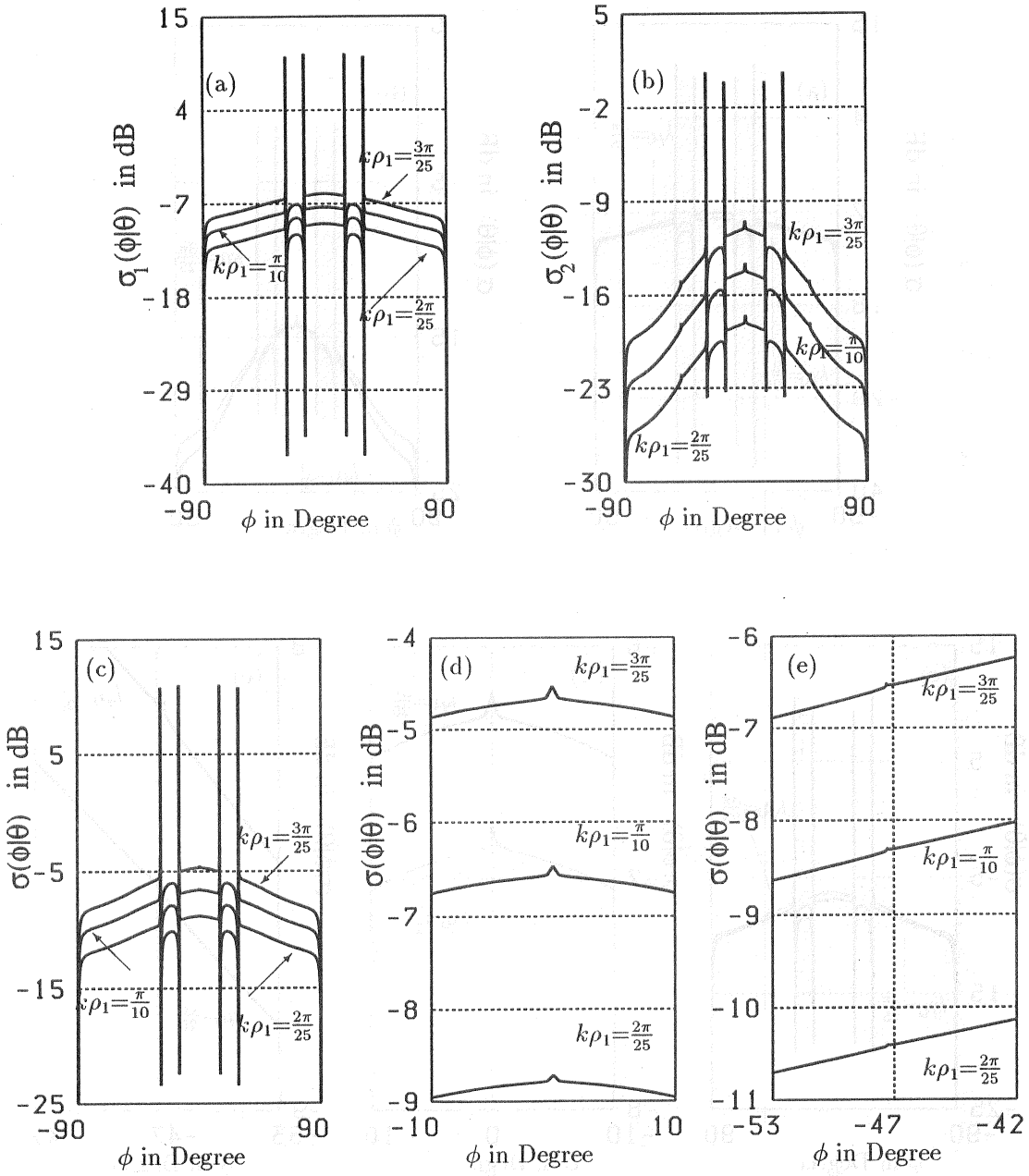

Figure 3.11: Comparisons of the scattering cross sections for several values of $k\rho_1$, where $k\rho_0 = 0.1\pi$, $k\kappa = 0.4\pi$, $kL = 2.7\pi$ and $\theta = 0°$. As $k\rho_1$ increases, both the scattering intensities and enhanced scattering peaks become strong. (a) $\sigma_1(\phi|\theta)$, (b) $\sigma_2(\phi|\theta)$, (c) the total $\sigma_1(\phi|\theta) + \sigma_2(\phi|\theta)$, (d) the backscattering peak at $\phi = 0°$ and (e) the diffracted backscattering peak at $\phi = -47.8°$.

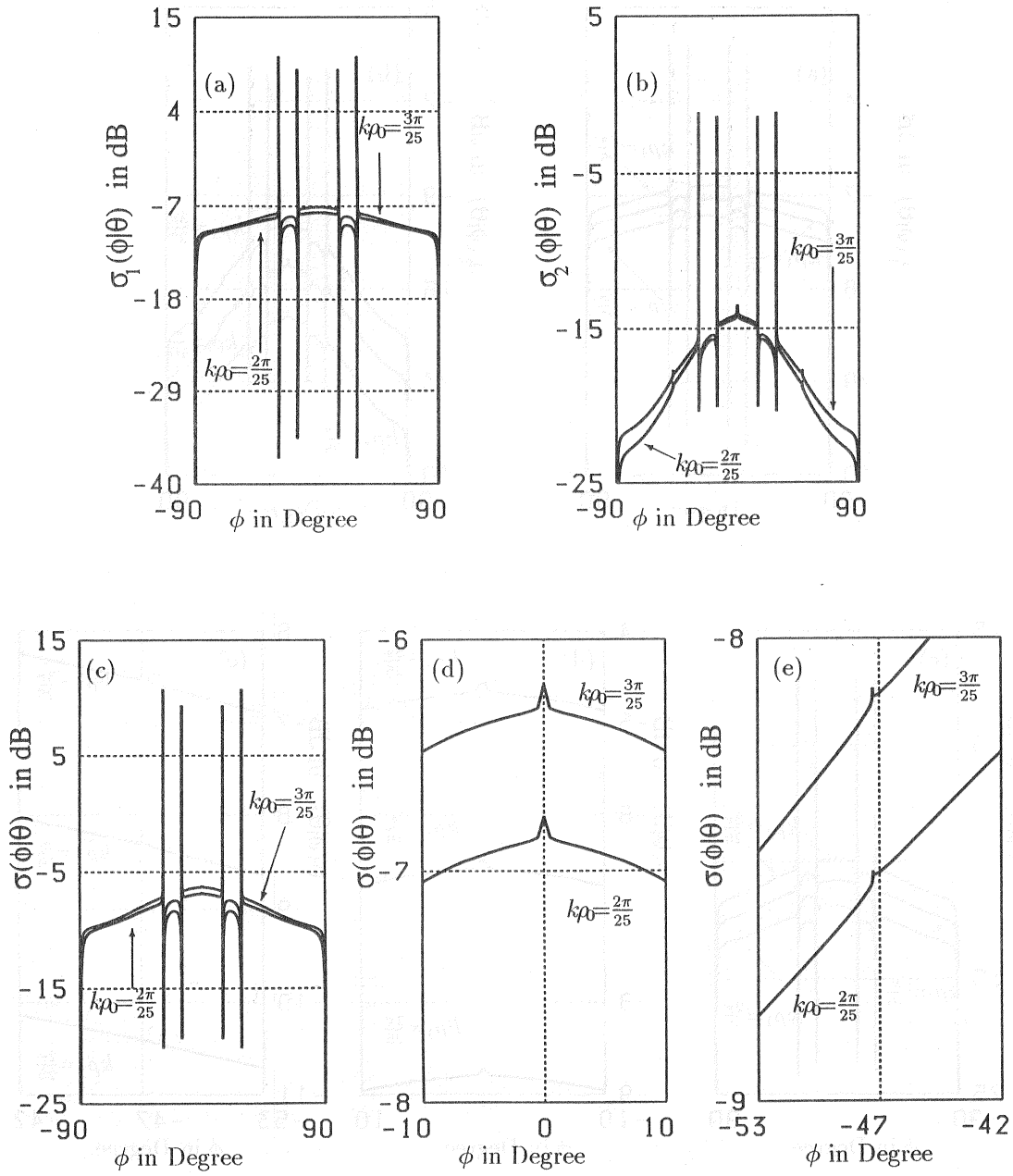

Figure 3.12: The scattering cross section for different values of $k\rho_0$. Here, parameters are $k\rho_1 = 0.1\pi$, $k\kappa = 0.4\pi$, $kL = 2.7\pi$ and $\theta = 0°$. As $k\rho_0$ becomes large, the scattering intensities increase. (a) $\sigma_1(\phi|\theta)$, (b) $\sigma_2(\phi|\theta)$, (c) the total $\sigma_1(\phi|\theta) + \sigma_2(\phi|\theta)$, (d) the backscattering peak at $\phi = 0°$ and (e) the diffracted backscattering peak at $\phi = -47.8°$.

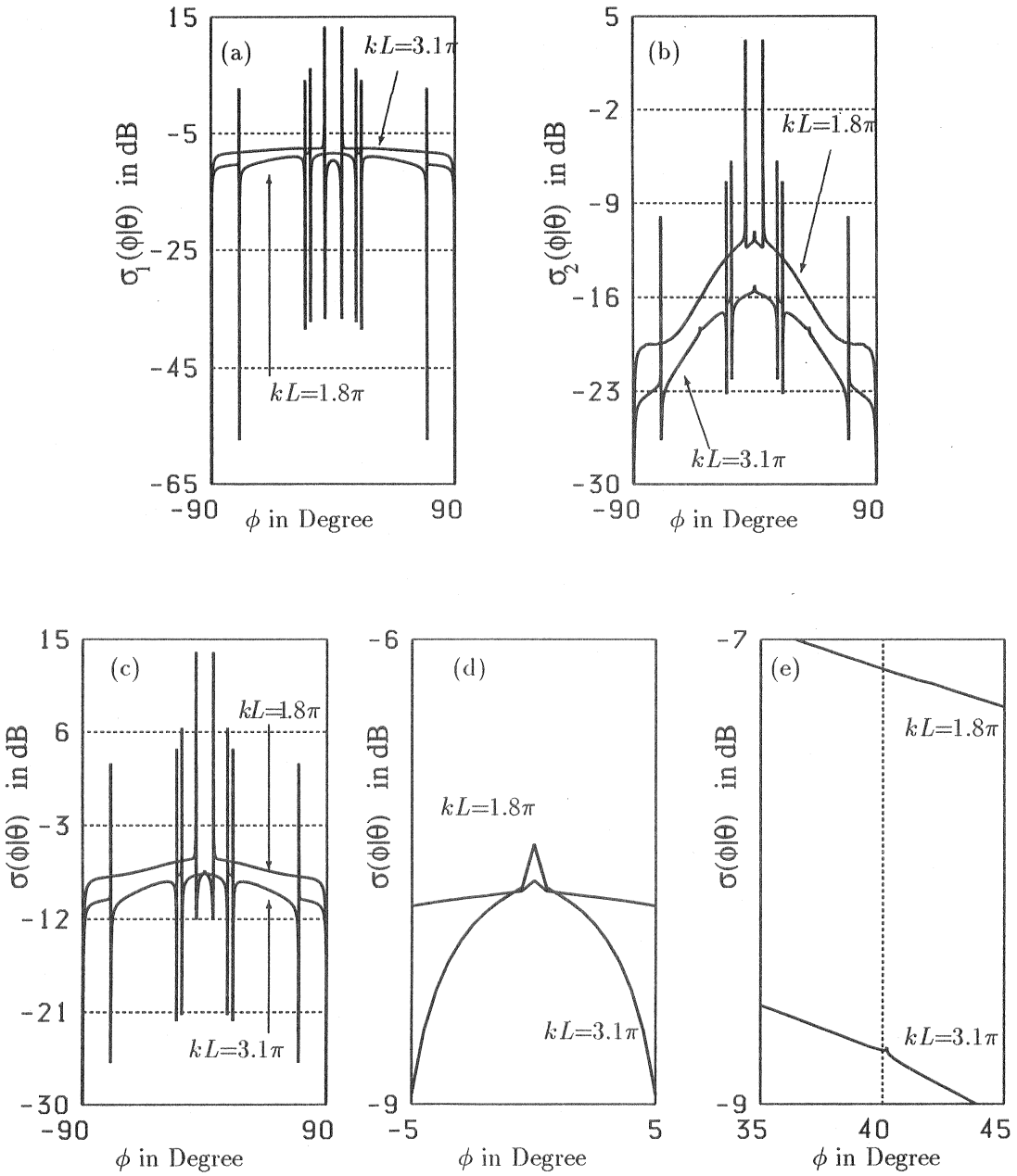

Figure 3.13: Comparisons of the scattering cross sections with parameters $k\rho_0 = k\rho_1 = 0.1\pi$, $k\kappa = 0.4\pi$ and $\theta = 0°$ for different period kL. The number and the positions of anomalies depend on only the period and wavelength. (a) $\sigma_1(\phi|\theta)$, (b) $\sigma_2(\phi|\theta)$, (c) the total $\sigma_1(\phi|\theta) + \sigma_2(\phi|\theta)$, (d) the backscattering peak at $\phi = 0°$ and (e) the diffracted backscattering peak at $\phi = 40.2°$.

Chapter 4

Orthogonal functionals of stochastic binary sequence

4.1 Introduction

Wiener's nonlinear theory is a stochastic functional theory which makes it possible to expand a nonlinear stochastic functional of a stationary Gaussian random process in a series of orthogonal stochastic functionals [82]-[84]. The theory has been applied to various problems in physics and engineering, such as the analysis and identification of nonlinear systems for noise input [60],[66],[82], theory of stochastic differential equation [85], the ergodic theory and the theory of turbulence [81]. However, Nakayama and Ogura et al have applied the theory to the wave propagation in random media and wave scattering from randomly rough surfaces [75],[86],[87], where the scattered wave field is regarded as a nonlinear stochastic functional of Gaussian random media or Gaussian rough surfaces. In chapters 2 and 3, we also used the theory to solve the problems of wave scattering from periodic surfaces randomly deformed by a Gaussian sequence.

Recentlyp, waves propagating in binary random media and scattering from binary rough surfaces have received much interest, because the Anderson localization in such media becomes a physical principle of new optical devices, and because digital data are stored by surface deformations called pits in recording devices such as compact disks. In principle, these binary random media and rough surfaces may be modeled by a stationary binary sequence, which takes two values with equal or unequal probability. Since the wave field in such a medium may be considered as a stochastic functional of a binary sequence, we need a systematic theory of a stochastic functional of binary sequence to represent the wave field.

In this chapter, we present some new formulas concerning orthogonal functionals of the stochastic binary sequence. In Sec.4.2, we prove an orthogonal relation concerning products of binary random variables. In Sec.4.3, we define the multivariate orthogonal polynomials, recurrence formula and generating function in explicit form. Using the orthogonal polynomials in Sec.4.4, we obtain the orthogonal expansion of a finitely di-

mensional function. We also prove that the multivariate orthogonal polynomials (finitely dimensional variables) are linear independent. In Sec.4.5, we show an orthogonal functional expansion of a stochastic functional of a binary sequence. A simple and significant example of the orthogonal functional expansion is discussed. In Sec.4.6, we represent a stationary sequence generated by the stationary binary sequence, where we prove the ergodicity. Next, however, we discuss a binary sequence taking ± 1 with unequal probability, because such unequal probability case is a realistic model of binary random media or binary random surfaces. We present several formulas on orthogonal functionals of such a binary sequence. These formulas obtained in this chapter can be applied to various random problems in physics and engineering. We will give an application in the next chapter.

4.2 Stationary binary sequence

To study a stationary binary sequence, we should consider two cases of equal probability and unequal probability. Let us start from the equal probability case. Assuming that $\{b_i, i = 0, \pm 1, \pm 2, \cdots\}$ is an independent stationary binary sequence taking ± 1 with equal probability

$$P(b_i = 1) = P(b_i = -1) = \frac{1}{2}, \tag{4.1}$$

one easily finds the average and correlation of b_i as

$$\langle b_i \rangle = 0, \quad \langle b_i b_j \rangle = \delta(i, j). \tag{4.2}$$

If $\{i_1, i_2, \cdots, i_m\}$ is a distinct set [1], $b_{i_1}, b_{i_2}, \cdots, b_{i_m}$ are mutually independent, so that one easily finds

$$\langle b_{i_1} b_{i_2} \cdots b_{i_m} \rangle = \langle b_{i_1} \rangle \langle b_{i_2} \rangle \cdots \langle b_{i_m} \rangle = 0. \tag{4.3}$$

When $\{i_1, i_2, \cdots, i_m\}$ and $\{j_1, j_2, \cdots, j_n\}$ are any two distinct sets, we get a relation:

$$\langle b_{i_1} b_{i_2} \cdots b_{i_m} \cdot b_{j_1} b_{j_2} \cdots b_{j_n} \rangle = \delta(m, n) \delta^{(m)}(i, j), \tag{4.4}$$

which is zero for $n \neq m$. Here, $\delta^{(m)}(i, j)$ indicates the sum of all distinct products of m delta functions of the form $\delta(i_s, j_t)$, $i = (i_1, i_2, \cdots, i_m)$, $j = (j_1, j_2, \cdots, j_m)$, all i_s and j_t

[1] By the word 'distinct set', we mean that i_1, i_2, $\cdots$, and i_m are distinct integers.

appearing just once in each product. Some concrete examples for $m = 2$ and $m = 3$ are

$$\delta^{(2)}(i,j) = \delta(i_1,j_1)\delta(i_2,j_2) + \delta(i_1,j_2)\delta(i_2,j_1), \tag{4.5}$$

$$\begin{aligned}\delta^{(3)}(i,j) = {} & \delta(i_1,j_1)\delta(i_2,j_2)\delta(i_3,j_3) + \delta(i_1,j_1)\delta(i_2,j_3)\delta(i_3,j_2) \\ & +\delta(i_1,j_2)\delta(i_2,j_1)\delta(i_3,j_3) + \delta(i_1,j_2)\delta(i_2,j_3)\delta(i_3,j_1) \\ & +\delta(i_1,j_3)\delta(i_2,j_1)\delta(i_3,j_2) + \delta(i_1,j_3)\delta(i_2,j_2)\delta(i_3,j_1).\end{aligned} \tag{4.6}$$

The $\delta^{(m)}(i,j)$ has been used for many years but no a concrete representation was given for a general case. Recently [69], however, we find an explicit expression as

$$\delta^{(m)}(i,j) = \sum_{l_1=1}^{m} \delta(i_1,j_{l_1}) \sum_{\substack{l_2=1 \\ l_2\neq l_1}}^{m} \delta(i_2,j_{l_2}) \times \cdots \times \sum_{\substack{l_m=1 \\ l_m\neq l_1,l_2,\cdots,l_{m-1}}}^{m} \delta(i_m,j_{l_m}), \tag{4.7}$$

which involves $m!$ terms. We prove the results (4.4) and (4.7) in terms of the moment generating function as follows.

Proof of the relation (4.4) and (4.7) : for a sufficiently large N, we define the moment generating function $M^{(2N+1)}(\Lambda_{2N+1})$ by

$$M^{(2N+1)}(\Lambda_{2N+1}) = \left\langle \exp\left\{ \sum_{k=-N}^{N} \lambda_k b_k \right\} \right\rangle = \prod_{k=-N}^{N} \cosh\lambda_k, \tag{4.8}$$

$$\Lambda_{2N+1} = (\lambda_{-N}, \lambda_{1-N}, \cdots, \lambda_0, \lambda_1, \cdots, \lambda_N), \tag{4.9}$$

where Λ_{2N+1} is a $2N+1$-dimensional vector. The moment generating function satisfies the relations:

$$M^{(2N+1)}(\Lambda_{2N+1})\Big|_{\Lambda_{2N+1}=0} = \left\langle \exp\left\{ \sum_{k=-N}^{N} \lambda_k b_k \right\}\Big|_{\Lambda_{2N+1}=0} \right\rangle = 1, \tag{4.10}$$

$$\langle b_{i_1} b_{i_2} \cdots b_{i_m} \rangle = \prod_{k=1}^{m} \frac{\partial}{\partial\lambda_{i_k}} M^{(2N+1)}(\Lambda_{2N+1})\Big|_{\Lambda_{2N+1}=0}, \tag{4.11}$$

$$\frac{\partial}{\partial\lambda_{i_k}} M^{(2N+1)}(\Lambda_{2N+1}) = \tanh\lambda_{i_k} M^{(2N+1)}(\Lambda_{2N+1}), \tag{4.12}$$

which holds for any values of $i_1, i_2, \cdots, i_m$. When $\{i_1, i_2, \cdots, i_m\}$ and $\{j_1, j_2, \cdots, j_n\}$ are two distinct sets, we obtain

$$\begin{aligned}\prod_{l=1}^{n} \frac{\partial}{\partial\lambda_{j_l}} M^{(2N+1)}(\Lambda_{2N+1}) &= \prod_{l=1}^{n} \tanh\lambda_{j_l} M^{(2N+1)}(\Lambda_{2N+1}), \\ \langle b_{i_1} b_{i_2} \cdots b_{i_m} \cdot b_{j_1} b_{j_2} \cdots b_{j_m} \rangle &= \prod_{k=1}^{m} \frac{\partial}{\partial\lambda_{i_k}} \prod_{l=1}^{n} \tanh\lambda_{j_l} M^{(2N+1)}(\Lambda_{2N+1})\Big|_{\Lambda_{2N+1}=0}.\end{aligned} \tag{4.13}$$

Therefore, without loss of generality, we assume $n \geq m$. Using the relation:

$$\frac{\partial}{\partial \lambda_{i_k}} \tanh \lambda_{j_l} = \tanh' \lambda_{i_k} \cdot \delta(i_k, j_l), \tag{4.14}$$

the prime denoting the differentiation, we first carry out the partial derivative with respect to λ_{i_1}, and then put $\lambda_{i_1} = 0$ to get

$$\begin{aligned} &\prod_{k=1}^{m} \frac{\partial}{\partial \lambda_{i_k}} \prod_{l=1}^{n} \tanh \lambda_{j_l} M^{(2N+1)}(\Lambda_{2N+1}) \Big|_{\Lambda_{2N+1}=0} \\ &= \prod_{k=2}^{m} \frac{\partial}{\partial \lambda_{i_k}} \sum_{l_1=1}^{n} \delta(i_1, j_{l_1}) \prod_{\substack{l=1 \\ l \neq l_1}}^{n} \tanh \lambda_{j_l} M^{(2N)}(\Lambda_{2N}) \Big|_{\Lambda_{2N}=0}, \end{aligned} \tag{4.15}$$

where $M^{(2N)}(\Lambda_{2N})$ is given by

$$M^{(2N)}(\Lambda_{2N}) = M^{(2N+1)}(\Lambda_{2N+1}) \Big|_{\lambda_{i_1}=0}, \tag{4.16}$$

and $\Lambda_{2N} = (\lambda_{-N}, \lambda_{1-N}, \cdots, \lambda_{i_1-1}, \lambda_{i_1+1}, \cdots, \lambda_N)$ is a $2N$-dimensional vector obtained from $2N+1$-dimensional vector Λ_{2N+1} by removing the λ_{i_1} component. To get (4.15), we have used such facts that i_1 is different from any one of $i_2, i_3, \cdot, i_m$, and

$$\tanh' \lambda_{i_1} \Big|_{\lambda_{i_1}=0} = 1, \quad \tanh \lambda_{i_1} \Big|_{\lambda_{i_1}=0} = 0. \tag{4.17}$$

Repeating this procedure, we obtain

$$\begin{aligned} &\prod_{k=1}^{m} \frac{\partial}{\partial \lambda_{i_k}} \prod_{l=1}^{n} \tanh \lambda_{j_l} M^{(2N+1)}(\Lambda_{2N+1}) \Big|_{\Lambda_{2N+1}=0} \\ &= \sum_{l_1=1}^{m} \delta(i_1, j_{l_1}) \sum_{\substack{l_2=1 \\ l_2 \neq l_1}}^{m} \delta(i_2, j_{l_2}) \cdots \sum_{\substack{l_m=1 \\ l_m \neq l_1, l_2, l_3, \cdots, l_{m-1}}}^{m} \delta(i_m, j_{l_m}) \\ &\quad \times \prod_{\substack{l=1 \\ l \neq l_1, l_2, \cdots, l_m}}^{n} \tanh \lambda_{j_l} M^{(2N+1-m)}(\Lambda_{2N+1-m}) \Big|_{\Lambda_{2N+1-m}=0}, \end{aligned} \tag{4.18}$$

where

$$M^{(2N+1-m)}(\Lambda_{2N+1-m}) = M^{(2N+1)}(\Lambda_{2N+1}) \Big|_{\lambda_{i_1}=\lambda_{i_2}=\cdots=\lambda_{i_m}=0}, \tag{4.19}$$

and Λ_{2N+1-m} is a $2N+1-m$-dimensional vector obtained from Λ_{2N+1} by removing $\lambda_{i_1}, \lambda_{i_2}, \cdots, \lambda_{i_m}$ components. As easily seen, (4.18) vanishes for $n > m$ because of the factor $\prod \tanh \lambda_{j_l}$ and relation (4.17). But the factor $\prod \tanh \lambda_{j_l}$ disappears when $n = m$. As a result, we finally obtain the relations (4.4) and (4.7).

4.3 Multivariate orthogonal polynomials

Let us define multivariate orthogonal polynomials associated with the binary sequence. However, it should be noted that, for example, $b_i b_j$ is a second order polynomial for $i \neq j$, but becomes a constant $b_i b_j = 1$ when $i = j$. Taking this fact in mind, first, we introduce a binary function $\Delta_m(i_1, i_2, \cdots, i_m)$ by

$$\Delta_m(i_1, i_2, \cdots, i_m) = \begin{cases} 1, & (i_1, i_2, \cdots, i_m \text{ are all distinct}) \\ 0, & (\text{ any other case }) \end{cases} \tag{4.20}$$

$$= \left[1 - \sum_{k=1}^{m-1} \delta(i_m, i_k)\right]\left[1 - \sum_{k=1}^{m-2} \delta(i_{m-1}, i_k)\right] \times \cdots \times \left[1 - \delta(i_3, i_2) - \delta(i_3, i_1)\right]\left[1 - \delta(i_2, i_1)\right], \tag{4.21}$$

which vanishes for any diagonal argument of $\{i_1, i_2, \cdots, i_m\}$ [2]. Then, we define the multivariate orthogonal polynomials $\{B_m(b_{i_1}, b_{i_2}, \cdots, b_{i_{m-1}}, b_{i_m}),\ m = 0, 1, 2, \cdots\}$ by

$$B_0 = 1, \tag{4.22}$$

$$B_1(b_i) = b_i, \tag{4.23}$$

$$B_2(b_i, b_j) = [1 - \delta(i, j)] b_i b_j, \tag{4.24}$$

$$B_3(b_i, b_j, b_k) = [1 - \delta(i, j) - \delta(i, k) - \delta(k, j) + 2\delta(i, k)\delta(i, j)] b_i b_j b_k, \tag{4.25}$$

$$\cdots \quad \cdots$$

$$B_m(b_{i_1}, b_{i_2}, \cdots, b_{i_m}) = \Delta_m(i_1, i_2, \cdots, i_m) b_{i_1} b_{i_2} \cdots b_{i_m} \quad (m \geq 1)$$

$$= \begin{cases} b_{i_1} b_{i_2} \cdots b_{i_m}, & (i_1, i_2, \cdots, i_m \text{ are all distinct}) \\ 0, & (\text{ any other case }) \end{cases} \tag{4.26}$$

which are symmetrical with respect to their variables. From (4.3), (4.4) and the definition (4.26), we easily find averages and orthogonality relation of the multivariate polynomials,

$$\langle B_m(b_{i_1}, b_{i_2}, \cdots, b_{i_{m-1}}, b_{i_m}) \rangle = \delta(m, 0), \tag{4.27}$$

$$\langle B_m(b_{i_1}, b_{i_2}, \cdots, b_{i_m}) B_n(b_{j_1}, b_{j_2}, \cdots, b_{j_n}) \rangle = \Delta_m(i_1, i_2, \cdots, i_m) \Delta_n(j_1, j_2, \cdots, j_n) \delta(m, n) \delta^{(m)}(i, j), \tag{4.28}$$

which holds for any non-negative integers m and n. Manipulating (4.26) and (4.21), we find the recurrence formula,

$$B_m(b_{i_1}, b_{i_2}, \cdots, b_{i_m}) = B_{m-1}(b_{i_1}, b_{i_2}, \cdots, b_{i_{m-1}}) B_1(b_{i_m})$$

[2] By the word of a diagonal argument of $\{i_1, i_2, \cdots, i_m\}$, we mean that there exists a number n $(n \leq m)$ such that $j_1 = j_2 = \cdots = j_n$, $j_k \in \{i_1, i_2, \cdots, i_m\}$, $(k = 1, 2, \cdots, n)$. For example, we call a case, where two variables out of $\{i_1, i_2, \cdots, i_m\}$ are equal, a diagonal argument of $\{i_1, i_2, \cdots, i_m\}$.

$$- \sum_{l=1}^{m-1} B_{m-2}(b_{i_1}, b_{i_2}, \cdots, b_{i_{l-1}}, b_{i_{l+1}}, \cdots, b_{i_{m-1}})\delta(i_m, i_l)$$
$$+ \sum_{l=1}^{m-1} \sum_{\substack{k=1 \\ k\neq l}}^{m-1} B_{m-2}(b_{i_1}, b_{i_2}, \cdots, b_{i_{l-1}}, b_{i_{l+1}}, \cdots, b_{i_{m-1}})\delta(i_m, i_l)\delta(i_k, i_l). \quad (4.29)$$

Here, we note that $k \neq l$ does not imply $i_k \neq i_l$ in the third term. Putting $m = 2$, we get a comprehensive example

$$B_1(b_i)B_1(b_j) = B_2(b_i, b_j) + \delta(i, j), \quad (4.30)$$

which is a second order polynomial for $i \neq j$, but becomes a zero order polynomial (constant) when $i = j$. On the other hand, the multivariate orthogonal polynomials may be obtained from the generating function Q,

$$Q = \prod_{k=-\infty}^{\infty} [1 + b_k t_k], \quad (4.31)$$

$$B_m(b_{i_1}, b_{i_2}, \cdots, b_{i_m}) = \frac{\partial}{\partial t_{i_1}} \frac{\partial}{\partial t_{i_2}} \cdots \frac{\partial}{\partial t_{i_m}} Q \Big|_{t_0 = t_{\pm 1} = t_{\pm 2} = \cdots = 0}. \quad (4.32)$$

We will explain how to obtain the generating function Q in subsection 4.5.2. Since $\partial t_k / \partial t_l = \delta(k, l)$, one easily gets (4.26) from (4.32). For example, we get

$$\begin{aligned} \frac{\partial Q}{\partial t_l} &= \sum_{m=-\infty}^{\infty} b_m \frac{\partial t_m}{\partial t_l} \prod_{k\neq m} [1 + b_k t_k] \\ &= \sum_{m=-\infty}^{\infty} b_m \delta(l, m) \prod_{k\neq m} [1 + b_k t_k], \end{aligned} \quad (4.33)$$

which yields $B_1(b_l)$ if we put $t_0 = t_{\pm 1} = t_{\pm 2} = \cdots = 0$. We note that explicit formulas (4.7)-(4.29) are first obtained in our paper [69].

4.4 Orthogonal expansion of functions

First, we consider a function $g(b_i)$ of single variable b_i. Since $b_i = \pm 1$, the function $g(b_i)$ takes only two values $g(1)$ and $g(-1)$, and can be expanded as

$$g(b_i) = g_0 + g_1 B_1(b_i) = [1, \ B_1(b_i)] \cdot [g_0, \ g_1]^t. \quad (4.34)$$

The two coefficients g_0 and g_1 can be determined by two methods: probabilistic method and non-probabilistic method. In the non-probabilistic method, we put $b_i = \pm 1$ in (4.34) to get

$$H_1 \cdot \begin{bmatrix} g_0 \\ g_1 \end{bmatrix} = \begin{bmatrix} g(1) \\ g(-1) \end{bmatrix}, \quad (4.35)$$

where H_1 is a 2×2 matrix with non-zero determinant:

$$H_1 = \begin{bmatrix} 1 & B_1(1) \\ 1 & B_1(-1) \end{bmatrix} = \begin{bmatrix} 1 & 1 \\ 1 & -1 \end{bmatrix}, \quad |H_1| = -2 \neq 0, \tag{4.36}$$

where $|\cdot|$ denotes determinant and H_1 is the 2×2 Hadamard matrix. Since $|H_1| \neq 0$, the two coefficients of (4.35) are determined uniquely. In the probabilistic method, we multiply a vector $[1, \ B_1(b_i)]^t$ from the left of (4.34) to obtain

$$\begin{bmatrix} 1 \\ B_1(b_i) \end{bmatrix} \cdot [1, \ B_1(b_i)] \cdot \begin{bmatrix} g_0 \\ g_1 \end{bmatrix} = \begin{bmatrix} g(b_i) \\ g(b_i)B_1(b_i) \end{bmatrix}. \tag{4.37}$$

Taking ensemble average, we get

$$\left\langle \begin{bmatrix} 1 \\ B_1(b_i) \end{bmatrix} \cdot [1, \ B_1(b_i)] \right\rangle = \begin{bmatrix} \langle 1 \rangle & \langle B_1(b_i) \rangle \\ \langle B_1(b_i) \rangle & \langle B_1^2(b_i) \rangle \end{bmatrix} = \begin{bmatrix} 1 & 0 \\ 0 & 1 \end{bmatrix}, \tag{4.38}$$

which becomes diagonal because of the orthogonality relation (4.28). Thus, we get

$$g_0 = \langle g(b_i) \rangle, \quad g_1 = \langle g(b_i) \cdot B_1(b_i) \rangle. \tag{4.39}$$

Next, we consider a function $g(b_i, b_j)$ of two variables. Here, we will employ a relation

$$B_1(b_i)B_1(b_j) = B_2(b_i, b_j), \quad i \neq j, \tag{4.40}$$

and the Kronecker product $\otimes$:

$$\begin{aligned} & [1, \ B_1(b_i)] \otimes [1, \ B_1(b_j)] \\ = \ & [1, \ B_1(b_i), \ B_1(b_j), \ B_1(b_j)B_1(b_i)] \\ = \ & [1, \ B_1(b_i), \ B_1(b_j), \ B_2(b_i, b_j)], \end{aligned} \tag{4.41}$$

where $i \neq j$. The function $g(b_i, b_j)$ may be expanded in terms of the multivariate polynomials as

$$g(b_i, b_j) = g_0 + g_1(i)B_1(b_i) + g_1(j)B_1(b_j) + 2g_2(i,j)B_2(b_j, b_i) \tag{4.42}$$

$$= [1, \ B_1(b_i), \ B_1(b_j), \ B_2(b_i, b_j)] \cdot [g_0, \ g_1(i), \ g_1(j), \ 2g_2(i,j)]^t, \tag{4.43}$$

where symmetry $g_2(i,j) = g_2(j,i)$ is assumed. Putting $b_i = \pm 1$ and $b_j = \pm 1$, we obtain four linear equations:

$$H_2 \cdot \begin{bmatrix} g_0 \\ g_1(i) \\ g_1(j) \\ 2g_2(i,j) \end{bmatrix} = \begin{bmatrix} g(1,1) \\ g(-1,1) \\ g(1,-1) \\ g(-1,-1) \end{bmatrix}, \tag{4.44}$$

where H_2 is a 4×4 matrix

$$\begin{aligned} H_2 &= \begin{bmatrix} 1 & B_1(1) & B_1(1) & B_1^2(1) \\ 1 & B_1(-1) & B_1(1) & B_1(1)B_1(-1) \\ 1 & B_1(1) & B_1(-1) & B_1(-1)B_1(1) \\ 1 & B_1(-1) & B_1(-1) & B_1^2(-1) \end{bmatrix} \\ &= \begin{bmatrix} H_1 & H_1 \\ H_1 & -H_1 \end{bmatrix} \\ &= H_1 \otimes H_1, \end{aligned} \tag{4.45}$$

$$|H_2| = (-2)^2 |H_1|^2 = 16, \tag{4.46}$$

where H_2 is the 4×4 Hadamard matrix. Because $|H_2| \neq 0$, the coefficients g_0, $g_1(i)$, $g_1(j)$ and $g_2(i,j)$ can be uniquely determined. In the probabilistic method, we multiply vector $[1,\ B_1(b_i),\ B_1(b_j),\ B_2(b_i,b_j)]^t$ from the left of (4.43) and take average. Then, we obtain

$$\begin{aligned} &\left\langle \begin{bmatrix} 1 \\ B_1(b_i) \\ B_1(b_j) \\ B_2(b_i,b_j) \end{bmatrix} \cdot [1,\ B_1(b_i),\ B_1(b_j),\ B_2(b_i,b_j)] \right\rangle \begin{bmatrix} g_0 \\ g_1(i) \\ g_1(j) \\ 2g_2(i,j) \end{bmatrix} \\ &\qquad = \left\langle \begin{bmatrix} g(b_i,b_j) \\ g(b_i,b_j)B_1(b_i) \\ g(b_i,b_j)B_1(b_j) \\ g(b_i,b_j)B_2(b_i,b_j) \end{bmatrix} \right\rangle. \end{aligned} \tag{4.47}$$

Because of the orthogonality relation, the 4×4 matrix $\langle [1,\ B_1(b_i),\ B_1(b_j),\ B_2(b_i,b_j)]^t \cdot [1,\ B_1(b_i),\ B_1(b_j),\ B_2(b_i,b_j)] \rangle$ becomes diagonal. Therefore, the coefficients can be given by averages

$$\begin{aligned} g_0 &= \langle g(i,j) \rangle, & g_2(i,j) &= \frac{\langle g(i,j) \cdot B_2(b_i,b_j) \rangle}{2}, \\ g_1(j) &= \langle g(i,j) \cdot B_1(b_j) \rangle, & g_1(i) &= \langle g(i,j) \cdot B_1(b_i) \rangle. \end{aligned} \tag{4.48}$$

To obtain (4.48), we have used the fact:

$$\langle B_n^2(b_{i_1}, b_{i_2}, \cdots, b_{i_n}) \rangle = 1, \tag{4.49}$$

$$n = 0, 1, 2, \cdots, \quad \{i_1, i_2, \cdots, i_n\} \text{ is any distinct set.} \tag{4.50}$$

Further, we consider a n-variable function $g(b_1, b_2, \cdots, b_n)$. Such a function may be represented in terms of the multivariate polynomials as

$$g(b_1, b_2, \cdots, b_n) = g_0 + \sum_{j=1}^{n} g_1(j) B_1(b_j) + \sum_{k,m=1}^{n} g_2(k,m) B_2(b_k, b_m)$$

$$+\cdots+\sum_{i_1,i_2,\cdots,i_n=1}^{n} g_n(i_1,i_2,\cdots,i_n)B_n(b_{i_1},b_{i_2},\cdots,b_{i_n}) \tag{4.51}$$

$$\begin{aligned}
&= g_0 + 1!\sum_{j=1}^{n} g_1(j)b_j + 2!\sum_{\substack{k,m=1\\k<m}}^{n} g_2(k,m)b_k b_m \\
&\quad +\cdots+ n!\sum_{\substack{i_1,i_2,\cdots,i_n=1\\i_1<i_2<\cdots<i_n}}^{n} g_n(i_1,i_2,\cdots,i_n)b_{i_1}b_{i_2}\cdots b_{i_n} \\
&= \Big[1,\ B_1(b_1),\ B_1(b_2),\ B_2(b_1,b_2),\cdots,B_1(b_n),\ B_2(b_1,b_n) \\
&\qquad \cdots,B_2(b_{n-1},b_n),\cdots,B_n(b_1,b_2,\cdots,b_n)\Big] \\
&\quad \cdot\Big[g_0,\ g_1(1),\ g_1(2),\ 2g_2(1,2),\ \cdots,\ g_1(n),\ 2g_2(1,n), \\
&\qquad \cdots,\ 2g_2(n-1,n),\ \cdots,\ n!g_n(1,2,\cdots,n)\Big]^t,
\end{aligned} \tag{4.52}$$

where we have used

$$\begin{aligned}
&[1,\ B_1(b_1)]\otimes[1,\ B_1(b_2)]\otimes\cdots\otimes[1,\ B_1(b_n)] \\
&= [1,\ B_1(b_1),\ B_1(b_2),\ B_2(b_1,b_2),\ \cdots,\ B_1(b_n),\ B_2(b_1,b_n), \\
&\qquad \cdots,\ B_2(b_{n-1},b_n),\ \cdots,\ B_n(b_1,b_2,\cdots,b_n)],
\end{aligned} \tag{4.53}$$

$$B_1(b_1)B_1(b_2)\cdots B_1(b_n) = B_k(b_1,b_2,\cdots,b_n). \tag{4.54}$$

Here, $g_k(i_1,i_2,\cdots,i_k)$ is also assumed to be symmetrical. Note that $g(b_1,b_2,\cdots,b_n)$ takes 2^n values and the number of the coefficients g_0, $g_1(1)$, $g_1(2)$, $g_2(1,2)$, $\cdots$, $g_1(n)$, $g_2(1,n)$, $\cdots$, $g_2(n-1,n)$, $\cdots$, $g_n(1,2,\cdots,n)$ is 2^n. Putting $b_k=\pm1$, we obtain a matrix equation to determine the 2^n coefficients from $g(b_{i_1},b_{i_2},\cdots,b_{i_n})$,

$$H_n\cdot\begin{bmatrix} g_0 \\ g_1(1) \\ g_1(2) \\ 2g_2(1,2) \\ \vdots \\ g_1(n) \\ 2g_2(1,n) \\ \vdots \\ 2g_2(n-1,n) \\ \vdots \\ n!g_n(1,2,\cdots,n) \end{bmatrix} = \begin{bmatrix} g(1,1,\cdots,1) \\ g(-1,1,\cdots,1) \\ g(1,-1,\cdots,1) \\ g(-1,-1,1,\cdots,1) \\ \vdots \\ g(1,1,\cdots,1,-1) \\ g(-1,1,\cdots,1,-1) \\ \vdots \\ g(1,1,\cdots,1,-1,-1) \\ \vdots \\ g(-1,-1,\cdots,-1) \end{bmatrix}. \tag{4.55}$$

Here, H_n is the $2^n\times 2^n$ matrix, which is made up from the arrange (4.53) of multivariate

polynomials. After some manipulations, we find a recurrence formula:

$$H_n = \begin{bmatrix} H_{n-1} & H_{n-1} \\ H_{n-1} & -H_{n-1} \end{bmatrix}, \quad n \geq 1, \tag{4.56}$$

$$|H_n| = (-2)^{2^{n-1}} |H_{n-1}|^2 \neq 0. \tag{4.57}$$

In fact, H_n is Hadamard matrix. Thus, the coefficients of (4.52) are uniquely determined from $g(b_{i_1}, b_{i_2}, \cdots, b_{i_n})$ when b_k's take ± 1 independently. On the other hand, those coefficients of (4.52) are also obtained from the orthogonality relation of the multivariate polynomials (4.28) as

$$\begin{aligned} g_0 &= \langle g^{(n)}(b_1, b_2, \cdots, b_n) \rangle, \\ g_k(i_1, i_2, \cdots, i_k) &= \frac{\left\langle g^{(n)}(b_1, b_2, \cdots, b_n) B_k(b_{i_1}, b_{i_2}, \cdots, b_{i_k}) \right\rangle}{k!}, \end{aligned} \tag{4.58}$$

where $\{i_1, i_2, \cdots, i_k\}$ is a distinct set and $k \geq 1$.

We have considered an orthogonal expansion of a function of binary variables. In the next section, we will consider the case where the number of variables becomes infinite.

4.5 Orthogonal functional expansion

We assume a sample point ω is an infinitely dimensional vector determined by an infinite binary sequence

$$\omega = (\cdots, b_{-2}, b_{-1}, b_0, b_1, \cdots) \quad \omega_i = b_i, \tag{4.59}$$

where ω_i is the i-th component of ω. Thus, an infinitely dimensional sample space Ω is composed of all these sample points. For any given components $b_{i_1}, b_{i_2}, \cdots, b_{i_n}$, we define a subset $\Omega(b_{i_1}, b_{i_2}, \cdots, b_{i_n})$ of Ω as

$$\begin{aligned} \Omega(b_{i_1}\, b_{i_2} \cdots b_{i_n}) &= \{\omega \in \Omega;\ \omega_{i_j} = b_{i_j},\ j = 1, 2, \cdots, n\} \\ &= \{\omega \in \Omega;\ \omega = (\cdots, b_{i_1}, \cdots, b_{i_2}, \cdots, b_{i_n}, \cdots)\}, \end{aligned} \tag{4.60}$$

which is an infinite set determined by finite components. In other words, $\Omega(b_{i_1}\, b_{i_2} \cdots b_{i_n})$ is a cylindrical set determined by only components $b_{i_1}\, b_{i_2} \cdots b_{i_n}$. It is clear that there exist 2^n subsets which are disjoint each other when the n components take ± 1 independently. Thus, the sample space Ω is made up of such 2^n subsets,

$$\Omega = \bigcup_{b_{i_1}, b_{i_2}, \cdots, b_{i_n} = \pm 1} \Omega(b_{i_1}, b_{i_2}, \cdots, b_{i_n}) \tag{4.61}$$

$$= \sum_{b_{i_1}, b_{i_2}, \cdots, b_{i_n} = \pm 1} \Omega(b_{i_1}, b_{i_2}, \cdots, b_{i_n}), \tag{4.62}$$

where the notation $\sum$ indicates these subsets are mutually disjoint. Let us explain the structure (4.62) by simple examples. For $n = 1$, Ω is consists of two subsets $\Omega(1)$ and $\Omega(-1)$ which are given by

$$\begin{aligned} \Omega(1) &= \{\omega \in \Omega; \quad \omega = (\cdots, b_i = 1, \cdots)\}, \\ \Omega(1) &= \{\omega \in \Omega; \quad \omega = (\cdots, b_i = -1, \cdots)\}. \end{aligned}$$

For $n = 2$, Ω is consists of four subsets given by

$$\begin{aligned} \Omega(1,1) &= \{\omega \in \Omega; \ \omega = (\cdots, b_i = 1, \cdots, b_j = 1, \cdots)\}, \\ \Omega(1,-1) &= \{\omega \in \Omega; \ \omega = (\cdots, b_i = 1, \cdots, b_j = -1, \cdots)\}, \\ \Omega(-1,1) &= \{\omega \in \Omega; \ \omega = (\cdots, b_i = -1, \cdots, b_j = 1 \cdots)\}, \\ \Omega(-1,-1) &= \{\omega \in \Omega; \ \omega = (\cdots, b_i = -1, \cdots, b_j = -1, \cdots)\}. \end{aligned}$$

Now, we have a Borel field or a finitely additive class given by (4.60). Since $\Omega(b_{i_1}, b_{i_2}, \cdots, b_{i_n})$ has the same probability as $\{b_{i_1}, b_{i_2}, \cdots, b_{i_n}\}$,

$$P[\Omega(b_{i_1}, b_{i_2}, \cdots, b_{i_n})] = P[b_{i_1}, b_{i_2}, \cdots, b_{i_n}], \tag{4.63}$$

where P indicates the probability, the sample space Ω turns out to be a measurable probabilistic space. For any function $f(\omega)$ on Ω, we may assume

$$\begin{aligned} \langle f(\omega) \rangle &= \int_\Omega f(\omega) P(d\omega) \\ &= \lim_{M,N \to \infty} \sum_{b_{-M}, \cdots, b_0, b_1, \cdots, b_N} f(\cdots, b_{-M}, \cdots, b_0, \cdots, b_N, \cdots) \\ &\quad \times P[\Omega(b_{-M}, \cdots, b_0, \cdots, b_N)]. \end{aligned} \tag{4.64}$$

In another words, the function on Ω is first considered as a step function which takes a constant value on subset $\Omega(b_{-M}, \cdots, b_0, \cdots, b_N)$, where the step function becomes a function of only $\{b_{-M}, \cdots, b_0, \cdots, b_N\}$ but is independent of other components. When the numbers M and N get large, the function on the sample space Ω becomes a functional of the stationary binary sequence $\{b_i, i = 0, \pm 1, \pm 2, \cdots\}$.

Further, we define $L^2(\Omega, P)$ as the set of Lebesgue measurable functionals on Ω. If a measurable functional $g(\omega) \in L^2(\Omega, P)$ with a finite variance

$$\langle |g(\omega)|^2 \rangle < \infty, \tag{4.65}$$

we may have an orthogonal functional expansion,

$$g(\omega) = g_0 + \sum_{k=-\infty}^{\infty} g_1(k)B_1(b_k) + \sum_{k,l=-\infty}^{\infty} g_2(k,l)B_2(b_k,b_l) + \cdots \tag{4.66}$$

$$= g_0 + 1! \sum_{k=-\infty}^{\infty} g_1(k)b_k + 2! \sum_{\substack{k,l=-\infty \\ k<l}}^{\infty} g_2(k,l)b_k b_l + \cdots \tag{4.67}$$

$$= \hat{g}_0 + \sum_{k=-\infty}^{\infty} \hat{g}_1(k)B_1(b_k) + \sum_{k,l=-\infty}^{\infty} \hat{g}_2(k,l)B_2(b_k,b_l) + \cdots, \tag{4.68}$$

which hold in ensemble mean square sense and may be proved in the end of this section. Here, g_0, $g_1(k)$, $g_2(k,l)$, $g_3(k,l,m)$, $\cdots$ and $\hat{g}_0$, $\hat{g}_1(k)$, $\hat{g}_2(k,l)$, $\hat{g}_3(k,l,m)$, $\cdots$ are deterministic kernel functions which are assumed to be symmetrical with respect to their arguments. Note that the right-hand side of (4.68) is written by zero-diagonal components of the kernel functions given by

$$\hat{g}_0 = g_0, \qquad \hat{g}_1(k) = g_1(k), \tag{4.69}$$
$$\hat{g}_m(i_1,i_2,\cdots,i_m) = \Delta_m(i_1,i_2,\cdots,i_m)g_m(i_1,i_2,\cdots,i_m),$$

which vanishes for m-dimensional diagonal arguments.

By the orthogonality relation (4.28), any two terms in (4.68) are orthogonal in ensemble mean sense. Then, kernel functions are determined by the cross correlation. From (4.28) and (4.68), we obtain an example,

$$\langle g(\omega)B_2(b_i,b_j)\rangle = \Delta_2(i,j)[\hat{g}_2(i,j) + \hat{g}_2(j,i)] \tag{4.70}$$

$$= 2!\hat{g}_2(i,j), \tag{4.71}$$

where we have used (4.21) and (4.69). Similarly, we obtain

$$\hat{g}_m(i_1,i_2,\cdots,i_m) = \frac{1}{m!}\langle g(\omega)B_m(b_{i_1}b_{i_2}\cdots b_{i_m})\rangle. \tag{4.72}$$

Since (4.68) is a complete expansion, one gets the Parseval relation,

$$\langle |g(\omega)|^2\rangle = \sum_{m=0}^{\infty} m! \sum_{i_1,i_2,\cdots,i_m=-\infty}^{\infty} |\hat{g}_m(i_1,i_2,\cdots,i_m)|^2, \tag{4.73}$$

which means that the right-hand side of the expansion (4.68) is convergent in ensemble mean square sense.

4.5.1 Proof of orthogonal functional expansion

Now, we prove the expansion (4.68). By the definition of $L^2(\Omega, P)$, there exist a step functional $g_{M,N}(\omega)$ and a set of subsets which are related with the $M+N$ variables $b_{-M}, \cdots, b_0, \cdots, b_N$ satisfying (4.60), such that

$$\lim_{M,N\to+\infty} \langle |g(\omega) - g_{M,N}(\omega)|^2 \rangle = 0, \tag{4.74}$$

where

$$\begin{aligned} g_{M,N}(\omega) &= g(b_{-M}, \cdots, b_0, \cdots, b_N), \quad \omega \in \Omega(b_{-M}, \cdots, b_0, \cdots, b_N), && (4.75) \\ \Omega &= \bigcup_{b_{-M},\cdots,b_0,\cdots,b_N} \Omega(b_{-M}, \cdots, b_0, \cdots, b_N) \\ &= \sum_{b_{-M},\cdots,b_0,\cdots,b_N} \Omega(b_{-M}, \cdots, b0, \cdots, b_N). && (4.76) \end{aligned}$$

Here, (4.74) means that the sequence function $g_{M,N}(\omega)$ converges to $g(\omega)$ in the ensemble mean square sense. (4.75) indicates the functional $g_{M,N}(\omega)$ is a step functional which takes a constant value on subset $\Omega(b_{-M}, \cdots, b_0, \cdots, b_N)$. In terms of the multivariate polynomials (4.51) of $N+M+1$ variables, we have

$$\begin{aligned} g_{N,M}(\omega) &= g(b_{-M}, \cdots, b_0, \cdots, b_N) && (4.77) \\ &= \hat{g}_0 + \sum_{k_1=-M}^{N} \hat{g}_1(k_1) B_1(b_{k_1}) + \sum_{k_1,k_2=-M}^{N} \hat{g}_2(k_1,k_2) B_2(b_{k_1}, b_{k_2}) \\ &\quad + \cdots + \sum_{k_1,k_2,\cdots,k_{N+M+1}=-M}^{N} \hat{g}_{N+M+1}(k_1, k_2, \cdots, k_{N+M+1}) \\ &\quad \times B_{N+M+1}(b_{k_1}, b_{k_2}, \cdots, k_{N+M+1}), && (4.78) \end{aligned}$$

which proves the orthogonal functional expansion (4.68).

4.5.2 An example of the orthogonal functional expansion

As a simple example, let us consider the orthogonal functional expansion of $g(\omega)$:

$$g(\omega) = \exp\left(\sum_{k=-\infty}^{\infty} f_1(k) b_k \right). \tag{4.79}$$

If $\sum_{k=-\infty}^{\infty} \left| Re[f_1(k)] \right| < \infty$, $g(\omega)$ belongs to $L^2(\Omega, P)$. Equation (4.79) is regarded as the output of a cascade system involving a linear filter and exponential nonlinear for the input of binary sequence. This example is important, because it gives the generating function

Q for the orthogonal polynomials $\{B_m(b_{i_1}, b_{i_2}, \cdots, b_{i_m})\}$. From (4.72) and (4.79), we may obtain the kernel functions as

$$\begin{aligned} \hat{g}_0 &= \prod_{k=-\infty}^{\infty} \cosh[f_1(k)], \\ \hat{g}_m(i_1, i_2, \cdots, i_m) &= \frac{\hat{g}_0}{m!} \Delta_m(i_1, i_2, \cdots, i_m) t_{i_1} t_{i_2} \cdots t_{i_m}, \quad m \geq 1, \\ t_k &= \tanh[f_1(k)]. \end{aligned} \tag{4.80}$$

Substituting the result (4.80) into (4.68), we get the orthogonal functional expansion

$$\begin{aligned} g(\omega) &= \hat{g}_0 + \frac{\hat{g}_0}{1!} \sum_k t_k \hat{B}_1(b_k) + \frac{\hat{g}_0}{2!} \sum_{k,l} t_k t_l \hat{B}_2(b_k, b_l) \\ &\quad + \frac{\hat{g}_0}{3!} \sum_{i,j,k} t_i t_j t_k \hat{B}_3(b_i, b_j, b_k) + \cdots. \end{aligned} \tag{4.81}$$

On the other hand, this expansion can be derived by another method. For $b_k = \pm 1$, we find an identity

$$e^{f_1(k) b_k} = \cosh[f_1(k)][1 + b_k t_k], \tag{4.82}$$

where t_k is given by (4.80). Then we have

$$\begin{aligned} g(\omega) &= \exp\left(\sum_{k=-\infty}^{\infty} f_1(k) b_k \right) \\ &= \hat{g}_0 \prod_{k=-\infty}^{\infty} [1 + t_k b_k] \\ &= \hat{g}_0 + \hat{g}_0 \sum_k t_k b_k + \hat{g}_0 \sum_{k<l} t_k t_l b_k b_l + \hat{g}_0 \sum_{i<j<k} t_i t_j t_k b_i b_j b_k + \cdots, \end{aligned} \tag{4.83}$$

which is the same expansion as (4.81). Equating (4.81) to (4.83), we find the generating function Q in (4.108).

4.6 Stationary sequence

We have considered the functional expansion of a stochastic functional $g(\omega)$, which is a random variable. This section discusses a stationary sequence generated by the stationary binary sequence.

Let us define the shift T which translates a sample vector ω into another sample vector $T\omega$ in the sample space Ω by

$$Tb_i = b_{i+1}, \quad T\omega = (\cdots, b_{-1}, b_0, b_1, b_2, \cdots). \tag{4.84}$$

Because b_i is a strictly stationary independent sequence, if a sample sequence ω exists with the probability $P(\omega)$, the shifted sequence $T\omega$ must exist with the same probability $P(T\omega) = P(\omega)$, which means measure-preserving. Thus, the shift T becomes a measure-preserving transformation in Ω with one parameter group properties:

$$T^0 = 1(\text{identity}); \quad T^m T^n = T^{m+n}, \tag{4.85}$$

where m and n are any integers. Applying the shift to the multivariate polynomials, we obtain

$$T^\beta B_m(b_{i_1}, b_{i_2}, \cdots, b_{i_{m-1}}, b_{i_m}) = B_m(b_{i_1+\beta}, b_{i_2+\beta}, \cdots, b_{i_{m-1}+\beta}, b_{i_m+\beta}), \tag{4.86}$$

where β is any integer. Using (4.86) and (4.68), we obtain the functional expansion for $g(T^\beta\omega)$

$$g(T^\beta\omega) = \hat{g}_0 + \sum_{k=-\infty}^{\infty} \hat{g}_1(k-\beta)B_1(b_k) + \sum_{k,l=\infty}^{\infty} \hat{g}_2(k-\beta, l-\beta)B_2(b_k, b_l) + \cdots, \tag{4.87}$$

which is a stationary sequence generated from the binary sequence $\{b_i\}$. The correlation function may be easily calculated as

$$\begin{aligned} \langle g(T^\beta\omega)g^*(\omega)\rangle &= |\hat{g}_0|^2 + 1! \sum_{k=-\infty}^{\infty} \hat{g}_1(k-\beta)\hat{g}_1^*(k) \\ &\quad + 2! \sum_{k\neq l} \hat{g}_2(k-\beta, l-\beta)\hat{g}_2^*(k,l) + \cdots. \end{aligned} \tag{4.88}$$

Note that any statistical properties of $g(T^\beta\omega)$ can be obtained from one sample sequence, because $g(T^\beta\omega)$ is ergodic.

4.6.1 Proof of ergodicity

The fundamental theorem of measure-preserving transformation is the ergodic theorem. It is usually stated as follows: the ensemble mean is equal to the time mean.

Ergodic theorem: when the mean $\langle g(\omega)\rangle$ and the variance $\langle |g(\omega)|^2\rangle$ are finite,

$$\text{l.i.m}_{n\to\infty} \frac{1}{2n+1} \sum_{\beta=-n}^{n} g(T^\beta\omega) = \langle g(\omega)\rangle \tag{4.89}$$

holds in ensemble mean square sense.

Proof: first, the condition $\langle |g(\omega)|^2\rangle < \infty$ means that

$$|\hat{g}_0|^2 + 1! \sum_{k=-\infty}^{\infty} |\hat{g}_1(k)|^2 + 2! \sum_{k,l=-\infty}^{\infty} |\hat{g}_2(k,l)|^2 + \cdots < \infty. \tag{4.90}$$

For any positive number ϵ, there exists a large integer P, such that when $p \geq P$,

$$\sum_{k<-p}^{k>p} |\hat{g}_1(k)|^2 + 2! \sum_{k,l<-p}^{k,l>p} |\hat{g}_2(k,l)|^2 + \cdots < \frac{\epsilon}{4}. \tag{4.91}$$

Then, there is a positive integer N_1 such that

$$N_1 < \frac{4(2P+1)\langle |g(\omega)|^2 \rangle - \epsilon}{2\epsilon} + 1, \quad N_1 > \frac{4(2P+1)\langle |g(\omega)|^2 \rangle - \epsilon}{2\epsilon}. \tag{4.92}$$

We can take a positive integer N such that $N = max\{P, N_1\}$, which means

$$\frac{2(2P+1)(2N+2P+1)}{(2N+1)^2} \langle |g(\omega)|^2 \rangle \leq \frac{\epsilon}{2}, \tag{4.93}$$

which will be used later. Assuming $n \geq N$, let us prove an inequality,

$$\left\langle \left| \frac{1}{2n+1} \sum_{\beta=-n}^{n} g(T^\beta \omega) - \hat{g}_0 \right|^2 \right\rangle \tag{4.94}$$

$$= \frac{1}{(2n+1)^2} \sum_{k=-\infty}^{\infty} \left| \sum_{\beta=-n}^{n} \hat{g}_1(k-\beta) \right|^2 + \frac{2!}{(2n+1)^2} \sum_{k,l=-\infty}^{\infty} \left| \sum_{\beta=-n}^{n} \hat{g}_2(k-\beta, l-\beta) \right|^2 + \cdots$$

$$< \epsilon. \tag{4.95}$$

For obtaining (4.95), we will repeately use an inequality for complex numbers $b_1, b_2, \cdots, b_n$,

$$\left| \sum_{i=1}^{n} b_i \right|^2 \leq n \sum_{i=1}^{n} |b_i|^2, \tag{4.96}$$

which may be proved by the Cauchy-Schwartz inequality [88]

$$\left(\sum_{i=1}^{n} a_i \right)^2 \leq n \left(\sum_{i=1}^{n} a_i^2 \right), \quad a_i \geq 0, \quad i = 1, 2, \cdots, n. \tag{4.97}$$

Because it is complicate to write the whole process of calculating (4.95), we only write explicitly the first term of (4.95),

$$\sum_{k=-\infty}^{\infty} \left| \sum_{\beta=-n}^{n} \hat{g}_1(k-\beta) \right|^2 + \cdots$$

$$= \left\{ \sum_{k=-(n+P)}^{n+P} \left| \sum_{\beta=-n}^{n} \hat{g}_1(k-\beta) \right|^2 + \cdots \right\} + \left\{ \sum_{k<-(n+P)}^{k>(n+P)} \left| \sum_{\beta=-n}^{n} \hat{g}_1(k-\beta) \right|^2 + \cdots \right\}$$

$$
\begin{aligned}
&\le 2\Big\{\sum_{k=-(n+P)}^{n+P}\Big|\sum_{\substack{\beta=-n\\|k-\beta|\le P}}^{n}\hat{g}_1(k-\beta)\Big|^2+\cdots\Big\}+2\Big\{\sum_{k=-(n+P)}^{n+P}\Big|\sum_{\substack{\beta=-n\\|k-\beta|>P}}^{n}\hat{g}_1(k-\beta)\Big|^2+\cdots\Big\}\\
&\quad+\Big\{\sum_{k<-(n+P)}^{k>n+P}\Big|\sum_{\beta=-n}^{n}\hat{g}_1(k-\beta)\Big|^2+\cdots\Big\}\\
&\le 2(2P+1)\Big\{\sum_{k=-(n+P)}^{n+P}\sum_{\substack{\beta=-n\\|k-\beta|\le P}}^{n}|\hat{g}_1(k-\beta)|^2+\cdots\Big\}\\
&\quad+2(2n+1)\Big\{\sum_{k=-(n+P)}^{n+P}\sum_{\substack{\beta=-n\\|k-\beta|>P}}^{n}|\hat{g}_1(k-\beta)|^2+\cdots\Big\}\\
&\quad+(2n+1)\Big\{\sum_{k<-(n+P)}^{k>(n+P)}\sum_{\beta=-n}^{n}|\hat{g}_1(k-\beta)|^2+\cdots\Big\}\\
&\le 2(2P+1)\sum_{k=-(n+P)}^{n+P}\langle|g(\omega)|^2\rangle+2(2n+1)\Big\{\sum_{k=-\infty}^{\infty}\sum_{\substack{\beta=-n\\|k-\beta|>P}}^{n}|\hat{g}_1(k-\beta)|^2+\cdots\Big\}\\
&\le 2(2P+1)(2n+2P+1)\langle|g(\omega)|^2\rangle+2(2n+1)^2\Big\{\sum_{k<-P}^{k>P}|\hat{g}_1(k)|^2+\cdots\Big\}. \qquad (4.98)
\end{aligned}
$$

Substituting (4.98) into (4.94) and using the relations (4.91) and (4.93), we get the inequality (4.95). Since ϵ is arbitrary, the ergodic theorem (4.89) holds in ensemble mean sense.

4.7 Stochastic binary sequence with unequal probability

In the previous sections, however, we only discuss a special case where a binary sequence takes two values with equal probability. In this section, we consider general probability case. For a stochastic binary sequence taking two values with unequal probability, we present explicit definition of the multivariate orthogonal polynomials and recurrence formula. These formulas can be applied to various random problems in physics and engineering.

Let $\{\hat{b}_i, i=0,\pm1,\pm2,\cdots\}$ be an independent stationary binary sequence taking ±1 with unequal probability

$$
P(\hat{b}_i=1)=\frac{1+\mu}{2},\quad P(\hat{b}_i=-1)=\frac{1-\mu}{2}, \qquad (4.99)
$$

where real μ is the average parameter with $|\mu|<1$. One easily finds the average and

correlation

$$\langle \hat{b}_i \rangle = \mu, \ \langle (\hat{b}_i - \mu)(\hat{b}_j - \mu) \rangle = (1 - \mu^2)\delta(i,j). \tag{4.100}$$

When $\mu = 0$, the binary sequence takes ± 1 with equal probability. When $\{i_1, i_2, \cdots, i_m\}$ and $\{j_1, j_2, \cdots, j_n\}$ are two distint sets, it is difficult to obtain the monent $\langle b_{i_1} b_{i_2} \cdots b_{i_m} \cdot b_{j_1} b_{j_2} \cdots b_{j_n} \rangle$, but we have

$$\begin{aligned} & \langle (b_{i_1} - \mu)(b_{i_2} - \mu) \cdots (b_{i_m} - \mu) \cdot (b_{j_1} - \mu)(b_{j_2} - \mu) \cdots (b_{j_n} - \mu) \rangle \\ = \ & (1 - \mu^2)^m \delta^{(m)}(i,j), \end{aligned} \tag{4.101}$$

which implies that we should regard $\frac{b_i - \mu}{\sqrt{1-\mu^2}}$ in unequal probability case as b_i in equal probability case.

4.7.1 Orthogonal polynomials

We also define multivariate orthogonal polynomials $\{\hat{B}_m(\hat{b}_{i_1}, \hat{b}_{i_2}, \cdots, \hat{b}_{i_{m-1}}, \hat{b}_{i_m}), \ m = 0, 1, 2, \cdots\}$ associated with the binary sequence by

$$\hat{B}_0 = 1, \tag{4.102}$$

$$\hat{B}_1(\hat{b}_i) = \hat{b}_i - \mu, \tag{4.103}$$

$$\hat{B}_2(\hat{b}_i, \hat{b}_j) = [1 - \delta(i,j)](\hat{b}_i - \mu)(\hat{b}_j - \mu), \tag{4.104}$$

$$\begin{aligned} \hat{B}_3(\hat{b}_i, \hat{b}_j, \hat{b}_k) = \ & [1 - \delta(i,j) - \delta(i,k) - \delta(k,j) \\ & + 2\delta(i,k)\delta(i,j)](\hat{b}_i - \mu)(\hat{b}_j - \mu)(\hat{b}_k - \mu), \end{aligned} \tag{4.105}$$

$$\cdots \quad = \quad \cdots$$

$$\hat{B}_m(\hat{b}_{i_1}, \hat{b}_{i_2}, \cdots, \hat{b}_{i_m}) = \Delta_m(i_1, i_2, \cdots, i_m)(\hat{b}_{i_1} - \mu)(\hat{b}_{i_2} - \mu) \cdots (\hat{b}_{i_m} - \mu), \tag{4.106}$$

$$(m \geq 1).$$

However, these polynomials may be obtained from a generating function $\hat{Q}$ as

$$\hat{B}_m(\hat{b}_{i_1}, \hat{b}_{i_2}, \cdots, \hat{b}_{i_m}) = \frac{\partial}{\partial t_{i_1}} \frac{\partial}{\partial t_{i_2}} \cdots \frac{\partial}{\partial t_{i_m}} \hat{Q} \Big|_{t_0 = t_{\pm 1} = t_{\pm 2} = \cdots = 0}. \tag{4.107}$$

The generating function Q is formally given as

$$\hat{Q} = \prod_{k=-\infty}^{\infty} \left[1 + (\hat{b}_k - \mu) \cdot t_k \right]. \tag{4.108}$$

Manipulating (4.102)-(4.106) and (4.21), we find the recurrence formula,

$$\begin{aligned}
&\hat{B}_m(\hat{b}_{i_1}, \hat{b}_{i_2}, \cdots, \hat{b}_{i_m}) \\
&= \hat{B}_{m-1}(\hat{b}_{i_1}, \hat{b}_{i_2}, \cdots, \hat{b}_{i_{m-1}})\hat{B}_1(\hat{b}_{i_m}) + 2\mu \sum_{l=1}^{m-1} \hat{B}_{m-1}(\hat{b}_{i_1}, \hat{b}_{i_2}, \cdots, \hat{b}_{i_{m-1}})\delta(i_m, i_l) \\
&-(1-\mu^2) \sum_{l=1}^{m-1} \hat{B}_{m-2}(\hat{b}_{i_1}, \hat{b}_{i_2}, \cdots, \hat{b}_{i_{l-1}}, \hat{b}_{i_{l+1}}, \cdots, \hat{b}_{i_{m-1}})\delta(i_m, i_l) \\
&+(1-\mu^2) \sum_{l=1}^{m-1} \sum_{\substack{k=1 \\ k\neq l}}^{m-1} \hat{B}_{m-2}(\hat{b}_{i_1}, \hat{b}_{i_2}, \cdots, \hat{b}_{i_{l-1}}, \hat{b}_{i_{l+1}}, \cdots, \hat{b}_{i_{m-1}})\delta(i_m, i_l)\delta(i_k, i_l). \quad (4.109)
\end{aligned}$$

The formula (4.109) can be proved by the same method as the case of equal probability. When $\mu = 0$, the binary sequence takes ± 1 with equal probability so that the formula (4.109) is reduced to formula (4.29). Putting $m = 2$ in (4.109), we get a comprehensive example

$$\hat{B}_1(\hat{b}_i)\hat{B}_1(\hat{b}_j) = \hat{B}_2(\hat{b}_i, \hat{b}_j) - 2\mu\hat{B}_1(\hat{b}_i)\delta(i,j) + (1-\mu^2)\delta(i,j). \quad (4.110)$$

Note that (4.110) is a second order polynomial for $i \neq j$, but becomes a first order polynomial when $i = j$. Replacing b_i by $\frac{b_i - \mu}{\sqrt{1-\mu^2}}$ in (4.3), (4.4) and using (4.102)-(4.106), we have

$$\langle \hat{B}_m(\hat{b}_{i_1}, \hat{b}_{i_2}, \cdots, \hat{b}_{i_{m-1}}, \hat{b}_{i_m}) \rangle = \delta(m, 0), \quad (4.111)$$

$$\begin{aligned}
&\langle \hat{B}_m(\hat{b}_{i_1}, \hat{b}_{i_2}, \cdots, \hat{b}_{i_m})\hat{B}_n(\hat{b}_{j_1}, \hat{b}_{j_2}, \cdots, \hat{b}_{j_n}) \rangle \\
&= (1-\mu^2)^n \Delta_m(i_1, i_2, \cdots, i_m)\Delta_n(j_1, j_2, \cdots, j_n)\delta(m,n)\delta^{(m)}(i,j), \quad (4.112)
\end{aligned}$$

which mean that the multivariate polynomials have zero averages for $m > 0$ and orthogonality relation. These results (4.109)-(4.112) are also obtain first in the paper [70].

4.7.2 Stationary sequence and orthogonal functional expansion

As same as the case of Sec.4.4, any function of ω is a functional of the binary sequence $\{\hat{b}_i\}$, enjoying an orthogonal functional expansion

$$\begin{aligned}
g(\omega) = g_0 &+ \sum_{k=-\infty}^{\infty} g_1(k)\hat{B}_1(\hat{b}_k) + \sum_{k,l=-\infty}^{\infty} g_2(k,l)\hat{B}_2(\hat{b}_k, \hat{b}_l) \\
&+ \sum_{k,l,m=-\infty}^{\infty} g_3(k,l,m)\hat{B}_3(\hat{b}_k, \hat{b}_l, \hat{b}_m) + \cdots, \quad (4.113)
\end{aligned}$$

which holds in ensemble mean square sense. Here, the deterministic coefficient functions can be given by

$$\begin{aligned}\hat{g}_m(i_1,i_2,\cdots,i_m) &= \Delta_m(i_1,i_2,\cdots,i_m)g_m(i_1,i_2,\cdots,i_m)\\ &= \frac{\langle g(\omega)\hat{B}_m(\hat{b}_{i_1}\hat{b}_{i_2}\cdots\hat{b}_{i_m})\rangle}{(1-\mu^2)^m m!},\end{aligned} \tag{4.114}$$

where we have used the fact that non-zero diagonal kernels are symmetrical for their arguments.

The stationary binary sequence $\{\hat{b}_i\}$ can also generate a stationary sequence

$$g(T^\beta\omega) = \hat{g}_0 + \sum_{k=-\infty}^{\infty}\hat{g}_1(k-\beta)\hat{B}_1(\hat{b}_k) + \sum_{k,l=\infty}^{\infty}\hat{g}_2(k-\beta,l-\beta)\hat{B}_2(\hat{b}_k,\hat{b}_l)+\cdots, \tag{4.115}$$

where β is any integer and operator T is a measure-preserving transformation in Ω satisfying the relation: $T(\cdots,\hat{b}_{-2},\hat{b}_{-1},\hat{b}_0,\hat{b}_1,\cdots) = (\cdots,\hat{b}_{-1},\hat{b}_0,\hat{b}_1,\hat{b}_2,\cdots)$.

4.8 Conclusions

By formal discussions, we have obtained some new formulas concerning the multivariate orthogonal polynomials of a stationary binary sequence. We also gave a simple example of orthogonal functional expansion. Since these formulas are given in explicit form, they can be applied to various problems in random theory. However, we are interested in application to the theory of wave scattering from binary random surfaces. Such an application will be studied in the next chapter.

There are limitations in our discussions, because we only consider the case where $\{b_i\}$ is a one-dimensional independent sequence. Extension from one-dimensional sequence to two-dimensional random field can be done formally. Only modifications for the extension are that the subscript i of b_i should be a two-dimensional index, and hence any summation and Kronecker's delta should be two-dimensional. However, the ordered summation in (4.68) or (4.83) becomes meaningless.

Besides, it seems difficult to get explicit forms of orthogonal multivariate polynomials for correlated binary sequence with any correlation function, because the multidimensional probability distribution is still unknown for a correlated binary sequence.

Chapter 5

Diffraction and scattering from randomly deformed periodic surfaces: binary case

5.1 Introduction

Diffraction and scattering of waves from randomly deformed periodic surfaces have been an important subject for many years, because natural and artificial periodic surfaces are often randomly deformed by inaccurate fabrication and other reasons [15]. Several authors studied such a scattering problem by several methods. In chapters 2 and 3, we introduced a probabilistic method [71], where the scattered wave field was determined as a stochastic functional of surface deformations. But, these works were restricted to a case where random deformations are Gaussian. In this chapter, however, we study a case of stochastic binary deformations, because such a case is related to digital recording devices which store random data by surface deformations [26],[27].

We assume that a randomly deformed periodic surface is generated by a periodic translation of a local surface profile, of which height is modulated by a stationary binary sequence. Since such a random surface is a periodic stationary process, the scattered wave is again shown to have a stochastic Floquet form: a product of a periodic stationary random function and an exponential phase factor. Using a harmonic series representation, we write such a periodic stationary random process as a sum of mutually correlated stationary processes, which are developed by binary functional expansions with unknown binary kernels; formulas of such a binary functional expansion have been obtained in chapter 4. Sec.5.3 and Sec.5.4 give several statistical properties of the diffraction and scattering, such as the coherently diffracted power, the scattering cross section and the optical theorem. In Sec.5.5, for the case of a slightly rough surface and TE plane incident wave, low order binary kernels involving multiple-scattering are determined from the boundary condition. Some numerical examples are illustrated in Sec.5.6. Then, it is shown that, even though diffraction efficiencies are related with both the height of average periodic surface and the amplitude of random deformation, the total diffraction power depends on only the amplitude of random deformation.

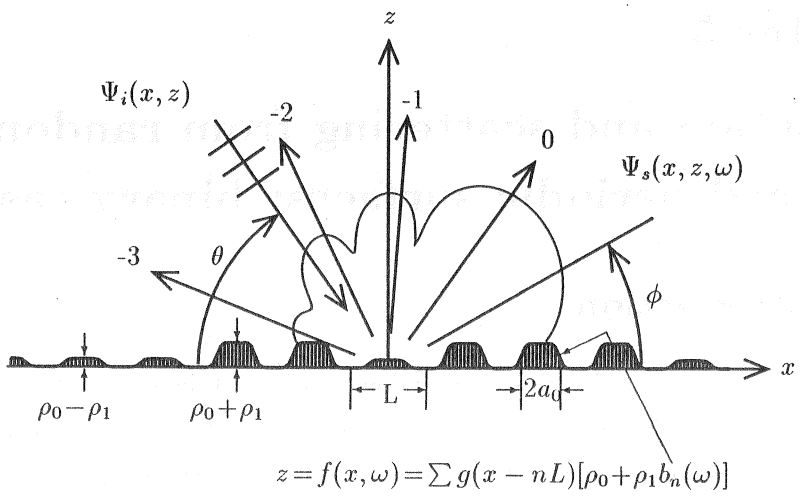

Figure 5.1: Diffraction and scattering of a TE plane wave from a randomly deformed periodic surface. L is the period, a_0 is half the width of the local surface profile, ρ_0 and ρ_1 are height parameters, θ is the angle of incidence and ϕ is a scattering (diffraction) angle. The coherent wave is diffracted into only discrete directions indicated by numbers. The incoherent wave is scattered into all directions.

5.2 Probabilistic formulation of the problem

Let us consider the randomly deformed periodic surface, shown in Fig.5.1, where the surface deformation is expressed by a periodic stationary binary random process $f(x,\omega)$,

$$z = f(x,\omega) = \sum_{n=-\infty}^{\infty} g(x - nL)[\rho_0 + \rho_1 b_n(\omega)], \tag{5.1}$$

where $g(x)$ is the local surface profile, L is the period, and $b_n(\omega)$ is an independent stationary binary sequence taking ± 1 with equal probability: $P(b_n = 1) = P(b_n = -1) = 1/2$. Then $b_n(\omega)$ has zero average and orthogonal correlation,

$$\langle b_n(\omega)\rangle = 0, \quad \langle b_n(\omega) b_m(\omega)\rangle = \delta(n,m), \tag{5.2}$$

where ω is a probability parameter denoting a sample point in the sample space Ω. From

(5.1) and (5.2), $f(x,\omega)$ has periodic average:

$$\langle f(x,\omega)\rangle = \rho_0 \sum_{n=-\infty}^{\infty} g(x-nL) = \langle f(x+L,\omega)\rangle, \tag{5.3}$$

where ρ_0 is the height parameter of the periodic component, and periodic correlation:

$$\begin{aligned} R(x,x') &= \Big\langle [f(x,\omega)-\langle f(x,\omega)\rangle]\cdot[f(x',\omega)-\langle f(x',\omega)\rangle]\Big\rangle \\ &= \rho_1^2 \sum_{n=-\infty}^{\infty} g(x-nL)g(x'-nL) \\ &= R(x+L,x'+L), \end{aligned} \tag{5.4}$$

where ρ_1 is the amplitude parameter of random deformation. Note that the random surface is made up of periodic component (average part) and random component.

By use of the shift operator T defined in (4.84), it holds that $b_n(\omega) = b_0(T^n\omega)$ for almost all ω, so that (5.1) has a shift invariance property

$$f(x,\omega) = f(x+mL, T^{-m}\omega). \tag{5.5}$$

Note that $f(x,\omega)$ is invariant under the two dimensional shift which takes (x,ω) into $(x+mL, T^{-m}\omega)$.

Let us denote the y component of the TE electric field by $\Psi(x,z,\omega)$, the incident wave by $\Psi_i(x,\omega)$, and the scattered field by $\Psi_s(x,z,\omega)$. These fields satisfy

$$\left[\frac{\partial^2}{\partial x^2}+\frac{\partial^2}{\partial z^2}+k^2\right]\Psi(x,z,\omega) = 0, \tag{5.6}$$

$$\Psi(x,z,\omega) = \Psi_i(x,z) + \Psi_s(x,z,\omega), \tag{5.7}$$

$$\Psi_i(x,z) = e^{ipx-i\beta_0(p)z}, \tag{5.8}$$

$$\Psi_s(x,z,\omega) = e^{ipx}U(x,z,\omega), \tag{5.9}$$

$$p = k\cos\theta, \quad \beta_n(\lambda) = \sqrt{k^2-\left(\lambda+\frac{2\pi n}{L}\right)^2},$$

$$\mathrm{Im}[\beta_n(p)] \geq 0, \quad n = 0,\pm1,\pm2,\cdots, \tag{5.10}$$

where $U(x,z,\omega)$ is a periodic stationary process of x with the period L, enjoying the shift invariance property

$$U(x,z,\omega) = U(x+mL,z,T^{-m}\omega), \ m = 0,\pm1,\cdots. \tag{5.11}$$

This implies that the average $\langle U(x,z,\omega)\rangle$ is a periodic function of x. The fact will be used below.

5.3 Stochastic representation for the periodic stationary process

We now consider the harmonic series representation for the periodic stationary random surface $f(x,\omega)$. First, we express the local surface profile $g(x)$ as,

$$\begin{aligned} g(x) &= \int_{-\infty}^{\infty} e^{i\lambda x} G(\lambda) d\lambda = \sum_{q=-\infty}^{\infty} e^{\frac{i2\pi qx}{L}} \int_{-\frac{\pi}{L}}^{\frac{\pi}{L}} e^{i\lambda x} G^{(q)}(\lambda) d\lambda, \\ G^{(q)}(\lambda) &= G\left(\lambda + \frac{2\pi q}{L}\right), \quad G^{(q)*}(\lambda) = G^{(-q)}(-\lambda). \end{aligned} \tag{5.12}$$

Substituting (5.12) into (5.1), we obtain the harmonic series representation for $f(x,\omega)$,

$$f(x,\omega) = \sum_{q=-\infty}^{\infty} e^{\frac{i2\pi qx}{L}} f^{(q)}(x,\omega), \tag{5.13}$$

$$f^{(q)}(x,\omega) = \frac{2\pi\rho_0}{L} G^{(q)}(0) + \rho_1 \sum_{n=-\infty}^{\infty} B^{(1)}[b_n] \int_{-\frac{\pi}{L}}^{\frac{\pi}{L}} e^{i\lambda(x-nL)} G^{(q)}(\lambda) d\lambda,$$

$$f^{(q)*}(x,\omega) = f^{(-q)}(x,\omega). \tag{5.14}$$

Note that (5.13) is a 'Fourier series', where a 'Fourier coefficient' $f^{(q)}(x,\omega)$ is not a deterministic constant but is a stationary process with constant average and mutual correlation function $R_{qq'}(x)$

$$\langle f^{(q)}(x,\omega) \rangle = \frac{2\pi\rho_0}{L} G^{(q)}(0), \tag{5.15}$$

$$R_{qq'}(x) = \frac{2\pi\rho_1^2}{L} \int_{-\frac{\pi}{L}}^{\frac{\pi}{L}} e^{i\lambda x} G^{(q)}(\lambda) G^{(q')*}(\lambda) d\lambda, \tag{5.16}$$

$$R^*_{qq'}(x) = R_{q'q}(-x), \qquad R_{qq}(0) \geq 0.$$

Because $U(x,z,\omega)$ is a periodic stationary process satisfying (5.11), we write it by the harmonic series representation

$$U(x,z,\omega) = \sum_{q=-\infty}^{\infty} e^{\frac{i2\pi qx}{L}} U^{(q)}(x,z,\omega), \tag{5.17}$$

where $U^{(q)}(x,z,\omega)$ is a stationary process of x. Since $U^{(q)}(x,z,\omega)$ is a stochastic functional of the binary sequence, it can be represented by a binary expansion (4.68) for each value of (x,z). Since $\Psi_s(x,z,\omega)$ satisfies (5.6) and the radiation condition for $z \to \infty$, we rewrite (4.68) and we put

$$U^{(q)}(x,z,\omega) = C_0^{(q)} e^{i\beta_q(p)z} + \sum_{m=-\infty}^{\infty} B^{(1)}[b_m] \int_{-\frac{\pi}{L}}^{\frac{\pi}{L}} C_1^{(q)}(\lambda) e^{i\lambda(x-mL)+i\beta_q(p+\lambda)z} d\lambda$$

$$+\sum_{m,n=-\infty}^{\infty} B^{(2)}[b_m, b_n] \int\int_{-\frac{\pi}{L}}^{\frac{\pi}{L}} C_2^{(q)}(\lambda_1,\lambda_2) e^{i\lambda_1(x-mL)+i\lambda_2(x-nL)+i\beta_q(p+\lambda_1+\lambda_2)z} d\lambda_1 d\lambda_2$$
$$+\cdots, \tag{5.18}$$

where $B^{(m)}[\cdot]$ is the multi-variate polynomial defined in chapter 4, and $C_0^{(q)}$, $C_1^{(q)}(\lambda)$, $C_2^{(q)}(\lambda_1,\lambda_2)$, $\cdots$ are binary kernels in the spectral domain. From (5.7), (5.9), (5.17) and (5.18), we obtain the coherent wave (average wave)

$$\langle \Psi(x,z,\omega)\rangle = e^{ipx-i\beta_0(p)z} + e^{ipx} \sum_{q=-\infty}^{\infty} e^{\frac{i2\pi qx}{L}+i\beta_q(p)z} C_0^{(q)}. \tag{5.19}$$

This is exactly Floquet's solution for a periodic grating, which means that the randomly deformed periodic surface works as a perfectly periodic surface for the coherent wave. As a result, the coherent wave is diffracted into only discrete directions. $C_0^{(q)}$ is the amplitude of the q-th order coherent wave diffracted into the direction $\phi_q(0)$, where

$$\phi_q(\lambda) = \cos^{-1}\frac{1}{k}\left(p+\lambda+\frac{2\pi q}{L}\right). \tag{5.20}$$

On the other hands, the incoherent wave is scattered into all directions. For example, $C_1^{(q)}(\lambda)$ is an amplitude factor of the incoherent wave scattered into the direction $\phi_q(\lambda)$.

5.4 Scattering cross section

In a loss-less case, we obtain the optical theorem,

$$\begin{aligned}\frac{\beta_0(p)}{k} &= \frac{1}{k}\sum_{n=-\infty}^{\infty} \mathrm{Re}[\beta_n(p)]|C_0^{(n)}|^2 \\ &+\frac{1}{k}\sum_{n=-\infty}^{\infty}\Big\{1!\Big(\frac{2\pi}{L}\Big)\int_{-\frac{\pi}{L}}^{\frac{\pi}{L}} \mathrm{Re}[\beta_n(p+\lambda)]|C_1^{(n)}(\lambda)|^2 d\lambda \\ &+2!\Big(\frac{2\pi}{L}\Big)^2\int\int_{-\frac{\pi}{L}}^{\frac{\pi}{L}} \mathrm{Re}[\beta_n(p+\lambda_1+\lambda_2)]|C_2^{(n)}(\lambda_1,\lambda_2)|^2 d\lambda_1 d\lambda_2 + \cdots\Big\},\end{aligned} \tag{5.21}$$

where the left-hand side is the incident power, $\frac{1}{k}\mathrm{Re}[\beta_n(p)]|C_0^{(n)}|^2$ is an coherent diffraction efficiency, the first term of the right-hand side is the total coherent power, and an integral indicates incoherently scattered power. The scattering cross section $\sigma_i(\phi|\theta)$ is given by

$$\begin{aligned}\sigma_i(\phi|\theta) &= 2\pi k\sin^2\phi\sum_{n=-\infty}^{\infty}\Big\{1!\Big(\frac{2\pi}{L}\Big)\Big|C_1^{(n)}(\lambda_n)\Big|^2 S(\lambda_n) \\ &+2!\Big(\frac{2\pi}{L}\Big)^2\int_{-\frac{\pi}{L}}^{\frac{\pi}{L}}\Big|C_2^{(n)}(\lambda_n-\lambda',\lambda')\Big|^2 S(\lambda_n-\lambda')d\lambda' + \cdots\Big\},\end{aligned} \tag{5.22}$$

where

$$S(\lambda) = \begin{cases} 1 & |\lambda| \le \pi/L \\ 0 & |\lambda| > \pi/L \end{cases}, \quad \lambda_n = k(\cos\phi - \cos\theta) - \frac{2\pi n}{L}, \tag{5.23}$$

where ϕ is a scattering angle shown in Fig.5.1. We will calculate numerically these quantities by use of low order binary kernels.

5.5 An approximate solution

Let us determine the binary kernels from the boundary condition. When the random surface is perfectly conductive, the wave function satisfies the Dirichlet condition:

$$\Psi(x, z, \omega) = 0 \quad \text{for } z = f(x, \omega). \tag{5.24}$$

For simplicity, however, we only consider the case where the random surface has small roughness and small slope. In this case, the boundary condition may be approximated by

$$\Psi(x, z, \omega) + f(x, \omega)\frac{\partial \Psi(x, z, \omega)}{\partial z} = 0 \quad (z = 0). \tag{5.25}$$

Substituting (5.7), (5.9), (5.17) and (5.13) into (5.25) and using orthogonality relation (4.28), we obtain hierarchical equations for the binary kernels.

the zero order equation

$$\sum_{r=-\infty}^{\infty}\left[\delta(n,r) + \frac{i2\pi\rho_0}{L}G^{(n-r)}(0)\beta_r(p)\right]C_0^{(r)} + \delta(n,0) - \frac{i2\pi\rho_0}{L}G^{(n)}(0)\beta_0(p)$$
$$+\frac{i2\pi\rho_1}{L}\sum_{r=-\infty}^{\infty}\int_{-\frac{\pi}{L}}^{\frac{\pi}{L}} G^{(n-r)}(-\lambda)\beta_r(p+\lambda)C_1^{(r)}(\lambda)d\lambda = 0, \tag{5.26}$$

the first order equation

$$\sum_{r=-\infty}^{\infty}\left[\delta(n,r) + \frac{i2\pi\rho_0}{L}G^{(n-r)}(0)\beta_r(p+\lambda)\right]C_1^{(r)}(\lambda)$$
$$+i\rho_1\sum_{r=-\infty}^{\infty} G^{(n-r)}(\lambda)\beta_r(p)C_0^{(r)} - i\rho_1\beta_0(p)G^{(n)}(\lambda)$$
$$+\frac{i4\pi\rho_1}{L}\sum_{r=-\infty}^{\infty}\int_{-\frac{\pi}{L}}^{\frac{\pi}{L}} G^{(n-r)}(-\lambda')\beta_r(p+\lambda+\lambda')C_2^{(r)}(\lambda,\lambda')d\lambda' = 0, \tag{5.27}$$

the second order equation

$$\sum_{r=-\infty}^{\infty}\left[\delta(n,r) + \frac{i2\pi\rho_0}{L}G^{(n-r)}(0)\beta_r(p+\lambda_1+\lambda_2)\right]C_2^{(r)}(\lambda_1,\lambda_2)$$

$$+\frac{i\rho}{2}\sum_{r=-\infty}^{\infty}\left[G^{(n-r)}(\lambda_2)\beta_r(p+\lambda_1)C_1^{(r)}(\lambda_1)+G^{(n-r)}(\lambda_1)\beta_r(p+\lambda_2)C_1^{(r)}(\lambda_2)\right]$$
$$-\frac{i\rho L}{4\pi}\sum_{r=-\infty}^{\infty}\int_{-\frac{\pi}{L}}^{\frac{\pi}{L}}G^{(n-r)}(\lambda_2-\Lambda)\beta_r(p+\lambda_1+\Lambda)C_1^{(r)}(\lambda_1+\Lambda)d\Lambda$$
$$-\frac{i\rho L}{4\pi}\sum_{r=-\infty}^{\infty}\int_{-\frac{\pi}{L}}^{\frac{\pi}{L}}G^{(n-r)}(\lambda_1-\Lambda)\beta_r(p+\lambda_2+\Lambda)C_1^{(r)}(\lambda_2+\Lambda)d\Lambda$$
$$+\frac{i6\pi\rho}{L}\sum_{r=-\infty}^{\infty}\int_{-\frac{\pi}{L}}^{\frac{\pi}{L}}G^{(n-r)}(-\lambda_3)\beta_r(p+\lambda_1+\lambda_2+\lambda_3)C_3^{(r)}(\lambda,\lambda_2,\lambda_3)d\lambda_3=0. \quad (5.28)$$

Neglecting $C_2^{(r)}(\lambda,\lambda')$ in (5.26) and (5.27), we obtain an approximate solution for $C_0^{(r)}$ and $C_1^{(r)}(\lambda)$, which are represented in matrix form,

$$\mathbf{C}_0=\left[\mathbf{I}+\mathbf{D}_0(0,p)-\mathbf{M}(p)\right]^{-1}\left[\mathbf{D}_0(0,p)-\mathbf{I}-\mathbf{M}(p)\right]\mathbf{I}^0, \quad (5.29)$$
$$\mathbf{C}_1(\lambda)=\left[\mathbf{I}+\mathbf{D}_0(0,p+\lambda)\right]^{-1}\mathbf{D}_1(\lambda,p)\left[\mathbf{I}^0-\mathbf{C}_0\right], \quad (5.30)$$

where $\mathbf{I}$ is the unit matrix, $\mathbf{D}_0(0,\lambda)$ and $\mathbf{D}_1(\lambda,p)$ are infinitely dimensional matrixes

$$\mathbf{D}_0(0,\lambda)=\frac{i2\pi\rho_0}{L}[G^{(n-r)}(0)\beta_r(\lambda)],$$
$$\mathbf{D}_1(\lambda,p)=i\rho_1[G^{(n-r)}(\lambda)\beta_r(p)], \quad (5.31)$$

where $G^{(n-r)}(\lambda)\beta_r(p)$ is the (n,r) element of the matrix $[G^{(n-r)}(\lambda)\beta_r(p)]$. On the other hand, $\mathbf{I}^0$, $\mathbf{C}_0$ and $\mathbf{C}_1(\lambda)$ are infinitely dimensional vectors

$$\begin{aligned}\mathbf{I}^0 &= (\cdots,\delta(r,0),\cdots)^t,\\ \mathbf{C}_0 &= (\cdots,C_0^{(-1)},C_0^{(0)},C_0^{(1)},\cdots)^t,\\ \mathbf{C}_1(\lambda) &= (\cdots,C_1^{(-1)}(\lambda),C_1^{(0)}(\lambda),C_1^{(1)}(\lambda),\cdots)^t,\end{aligned} \quad (5.32)$$

and $\mathbf{M}(p)$ is a mass operator matrix involving multiple-scattering,

$$\mathbf{M}(p)=\frac{2\pi}{L}\int_{-\frac{\pi}{L}}^{\frac{\pi}{L}}\mathbf{D}_1(-\lambda,p+\lambda)\left[\mathbf{I}+\mathbf{D}_0(0,p+\lambda)\right]^{-1}\mathbf{D}_1(\lambda,p)d\lambda. \quad (5.33)$$

We show the real and imaginary parts of the mass operator (the component of the matrix) in Fig.5.2.

From (5.29) and (5.30), $C_1^{(n)}(\lambda)$ can be written as

$$C_1^{(n)}(\lambda)=i\rho_1\sum_{r,j=-\infty}^{\infty}q_{n,r}(p+\lambda)G^{(r-j)}(\lambda)\beta_j(p)\left[\delta(j,0)-C_0^{(j)}\right], \quad (5.34)$$
$$[q_{n,r}(\lambda)]=[\mathbf{I}+\mathbf{D}_0(0,\lambda)]^{-1},$$

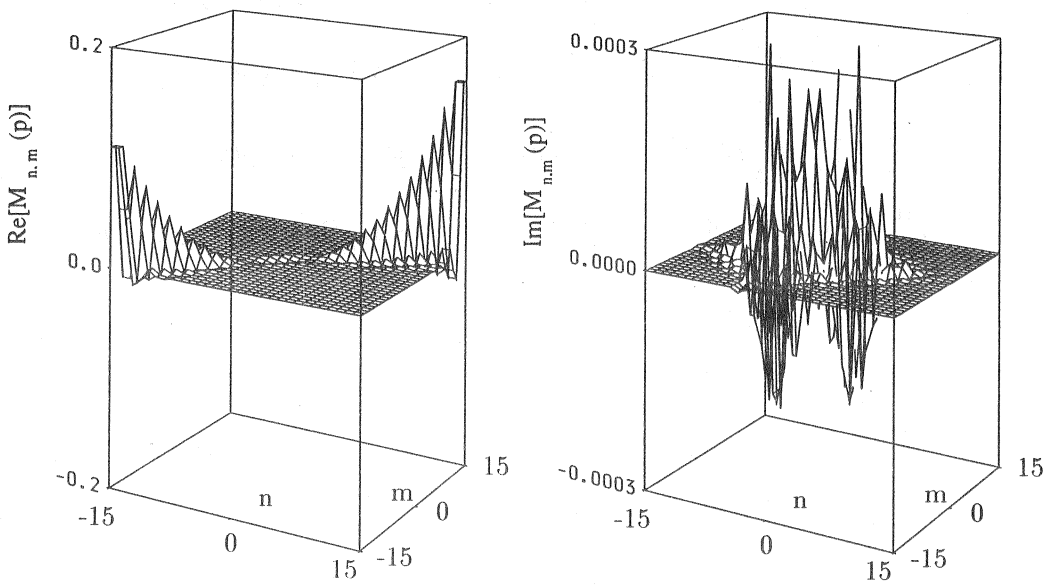

Figure 5.2: Real part and imaginary part of mass operator matrix $M(p)$ with parameters $L = 3\Lambda$, $\theta = 60°$, $a_0 = \Lambda$ and $\rho_0 = \rho_1 = \Lambda/40$. The diagonal element of real part is relatively large. The imaginary part is quite small.

where $q_{n,r}(\lambda)$ is the (n,r) component. Substituting (5.34) into (5.22), the scattering cross section $\sigma_i(\phi|\theta)$ is approximately expressed as

$$\sigma_i(\phi|\theta) \approx \frac{4\pi^2 k\rho_1^2}{L}\sin^2\phi \left| \sum_{r,j=-\infty}^{\infty} q_{0,r}(k\cos\phi) \right.$$
$$\left. \times G^{(r-j)}(k\cos\phi - k\cos\theta)\beta_r(k\cos\theta)\left[\delta(j,0) - C_0^{(j)}\right] \right|^2 + \cdots . \quad (5.35)$$

Since $C_0^{(j)}$ is an amplitude of the coherent diffraction, (5.34) and (5.35) imply the physical mechanism such that the j-th order coherently diffracted wave generates an incoherently scattered wave with $C_1^{(n)}(\lambda)$, and $\sigma_i(\phi|\theta)$ is determined by the contributions from these coherently diffracted waves. This fact agrees with other papers [17,18,71].

5.6 Numerical examples

For numerical calculations, we assume that the local surface profile $g(x)$ is a rectangular boss with smooth edges shown in Fig.5.1, and we put

$$g(x) = \frac{1}{2}[\mathrm{erf}(\frac{x+a_0}{\kappa}) - \mathrm{erf}(\frac{x-a_0}{\kappa})], \tag{5.36}$$

$$\mathrm{erf}(x) = \frac{2}{\sqrt{\pi}}\int_0^x e^{-t^2}dt, \tag{5.37}$$

$$G(\lambda) = \frac{\sin(a_0\lambda)}{\pi\lambda}e^{-\frac{(\kappa\lambda)^2}{4}}, \quad G(\frac{n\pi}{a_0}) = 0, \quad n \neq 0, \tag{5.38}$$

where a_0 is a width parameter, $\mathrm{erf}(x)$ is error function and κ is a constant determining the surface shape. For concrete calculations, we put $\kappa = 0.2\Lambda$, $L = 3\Lambda$, $a_0 = \Lambda$, $\rho_0 = \rho_1 = \Lambda/40$ and $\theta = 60°$, where Λ is wavelength. Further, we approximate (5.29) and (5.30) by 61×61 matrices and 61 dimensional vectors.

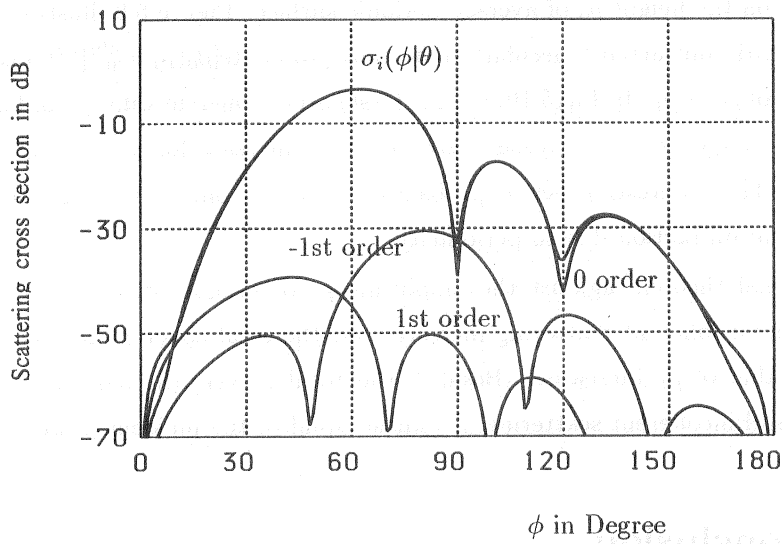

Figure 5.3: The contribution from 0, 1st and -1st order coherently diffracted waves with parameters $a_0 = \Lambda$, $\theta = 60°$, $\rho_0 = \rho_1 = \Lambda/40$ and $L = 3\Lambda$. The contribution from 0 order coherently diffracted wave is much larger than that from the other orders.

As is pointed out above, the $\sigma_i(\phi|\theta)$ is made up of contributions from each coherently

diffracted wave. Fig.5.3 shows contributions from each coherently diffracted wave separately. Since $C_0^{(0)}$ is relatively large but $C_0^{(j)}$ is small for $j \neq 0$, the contribution from the 0 order coherently diffracted wave is much larger than that from 1st or -1st order coherently diffracted wave. In other words, $\sigma_i(\phi|\theta)$ is mainly determined by the 0 term in the summation in equation (5.35). The scattering cross section $\sigma_i(\phi|\theta)$ is calculated against the scattering angle ϕ. Figure 5.4 shows that the incoherent scattering spreads widely and is relatively strong in the direction of specular reflection. Since $g(x)$ is a smooth rectangular and $G(\lambda)$ has zeros, $\sigma_i(\phi|\theta)$ has ripples. However, such ripples may disappear when a_0 is relatively short, as is shown in Fig.5.5. By (5.35), the scattering cross section is inversely proportional to the period L, as illustrated in Fig.5.6. Fig.5.7 illustrates, for several values of ρ_1, the backscattering cross section $\sigma_i(\phi|180° - \phi)$ which is relatively strong when the incident angle is 90°.

As is mentioned above, the coherent wave is only diffracted into discrete directions. Fig.5.8 shows that the total coherent power, given by the first term in the right-hand side of (5.21), decreases when the amplitude of random deformation increases, but has little dependence on the height ρ_0 of average periodic surface. Figure 5.9 illustrates that the 0 order coherently diffracted (specularly reflected) power $\mathrm{Re}[\beta_0(p)]|C_0^{(0)}|^2/k$ decreases with the increase of ρ_0 or ρ_1. In Fig.5.10, the 1st (-1st) order coherent diffraction becomes large when ρ_0 gets large. As ρ_1 increases, however, they increase for $\rho_0 = 0$ but decrease for $\rho_0 = \Lambda/40$. This interesting fact is probably caused by combinations between multiple-scattering and diffraction due to periodicity.

The optical theorem against the amplitude ρ_1 of random deformation is shown in Fig.5.11. The incoherent scattering increases but the total coherent scattering decreases when the value of ρ_1 increases. Besides, the total power, the sum of total coherent diffraction and incoherent scattering, is almost equal to the incident power.

5.7 Conclusion

In this chapter, we discussed a probabilistic formulation of the diffraction and scattering of a plane wave from periodic surfaces randomly deformed by a binary sequence. The scattered wave is shown to have a stochastic Floquet form, that is a product of a periodic stationary random function and an exponential phase factor. Such a periodic stationary random function is then represented in terms of a harmonic series representation, where

coefficient functions are mutually correlated stationary processes rather than constants. The mutually correlated stationary processes are written by binary orthogonal functionals with unknown binary kernels. When the surface deformations are small compared with wavelength, an approximate solution is obtained for low order binary kernels, from which the scattering cross section, coherently diffracted power and the optical theorem were numerically calculated.

The properties of scattering from periodic random surfaces have been studied in chapters 2 and 3 for the Gaussian case but in chapter 5 for the binary case. Though the Gaussian sequence and the binary sequence are two different sequences in probability distribution, they are same in average and correlation function. Further, they have same forms of the orthogonal Hermite polynomials (4.102)-(4.24), (A.3)-(A.5) and the recurrence formulas (4.29), (A.7) up to the second order. Thus, when we determine the kernel functions neglecting the second order kernel functions, the first order Wiener kernel is same as the first order binary kernel, and the scattering properties calculated by only the first order Wiener kernel is completely identical to that given by the first order binary kernel. However, the multi-variable orthogonal polynomials and the recurrence formulas for the third order in the two case are different, we think that the second order Wiener kernel and the second order binary kernel are different. Though we have not determined the second order binary kernel, we can see the difference from the equation (2.57) and (5.28). That is because that the integral terms on the first order kernels in (5.28) do not appear at equation (2.41). As a further research problem, we will determine the second order binary kernel and compare the Gaussian case and the binary case.

Besides, for the TM incident wave, we have not discussed the binary case. The work will be remained further study.

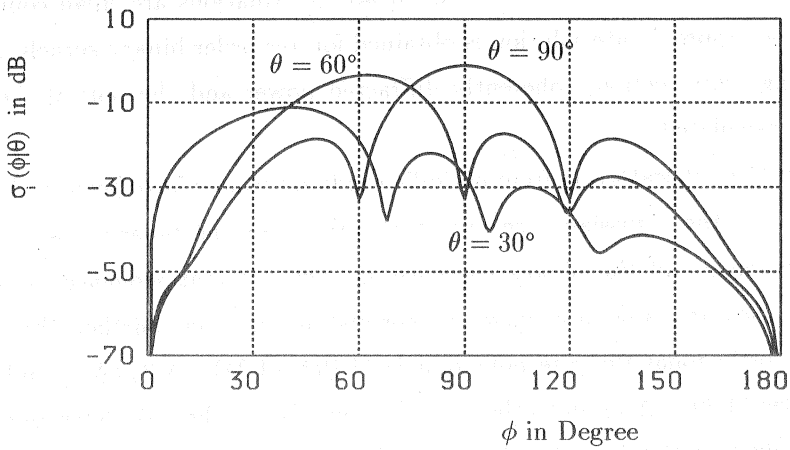

Figure 5.4: Scattering cross section against scattering angle ϕ for several angles of incidence. Parameters are $a_0 = \Lambda$, $\rho_0 = \rho_1 = \Lambda/40$ and $L = 3\Lambda$ Scattering cross section is relatively strong in the direction of specular reflection.

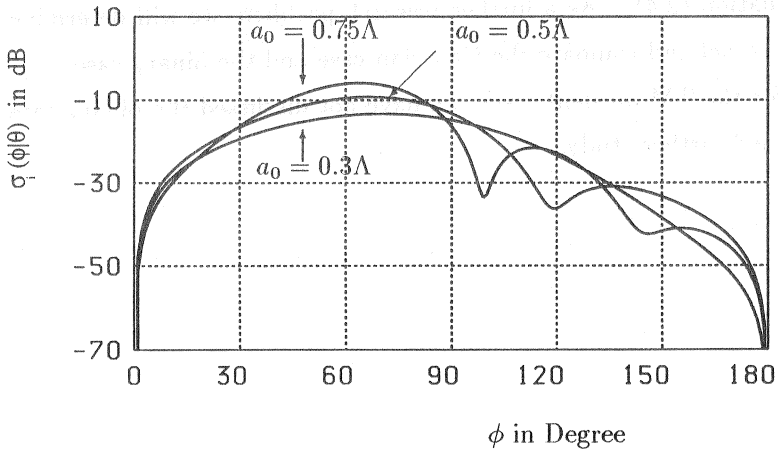

Figure 5.5: Scattering cross section for several values of a_0 with parameters $\theta = 60°$, $\rho_0 = \rho_1 = \Lambda/40$ and $L = 3\Lambda$. When the width parameter a_0 is small, no ripples appear. The number of ripples increases with the increase of a_0.

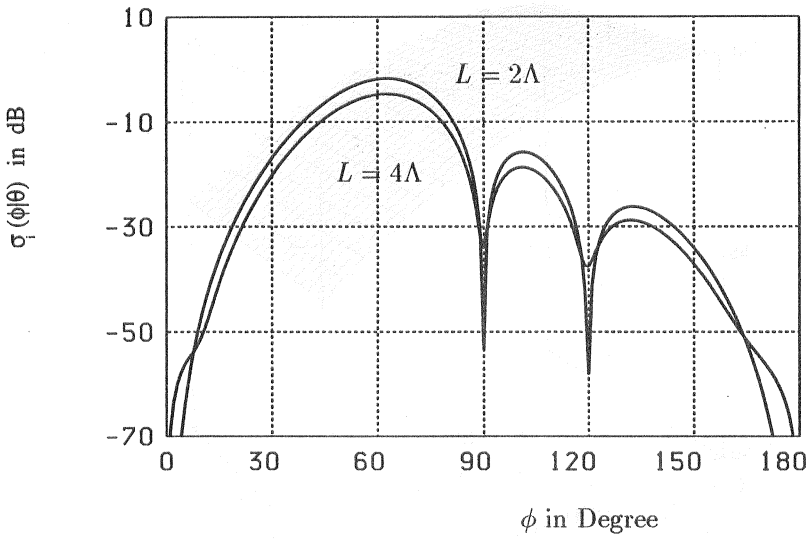

Figure 5.6: Scattering cross section for several values of period L with parameters $a_0 = \Lambda$, $\rho_0 = \rho_1 = \Lambda/40$ and $\theta = 60°$. The scattering cross section is almost inverse proportional to the period L.

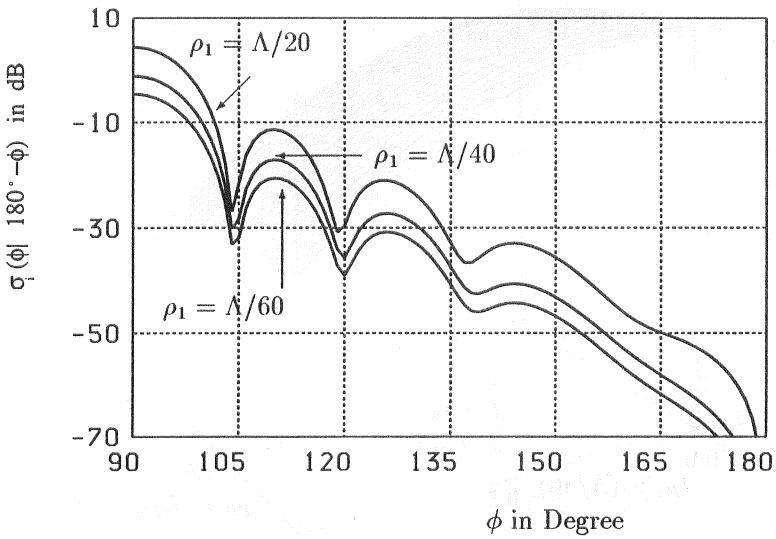

Figure 5.7: Backscattering cross section $\sigma_i(\phi|180° - \phi)$ for different values of ρ_1. Parameters are $a_0 = \Lambda$, $L = 3\Lambda$ and $\rho_0 = \Lambda/40$ The backscattering is relatively strong when the incident angle is 90°.

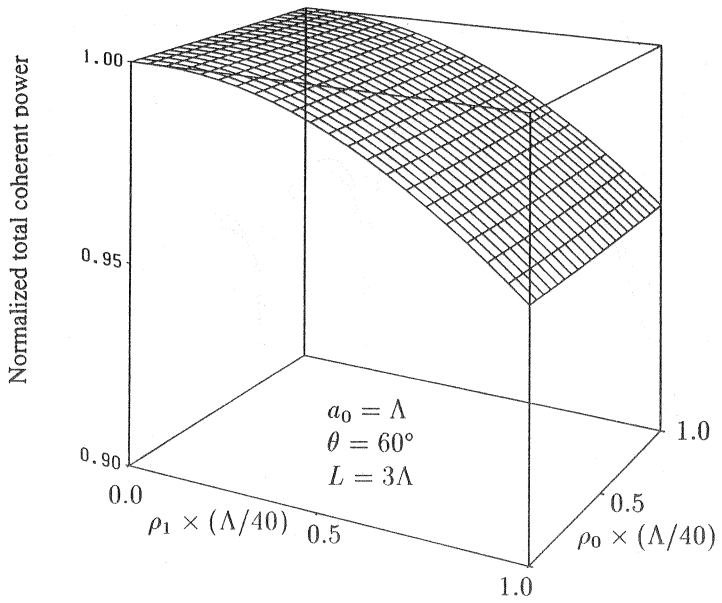

Figure 5.8: The total coherent power $\sum \mathrm{Re}[\beta_n(p)] \left|C_0^{(n)}\right|^2 / k$ against height parameters ρ_0 and ρ_1. The power decreases when the amplitude ρ_1 of random deformation increases, but has little dependence on the height ρ_0 of average periodic surface.

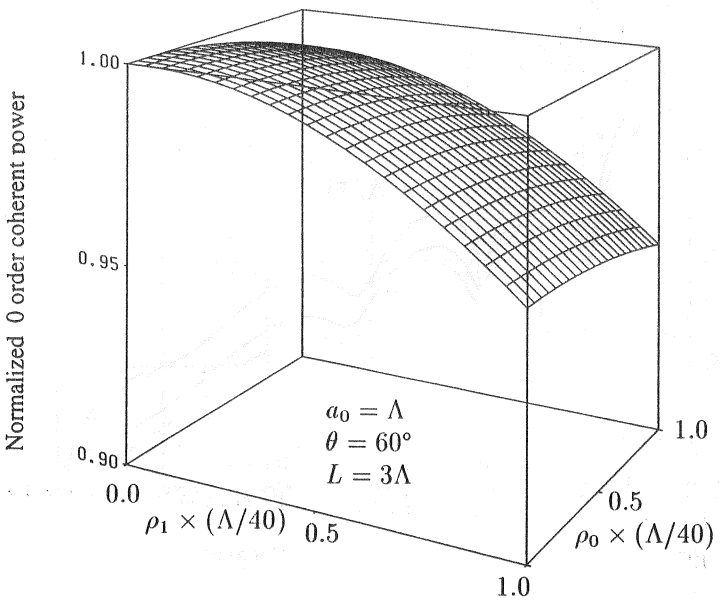

Figure 5.9: The 0 order coherently diffracted (specularly reflected) power $\mathrm{Re}[\beta_0(p)] \left|C_0^{(0)}\right|^2 / k$ against height parameters ρ_0 and ρ_1. The power decreases with increasing of ρ_0 or ρ_1. The diffraction angle is 60°.

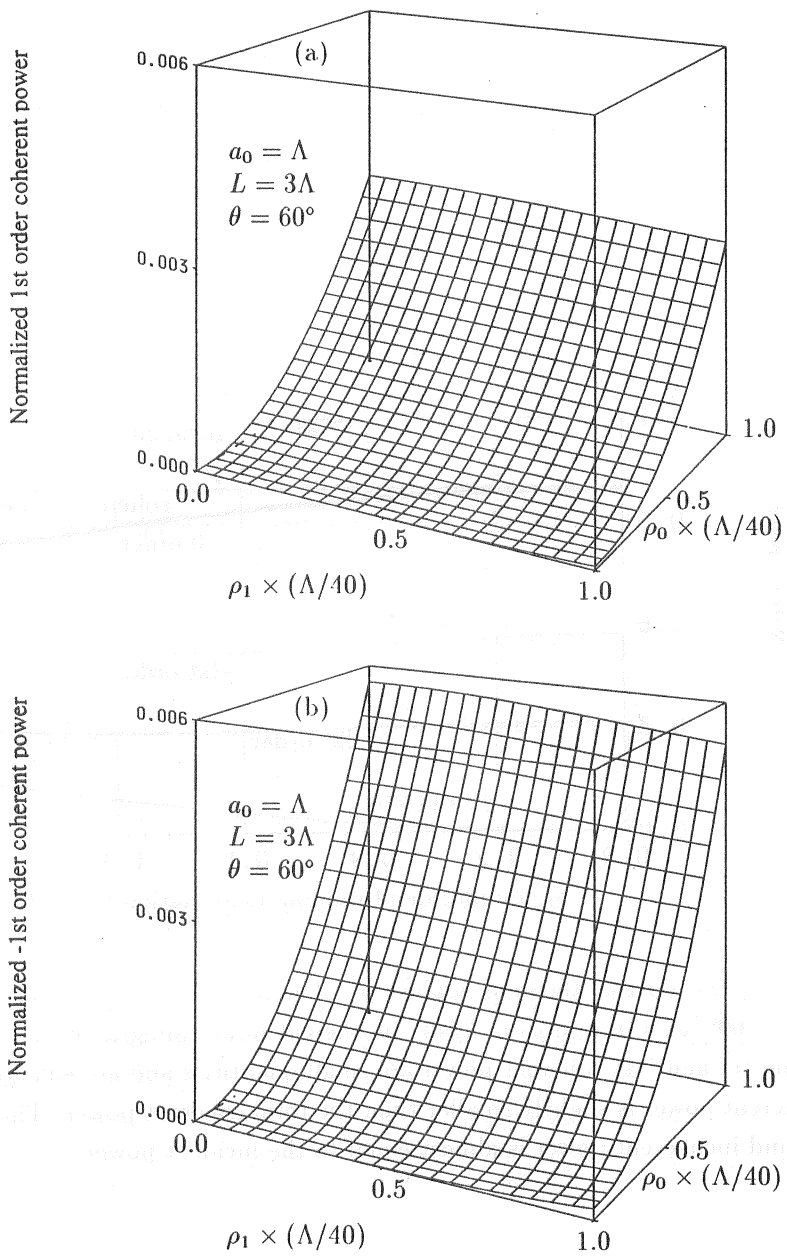

Figure 5.10: The coherent diffraction efficiencies again height parameters ρ_0 and ρ_1. (a) the 1st order diffracted power $\mathrm{Re}[\beta_1(p)]\left|C_0^{(1)}\right|^2/k$ with diffraction angle $\phi_1(0) = \cos^{-1}(5/6) \approx 33.6°$. (b) the -1st order diffracted power $\mathrm{Re}[\beta_{-1}(p)]\left|C_0^{(-1)}\right|^2/k$ with diffraction angle $\phi_{-1}(0) = \cos^{-1}(1/6) \approx 88.4°$. As ρ_1 becomes large, the coherent diffraction increases for $\rho_0 = 0$ but decreases for $\rho_0 = \Lambda/40$.

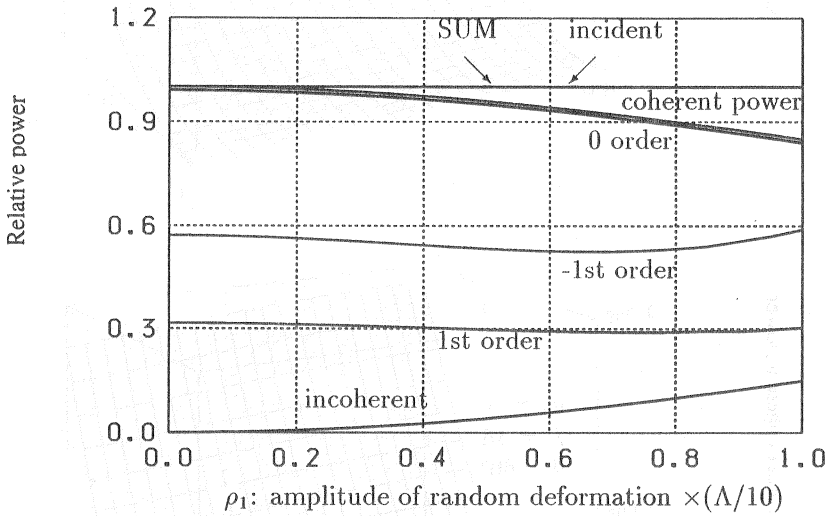

Figure 5.11: The optical theorem against ρ_1 of random deformation with parameters $L = 3\Lambda$, $\theta = 60°$, $a_0 = \Lambda$ and $\rho_0 = \Lambda/40$. Incoherent power integrated over all scattering angles. The 1st and -1st coherent power are small quantities and are enlarged 100 times. The 0 coherent power is slightly smaller than the total coherent power. The sum of total coherent and incoherent power is almost equal to the incident power.

Chapter 6

Scattering from a thin film with volume disorder

6.1 Introduction

The scattering problems may be divided into two categories by the physical reasons: surface factors and volume factors. In previous chapters, we have considered incoherent scattering of waves whose random nature was caused by random surfaces, i.e. by surface factors. In this chapter, however, we investigate random wave fields generated by a thin film with volume disorder, where the scattering takes place by volume factor. Several authors have studied the backscattering from such a random thin film by Born approximation [89] and multiple-scattering analysis [90]. However, we discuss the scattering problem by a systematic theory of stochastic functionals in this chapter.

In Sec.6.2, we consider the formulation of the problem, where the volume disorder of the thin film is mathematically given by a homogeneous Gaussian random field. We know that the diffracted wave may have Floquet's form for a periodic case and scattered wave may have stochastic Floquet's form for periodic random cases. In this chapter, we first determine a form of the scattered wave using the shift invariance property of the homogeneous Gaussian disorder. It is shown that, in regions outside of the thin film, the scattered wave has stochastic extension of Floquet's form: a product of a homogeneous random field and an exponential function. In Sec.6.3, we express such wave functions by the Wiener expansions which have deterministic coefficient functions called Wiener kernels. In Sec.6.4, we obtain several statistical properties such as coherent wave, scattering cross section and the optical theorem, which are all represented in terms of the Wiener kernels. On the other hand, the wave function inside the thin film is represented by a linear combination of homogeneous random fields with complex parameters. Since the thin film is finite in thickness, such homogeneous random fields become analytic in the complex s plane. Representing such homogeneous random field by the Wiener expansion, we approximately determine low order Wiener kernels on the basis of the analytical property of the Wiener kernels in the complex s plane. Further, we give numerical results in Sec.6.6. Then, we

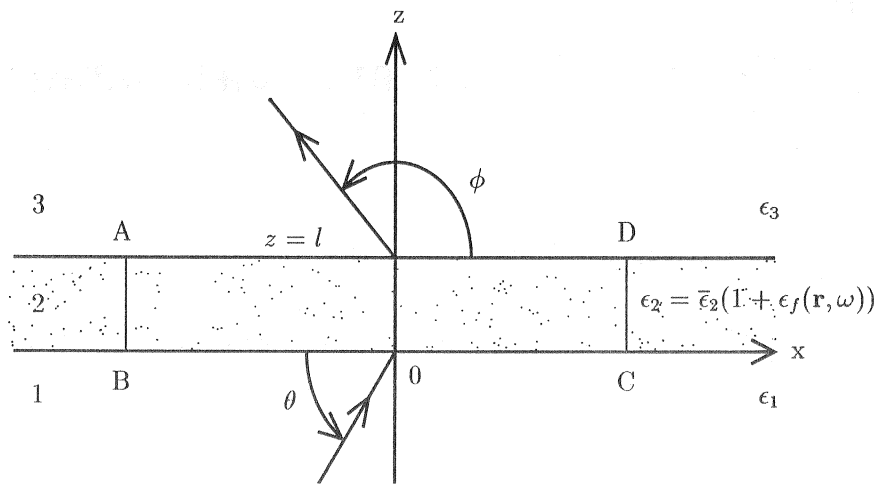

Figure 6.1: The scattering of a TE plane wave from a random thin film (thickness l). θ and ϕ are the angle of incidence and a scattering angle. The rectangle ABCD is an integral area for obtaining the optical theorem.

find that the incoherent scattering is enhanced in the directions of backscattering and specular reflection. We discuss the physical mechanism of the enhanced scattering.

6.2 Formulation of the problem

We consider a TE wave scattering from a thin film with volume disorder as shown in Fig.6.1. The media 1 and 3 have permittivities ϵ_1 and ϵ_3, respectively. Since the medium 2 is randomly inhomogeneous, we write

$$\epsilon_2 = \bar{\epsilon}_2 \left(1 + \epsilon_f(\mathbf{r}, \omega)\right), \tag{6.1}$$

where $\bar{\epsilon}_2$ is the average permittivity, $\mathbf{r} = x\mathbf{e}_x + z\mathbf{e}_z$ ($\mathbf{e}_x$ and $\mathbf{e}_z$ are the unit vectors in the x and z directions, respectively) is a two-dimensional position vector, ω denotes a probability parameter describing a sample point in the sample space Ω and $\epsilon_f(\mathbf{r}, \omega)$ is a strictly homogeneous random function representing permittivity fluctuation. We assume

that $\epsilon_f(\mathbf{r},\omega)$ has zero average and the variance σ^2,

$$\langle \epsilon_f(\mathbf{r},\omega)\rangle = 0, \quad \langle \epsilon_f^2(\mathbf{r},\omega)\rangle = \sigma^2. \tag{6.2}$$

Because $\epsilon_f(\mathbf{r},\omega)$ is a strictly stationary process, a two-dimensional translation $\mathbf{r} \to \mathbf{r}+\mathbf{a}$ of a sample function yields a shift $T^{\mathbf{a}}$ in the sample space Ω such that

$$\epsilon_f(\mathbf{r}+\mathbf{a},\omega) = \epsilon_f(\mathbf{r}, T^{\mathbf{a}}\omega), \tag{6.3}$$

which means that $\epsilon_f(\mathbf{r},\omega) = \epsilon_f(\mathbf{r}+\mathbf{a}, T^{-\mathbf{a}}\omega)$. Therefore, $\epsilon_f(\mathbf{r},\omega)$ is invariant under the translation from $(\mathbf{r},\omega)$ into $(\mathbf{r}+\mathbf{a}, T^{-\mathbf{a}}\omega)$. The fact will be used to determine the wave function later. Here, $T^{\mathbf{a}}$ describes the measure-preserving transformation taking ω into another sample point $T^{\mathbf{a}}\omega$ with the group property:

$$T^{\mathbf{a}}T^{\mathbf{b}} = T^{\mathbf{a}+\mathbf{b}}, \quad T^0 = 1(identity), \quad \mathbf{a},\mathbf{b} \in R^2. \tag{6.4}$$

Because of the layer structure as shown in Fig.6.1, we decompose T into x and z directions and introduce operators T_x and T_z by the relations:

$$\begin{aligned} &T^{a\mathbf{e}_x} = T_x^a, \quad T_x^0 = 1(identity), \quad T_x^a T_x^b = T_x^{a+b}, \\ &T^{b\mathbf{e}_z} = T_z^b, \quad T_z^0 = 1(identity), \quad T_z^a T_z^b = T_z^{a+b}, \quad -\infty < a,b < \infty. \end{aligned} \tag{6.5}$$

We denote the y component of the TE electric field by $\Psi(\mathbf{r},\omega)$, which satisfies the two-dimensional wave equation in each areas,

$$\begin{aligned} [\nabla^2 + k_1^2]\Psi(\mathbf{r},\omega) &= 0, \quad z < 0 \\ [\nabla^2 + k_2^2(1+\epsilon_f(\mathbf{r},\omega))]\Psi(\mathbf{r},\omega) &= 0, \quad l \geq z \geq 0 \\ [\nabla^2 + k_3^2]\Psi(\mathbf{r},\omega) &= 0, \quad z > l, \end{aligned} \tag{6.6}$$

where, k_1, k_2 and k_3 are wavenumbers in medium 1, medium 2 and medium 3, respectively. In medium 1, the wave function $\Psi_1(\mathbf{r},\omega)$ is written as a linear combination of the incident plane wave $e^{ipx+i\beta_1(p)z}$ which is independent of ω and the scattered wave $\Psi_s(\mathbf{r},\omega)$ that is a random function,

$$\begin{aligned} &\Psi_1(\mathbf{r},\omega) = e^{ipx+i\beta_1(p)z} + \Psi_s(\mathbf{r},\omega), \\ &p = k_1\cos\theta, \quad \beta_1(p) = \sqrt{k_1^2 - p^2}, \quad \mathrm{Im}[\beta_1(p)] \geq 0, \end{aligned} \tag{6.7}$$

where θ is the angle of incidence. Since the incident wave is a plane wave and the thin film is homogeneous in the x direction, the scattered wave becomes a product of

a homogeneous random field of x and an exponential function of x. This should be understood as a stochastic extension of Floquet's theorem for a periodic case. Therefore, wave functions in the other media are also expressed by products of homogeneous random fields of x and the exponential function of x,

$$\Psi_1(\mathbf{r},\omega) = e^{ipx}[e^{i\beta_1(p)z} + u_1(z,T_x^x\omega)], \tag{6.8}$$

$$\Psi_2(\mathbf{r},\omega) = e^{ipx}u_2(z,T_x^x\omega), \tag{6.9}$$

$$\Psi_3(\mathbf{r},\omega) = e^{ipx}u_3(z,T_x^x\omega), \tag{6.10}$$

where $u_1(z,T_x^x\omega)$, $u_2(z,T_x^x\omega)$ and $u_3(z,T_x^x\omega)$ are homogeneous random fields of x but inhomogeneous in the z direction.

Since the electromagnetic field is continuous in space, the homogeneous random functions satisfy the boundary conditions at $z=0$ and $z=l$,

$$\begin{aligned} 1+u_1(0,T_x^x\omega) &= u_2(0,T_x^x\omega), \\ i\beta_1(p)+u_1'(0,T_x^x\omega) &= u_2'(0,T_x^x\omega), \\ u_2(l,T_x^x\omega) &= u_3(l,T_x^x\omega), \\ u_2'(l,T_x^x\omega) &= u_3'(l,T_x^x\omega), \end{aligned} \tag{6.11}$$

where the prime expresses the differentiation with respect to z.

Next, let us determine a form of the wave function in the direction z within the thin film. On the basis of a fact that $\epsilon_f(\mathbf{r},\omega)$ is invariant under the translation from (z,ω) into $(z+a,T_z^{-a}\omega)$, we introduce a translation operator D_z^a acting on the function $u_2(z,\omega)$ by the relation,

$$D_z^a u_2(z,\omega) = u_2(z+a,T_z^{-a}\omega), \tag{6.12}$$

which also translates (z,ω) into $(z+a,T_z^{-a}\omega)$. Using Fourier transformation on D_z^a, we obtain

$$\int_{-z}^{-z+l} e^{-isa}D_z^a u_2(z,\omega)da = e^{isz}v(T_z^z\omega|s), \tag{6.13}$$

$$v(T_z^z\omega|s) = \int_0^l e^{isa'}u_2(a',T_z^{a'}T_z^z\omega)da', \tag{6.14}$$

where the interval $[-z,-z+l]$ of the integration is finite since $u_2(z,\omega)=0$ outside the thin film. From (6.13) and (6.14), we find that $v(T_z^z\omega|s)$ is a homogeneous random field of z and invariant under operator D_z^a

$$D_z^a v(T_z^z\omega|s) = v(T_z^z\omega|s). \tag{6.15}$$

Thus the transformation (6.13) changes the inhomogeneous random field $u_2(z,\omega)$ of z into a homogeneous random field $v(T_z^z\omega|s)$ of z. This can be also considered as a transformation into the complex s plane. In fact, $v(T_z^z\omega|s)$ becomes an analytic function of s when l is finite. From this analytical property, we will determine $v(T_z^z\omega|s)$ and the boundary values in (6.11), simultaneously. Integrating (6.13) with respect to s, we obtain the inverse transformation,

$$\frac{1}{2\pi}\int_{-\infty}^{\infty} e^{isz}v(T_z^z\omega|s)ds = \begin{cases} u_2(z,\omega), & 0 \le z \le l, \\ 0, & z < 0, z > l. \end{cases} \tag{6.16}$$

Therefore, $\Psi_2(\mathbf{r},\omega)$ can be expressed by the homogeneous random field $v(T^{\mathbf{r}}\omega|s)$,

$$\Psi_2(x,z,\omega) = \frac{e^{ipx}}{2\pi}\int_{-\infty}^{\infty} e^{isz}v(T^{\mathbf{r}}\omega|s)ds. \tag{6.17}$$

Now we take the Fourier transformation of (6.6) with respect to D_z^a over the interval $(-z,-z+l)$ to obtain an equation for $v(T_z^z\omega|s)$. By integration by parts, we get a stochastic equation for $v(T_z^z\omega|s)$ (see the next subsection)

$$\begin{aligned} & [(ip+\nabla_x)^2 + (is+\nabla_z)^2 + k_2^2(1+\epsilon_f(\mathbf{r},\omega))]v(T^{\mathbf{r}}\omega|s) \\ = & -[e^{-isl}u_2'(l,T^{\mathbf{r}}T_z^{-l}\omega) - u_2'(0,T^{\mathbf{r}}\omega)] - (is+\nabla_z)[e^{-isl}u_2(l,T^{\mathbf{r}}T_z^{-l}\omega) - u_2(0,T^{\mathbf{r}}\omega)] \\ = & [i\beta_1(p) + u_1'(0,\omega)] + (is+\nabla_z)[1+u_1(0,T^{\mathbf{r}}\omega)] \\ & -e^{-isl}[u_3'(l,T^{\mathbf{r}}T_z^{-l}\omega) + (is+\nabla_z)u_3(l,T^{\mathbf{r}}T_z^{-l}\omega)], \end{aligned} \tag{6.18}$$

where $\nabla_x = \partial/\partial x$ and $\nabla_z = \partial/\partial z$. Here we have applied the boundary conditions in (6.11) to get (6.18).

6.2.1 Derivation of the equation (2.18)

Let us calculate the Fourier transformation of (6.6) with respect to D_z^a over the interval $(-z,-z+l)$. Since $\epsilon_f(\mathbf{r},\omega)$ is invariant under the translation operator D_z^a by (6.3), we obtain

$$\begin{aligned} & \int_{-z}^{-z+l} e^{-isa}D_z^a[\nabla_x^2 + k_2^2(1+\epsilon_f(\mathbf{r},\omega))]\Psi(\mathbf{r},\omega)da \\ = & \int_{-z}^{-z+l} e^{-isa}D_z^a[(ip+\nabla_x)^2 + \nabla_z^2 + k_2^2(1+\epsilon_f(\mathbf{r},\omega))]u_2(z,T_x^x\omega)da \\ = & e^{isz}[(ip+\nabla_x)^2 + k_2^2(1+\epsilon_f(\mathbf{r},\omega))]v(T^{\mathbf{r}}\omega) + \int_{-z}^{-z+l} e^{-isa}D_z^a\nabla_z^2u_2(z,T_x^x\omega)da, \end{aligned} \tag{6.19}$$

where (6.19) is obtained from (6.9) and (6.13). Next, for calculating the integral in (6.19), we consider the Fourier transformation of $\nabla_z u_2(z+a, T_z^{-a}T_x^x\omega)$,

$$\begin{aligned}
&\int_{-z}^{-z+l} e^{-isa}\nabla_z u_2(z+a, T_z^{-a}T_x^x\omega)da \\
&= \int_{-z}^{-z+l} e^{-isa}\frac{\partial}{\partial a}u_2(z+a, T_z^{-a}T_x^x\omega)da - \frac{\partial}{\partial b}\int_{-z}^{-z+l} e^{-isa}u_2(z+a, T_z^{-a-b}T_x^x\omega)da\Big|_{b=0} \\
&= e^{-isa}u_2(z+a, T_z^{-a}T_x^x\omega)\Big|_{a=-z}^{a=-z+l} + is\int_{-z}^{-z+l} e^{-isa}u_2(z+a, T_z^{-a}T_x^x\omega)da \\
&\quad -\frac{\partial}{\partial b}e^{isz}v(T^{\mathbf{r}}T^{-b}\omega)\Big|_{b=0} \qquad (6.20) \\
&= e^{-isa}u_2(z+a, T_z^{-a}T_x^x\omega)\Big|_{a=-z}^{a=-z+l} + e^{isz}(is+\nabla_z)v(T^{\mathbf{r}}\omega) \\
&= e^{-isa}u_2(z+a, T_z^{-a}T_x^x\omega)\Big|_{a=-z}^{a=-z+l} \\
&\quad + e^{isz}(is+\nabla_z)\Big[e^{-isz}\int_{-z}^{-z+l} e^{-isa}u_2(z+a, T_z^{-a}T_x^x\omega)da\Big], \qquad (6.21)
\end{aligned}$$

where we have used integration by parts and (6.13) to get (6.20). Replacing $u_2(z+a, T_z^{-a}T_x^x\omega)$ by $\nabla_z u_2(z+a, T_z^{-a}T_x^x\omega)$ in (6.20) and (6.21), we have

$$\begin{aligned}
&\int_{-z}^{-z+l} e^{-isa}D_z^a\nabla_z^2 u_2(z, T_x^x\omega)da = e^{-isa}\nabla_z u_2(z+a, T_z^{-a}T_x^x\omega)\Big|_{a=-z}^{a=-z+l} \\
&\quad + e^{isz}(is+\nabla_z)\Big[e^{-isz}\int_{-z}^{-z+l} e^{-isa}\nabla_z u_2(z+a, T_z^{-a}T_x^x\omega)da\Big] \qquad (6.22) \\
&= e^{isz}[e^{-isl}u_2'(l, T_z^{-l}T^{\mathbf{r}}\omega) - u_2'(0, T^{\mathbf{r}}\omega)] \\
&\quad + e^{isz}(is+\nabla_z)\Big[e^{-isz}e^{-isa}u_2(z+a, T_z^{-a}T_x^x\omega)\Big|_{a=-z}^{a=-z+l}\Big] \\
&\quad + e^{isz}(is+\nabla_z)^2\Big[e^{-isz}\int_{-z}^{-z+l} e^{-isa}u_2(z+a, T_z^{-a}T_x^x\omega)da\Big] \qquad (6.23) \\
&= e^{isz}[e^{-isl}u_2'(l, T_z^{-l}T^{\mathbf{r}}\omega) - u_2'(0, T^{\mathbf{r}}\omega)] \\
&\quad + e^{isz}(is+\nabla_z)[e^{-isl}u_2(l, T_z^{-l}T^{\mathbf{r}}\omega) - u_2(0, T^{\mathbf{r}}\omega)] + e^{isz}(is+\nabla_z)^2 v(T^{\mathbf{r}}\omega). \qquad (6.24)
\end{aligned}$$

Note that (6.23) is obtained by applying (6.21) again. Substituting (6.24) into (6.19) and using the boundary conditions in (6.11), we easily obtain the equation (6.18).

Here, we should note that $\nabla_z u_2(l, T_z^{-l}T^{\mathbf{r}}\omega)$ and $u_2'(l, T_z^{-l}T^{\mathbf{r}}\omega)$ are different. By definition, we obtain

$$u_2'(l, T_z^{-l}T^{\mathbf{r}}\omega) = \frac{\partial u_2(z,\omega)}{\partial z}\Big|_{z=l,\omega=T_z^{-l}T^{\mathbf{r}}\omega}, \qquad (6.25)$$

which means that the derivative $\partial u_2(z,\omega)/\partial z$ at $z=l$ is translated by the shift from ω into $T^{-l}T^{\mathbf{r}}\omega$. In other words, we first calculate the derivative $\partial u_2(z,\omega)/\partial z$ at $z=l$, and

then translate it from ω into $T^{-l}T^{\mathbf{r}}\omega$. On the other hand, we obtain

$$\nabla_z u_2(l, T_z^{-l}T^{\mathbf{r}}\omega) = \frac{\partial u_2(l, T_z^{-l}T^{\mathbf{r}}\omega)}{\partial z}, \tag{6.26}$$

where we first shift $u_2(l,\omega)$ into $u_2(l, T^{-l}T^{\mathbf{r}}\omega)$, and then calculate it's derivative with respect to z.

6.3 Stochastic Functional

We assume that the permittivity $\epsilon_f(\mathbf{r},\omega)$ is a Gaussian process generated by the complex Gaussian random measure $dB(\mathbf{\Lambda},\omega)$ (see Ref.[61]) and is represented as a Wiener integral,

$$\epsilon_f(\mathbf{r},\omega) = \int_{R^2} e^{i\mathbf{\Lambda}\cdot\mathbf{r}} G(\mathbf{\Lambda}) dB(\mathbf{\Lambda},\omega), \tag{6.27}$$

where $\mathbf{\Lambda} = \Lambda_x \mathbf{e}_x + \Lambda_z \mathbf{e}_z$ is a two-dimensional vector. The $dB(\mathbf{\Lambda},\omega)$ has zero average, δ correlation function and shift invariance property under $T^{\mathbf{r}}$,

$$\begin{aligned}
\langle dB(\mathbf{\Lambda},\omega)\rangle &= 0, && (6.28)\\
\langle dB(\mathbf{\Lambda},\omega) dB^*(\mathbf{\Lambda}',\omega)\rangle &= \delta(\mathbf{\Lambda}-\mathbf{\Lambda}') d\mathbf{\Lambda} d\mathbf{\Lambda}', && (6.29)\\
dB(\mathbf{\Lambda}, T^{\mathbf{r}}\omega) &= e^{i\mathbf{\Lambda}\cdot\mathbf{r}} dB(\mathbf{\Lambda},\omega), && (6.30)\\
dB(\mathbf{\Lambda},\omega) &= dB^*(-\mathbf{\Lambda},\omega). && (6.31)
\end{aligned}$$

When $\epsilon_f(\mathbf{r},\omega)$ is isotropic and $|G(\mathbf{\Lambda})|^2 = |G(|\mathbf{\Lambda}|)|^2$ holds, we have the correlation function of $\epsilon_f(\mathbf{r},\omega)$,

$$\begin{aligned}
R_\epsilon(|\mathbf{r}-\mathbf{r}'|) &= \langle \epsilon_f(\mathbf{r},\omega)\epsilon_f(\mathbf{r}',\omega)\rangle \\
&= 2\pi \int_0^\infty J_0(\Lambda|\mathbf{r}-\mathbf{r}'|)|G(\Lambda)|^2 \Lambda d\Lambda, && (6.32)
\end{aligned}$$

where $J_0(\cdot)$ is Bessel function.

Next, we consider $u_1(z, T_x^x\omega)$ and $u_3(z, T_x^x\omega)$ as functionals of $dB(\mathbf{\Lambda},\omega)$. For making $e^{ipx}u_1(z, T_x^x\omega)$ and $e^{ipx}u_3(z, T_x^x\omega)$ satisfy the wave equations (6.6) and the radiation condition for $|z| \to \infty$, we write Wiener expansions [1] for $u_1(z, T_x^x\omega)$ and $u_3(z, T_x^x\omega)$ as

$$\begin{aligned}
u_1(z, T_x^x\omega) &= A_0 e^{-i\beta_1(p)z} + \int A_1(\mathbf{\Lambda}) e^{i\Lambda_x x - i\beta_1(p+\Lambda_x)z} h^{(1)}[dB(\mathbf{\Lambda})] \\
&+ \int\int A_2(\mathbf{\Lambda}_1,\mathbf{\Lambda}_2) e^{i(\Lambda_{x1}+\Lambda_{x2})x - i\beta_1(p+\Lambda_{x1}+\Lambda_{x2})z} h^{(2)}[dB(\mathbf{\Lambda}_1), dB(\mathbf{\Lambda}_2)] + \cdots, && (6.33)
\end{aligned}$$

[1] Note that these Wiener expansions are the two-dimensional form on multiple Wiener integrals.

$$u_3(z, T_x^x\omega) = C_0 e^{i\beta_3(p)z} + \int C_1(\mathbf{\Lambda}) e^{i\Lambda_x x + i\beta_3(p+\Lambda_x)z} h^{(1)}[dB(\mathbf{\Lambda})]$$
$$+ \int\int C_2(\mathbf{\Lambda}_1, \mathbf{\Lambda}_2) e^{i(\Lambda_{x1}+\Lambda_{x2})x + i\beta_3(p+\Lambda_{x1}+\Lambda_{x2})z} h^{(2)}[dB(\mathbf{\Lambda}_1), dB(\mathbf{\Lambda}_2)] + \cdots, \quad (6.34)$$
$$\beta_3(p) = \sqrt{k_3^2 - p^2}, \qquad \mathrm{Im}[\beta_3(p)] \geq 0,$$

where A_0, C_0, $A_1(\mathbf{\Lambda})$, $C_1(\mathbf{\Lambda})$, $\cdots$ are deterministic coefficients called Wiener kernels and $h^{(1)}[dB(\mathbf{\Lambda})]$, $h^{(2)}[dB(\mathbf{\Lambda}_1), dB(\mathbf{\Lambda}_2)], \cdots$ are Wiener differentials. Here, we have dropped ω in $dB(\mathbf{\Lambda}, \omega)$.

For solving (6.18), we need functional expressions for $u_1'(0,\omega)$, $u_1(0, T^{\mathbf{r}}\omega)$, $u_3'(l, T^{\mathbf{r}}T_z^{-l}\omega)$ and $u_3(l, T^{\mathbf{r}}T_z^{-l}\omega)$. These functional expressions are easily obtained from (6.33), (6.34) and the translation property (6.30). Similarly, we regard $v(T^{\mathbf{r}}\omega)$ as a functional of $dB(\mathbf{\Lambda}, \omega)$, and we write its Wiener expansion as

$$v(T^{\mathbf{r}}\omega|s) = F_0(s) + \int F_1(\mathbf{\Lambda}|s) e^{i\mathbf{\Lambda}\cdot\mathbf{r}} dB(\mathbf{\Lambda})$$
$$+ \int\int F_2(\mathbf{\Lambda}_1, \mathbf{\Lambda}_2|s) e^{i(\mathbf{\Lambda}_1+\mathbf{\Lambda}_2)\cdot\mathbf{r}} h^{(2)}[dB(\mathbf{\Lambda}_1), dB(\mathbf{\Lambda}_2)] + \cdots. \quad (6.35)$$

Since $v(T^{\mathbf{r}}\omega|s)$ is an analytic function on the s plane, Wiener kernels $F_0(s)$, $F_1(\mathbf{\Lambda}|s)$, $\cdots$ are assumed to be analytic on the s plane. By (6.33), (6.34) and (6.35) the scattered wave can be determined as a stochastic function, if we determine coefficients A_0, C_0, $A_1(\mathbf{\Lambda})$, $C_1(\mathbf{\Lambda})$, $F_0(s)$, $F_1(\mathbf{\Lambda}|s)$, etc.

6.4 Coherent wave, optical theorem and scattering cross section

In the preceding section, we have obtained a representation of the scattered wave as a stochastic functional. In this section, we will obtain representations for the coherent wave, optical theorem and incoherent scattering cross section. From the orthogonality of Wiener differentials, the coherent wave (average wave) can be expressed as

$$\langle \Psi_1(\mathbf{r}, \omega) \rangle = e^{ipx}[e^{i\beta_1(p)z} + A_0 e^{-i\beta_1(p)z}],$$
$$\langle \Psi_2(\mathbf{r}, \omega) \rangle = \frac{e^{ipx}}{2\pi} \int_{-\infty}^{\infty} e^{isz} F_0(s) ds,$$
$$\langle \Psi_3(\mathbf{r}, \omega) \rangle = C_0 e^{i[px + \beta_3(p)z]}. \quad (6.36)$$

Clearly, A_0 is the coherent reflection coefficient and C_0 is the coherent transmission coefficient. Next, we consider the optical theorem. For a loss-less case, it holds that

$$\mathrm{div}\left[\mathrm{Im}\left(\frac{\Psi_2^*}{k_2} \cdot \mathrm{grad}\Psi_2\right)\right] = 0, \quad (6.37)$$

which is deduced from wave equation (6.6). Integrating (6.37) over the box ABCDA in Fig.6.1 and applying the Gauss theorem, we obtain

$$\left(\int_{\mathrm{AD}} dx + \int_{\mathrm{DC}} dz + \int_{\mathrm{CB}} dx + \int_{\mathrm{BA}} dz\right) \mathrm{Im}\left(\frac{\Psi_2^*}{k_2} \cdot \mathrm{grad}\Psi_2\right) = 0. \tag{6.38}$$

Because the integral intervals of DC and BA are finite, calculating the integral per unit length (of BC), we have

$$\lim_{\substack{|\mathrm{OB}|\to\infty \\ |\mathrm{OC}|\to\infty}} \frac{1}{|\mathrm{BC}|}\left(\int_{\mathrm{AD}} dx + \int_{\mathrm{CB}} dx\right) \mathrm{Im}\left(\frac{\Psi_2^*}{k_2} \cdot \mathrm{grad}\Psi_2\right) = 0, \tag{6.39}$$

where |OB|, |OC| and |BC| are the lengths of intervals OB, OC and BC, respectively. By ergodic theorem that the mean over space is equal to the ensemble mean over all sample points, (6.39) becomes

$$\frac{1}{k_2}\langle \mathrm{Im}(\Psi_2^* \cdot \mathrm{grad}\Psi_2)\rangle = 0. \tag{6.40}$$

Considering the boundary conditions (6.11) and substituting the Wiener expansions (6.33) and (6.34) into (6.40), we get the optical theorem.

$$\begin{aligned} \sin\theta \;=\; & \sin\theta|A_0|^2 + \mathrm{Re}[\beta_3(k_1\cos\theta)]|C_0|^2/k_1 \\ & + \frac{1}{2\pi}\int_{\pi}^{2\pi} \sigma_b(\phi|\theta)d\phi + \frac{1}{2\pi}\int_0^{\pi} \sigma_f(\phi|\theta)d\phi, \end{aligned} \tag{6.41}$$

where ϕ is a scattering angle. The left-hand side is the incident power per unit length, whereas the first and second terms in the right hand side are coherently reflected and transmitted power, respectively. The $\sigma_f(\phi|\theta)$ and $\sigma_b(\phi|\theta)$ are scattering cross sections in the forward ($0 < \phi < \pi$) and backward ($\pi < \phi < 2\pi$) directions, respectively.

$$\sigma_b(\phi|\theta) = 2\pi k_1 \sin^2\phi \int_{-\infty}^{\infty} |A_1\left(k_1(\cos\phi - \cos\theta)\mathbf{e}_x + \lambda_z\mathbf{e}_z\right)|^2 d\lambda_z \;+\cdots, \tag{6.42}$$

$$\sigma_f(\phi|\theta) = \frac{2\pi k_3^2 \sin^2\phi}{k_1} \int_{-\infty}^{\infty} |C_1\left((k_3\cos\phi - k_1\cos\theta)\mathbf{e}_x + \lambda_z\mathbf{e}_z\right)|^2 d\lambda_z + \cdots. \tag{6.43}$$

We will calculate scattering cross section by use of the first order Wiener kernels.

6.5 Approximate solution

For concrete discussion, we assume an isotropic Gaussian correlation function as

$$R_\epsilon(r) = \sigma^2 \exp\left(-\frac{r^2}{\kappa^2}\right), \tag{6.44}$$

where κ is the correlation length. Substituting (6.33), (6.34) and (6.35) into (6.18), we obtain a hierarchy of equations for F_n's

the zero order equation

$$\begin{aligned}&[k_2^2-p^2-s^2]F_0(s)+k_2^2\int G^*(\mathbf{\Lambda})F_1(\mathbf{\Lambda}|s)d\mathbf{\Lambda}\\ =\;& i[s+\beta_1(p)]+i[s-\beta_1(p)]A_0-i[s+\beta_3(p)]e^{i(\beta_3(p)-s)l}C_0,\end{aligned}\tag{6.45}$$

the first order equation

$$\begin{aligned}&[k_2^2-(p+\Lambda_x)^2-(s+\Lambda_z)^2]F_1(\mathbf{\Lambda}|s)+k_2^2G(\mathbf{\Lambda})F_0(s)\\ &+2k_2^2\int G^*(\mathbf{\Lambda}')F_2(\mathbf{\Lambda},\mathbf{\Lambda}'|s)d\mathbf{\Lambda}'\\ =\;& i[s+\Lambda_z-\beta_1(p+\Lambda_x)]A_1(\mathbf{\Lambda})\\ &-i[s+\Lambda_z+\beta_3(p+\Lambda_x)]e^{i(\beta_3(p+\Lambda_x)-\Lambda_z-s)l}C_1(\mathbf{\Lambda}),\end{aligned}\tag{6.46}$$

the second order equation

$$\begin{aligned}&[k_2^2-(p+\Lambda_{x1}+\Lambda_{x2})^2-(s+\Lambda_{z1}+\Lambda_{z2})^2]F_2(\mathbf{\Lambda}_1,\mathbf{\Lambda}_2|s)\\ &+\frac{k_2^2}{2}[G(\mathbf{\Lambda}_1)F_1(\mathbf{\Lambda}_2|s)+G(\mathbf{\Lambda}_2)F_1(\mathbf{\Lambda}_1|s)]\\ &+3k_2^2\int G^*(\mathbf{\Lambda}')F_3(\mathbf{\Lambda}_1,\mathbf{\Lambda}_2,\mathbf{\Lambda}'|s)d\mathbf{\Lambda}'\\ =\;& i[s+\Lambda_{z1}+\Lambda_{z2}-\beta_1(p+\Lambda_{x1}+\Lambda_{x2})]A_2(\mathbf{\Lambda}_1,\mathbf{\Lambda}_2)\\ &-i[s+\Lambda_{z1}+\Lambda_{z2}+\beta_3(p+\Lambda_{x1}+\Lambda_{x2})]e^{i[\beta_3(p+\Lambda_{x1}+\Lambda_{x2})-\Lambda_{z1}-\Lambda_{z2}-s]l}C_2(\mathbf{\Lambda}_1,\mathbf{\Lambda}_2)\\ &+\cdots.\end{aligned}\tag{6.47}$$

Neglecting the integral term and the right-hand side in (6.46), we roughly obtain

$$F_1(\mathbf{\Lambda}|s)\approx-\frac{k_2^2G(\mathbf{\Lambda})F_0(s)}{k_2^2-(p+\Lambda_x)^2-(s+\Lambda_z)^2}.\tag{6.48}$$

Because (6.48) has poles in the s-plane, (6.48) can't become an approximation solution of $F_1(\mathbf{\Lambda}|s)$. But it can be used as the correction of $F_0(s)$. Substituting (6.48) into (6.45), we have

$$\begin{aligned}&[k_2^2-p^2-s^2+m(\sqrt{p^2+s^2})]F_0(s)\\ =\;& i[s+\beta_1(p)]+i[s-\beta_1(p)]A_0-i[s+\beta_3(p)]e^{i(\beta_3(p)-s)l}C_0,\end{aligned}\tag{6.49}$$

where $m(\sqrt{p^2+s^2})$ is the mass operator describing a multiple-scattering effect. For an isotropic random medium, we obtain

$$m(\sqrt{p^2+s^2})\;=\;k_2^4\int_{R^2}\frac{|G(\mathbf{\Lambda})|^2}{(s+\Lambda_z)^2+(p+\Lambda_x)^2-k_2^2}d\mathbf{\Lambda}\tag{6.50}$$

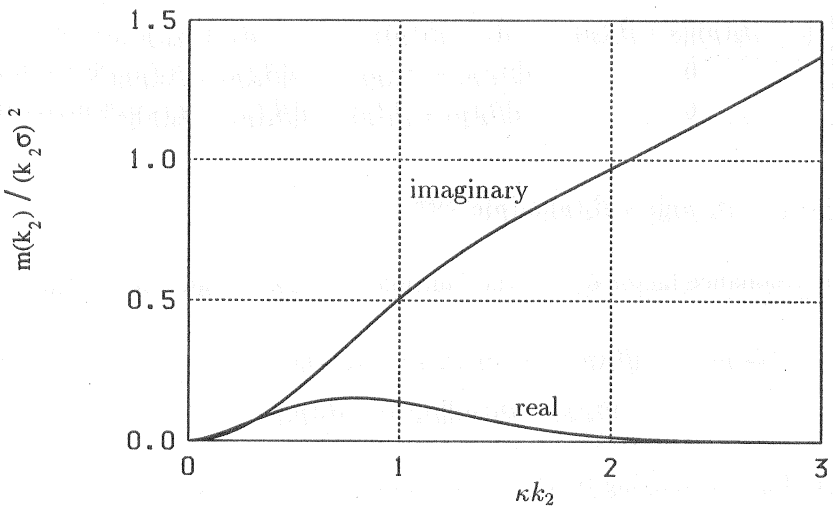

Figure 6.2: The real and imaginary parts of $m(k_2)$ for Gaussian correlation function. κ is the correlation length. Because the imaginary of $m(k_2)$ is positive, the coherent wave decays exponentially.

$$= \frac{i\pi k_2^4}{2}\int_0^\infty H_0^{(1)}(k_2 r)J_0(r\sqrt{p^2+s^2})R_\epsilon(r)r\,dr. \tag{6.51}$$

Particularly, the mass operator $m(k_2)$ can is calculated as

$$m(k_2) = \frac{i\pi k_2^2\sigma^2}{2}\int_0^\infty H_0^{(1)}(r_1)J_0(r_1)\exp\left(-\frac{r_1^2}{\kappa^2 k_2^2}\right)r_1 dr_1, \tag{6.52}$$

which is shown in Fig.6.2.

Now, we determine $F_0(s)$, A_0 and C_0 from (6.49). The coefficient of $F_0(s)$ in (6.49) has zeros

$$s \approx \pm\bar{\beta}_2(p), \quad \bar{\beta}_2(p) = \sqrt{k_2^2 - p^2 + m(k_2)}. \tag{6.53}$$

Since $F_0(s)$ is an analytic function of s, the right-hand side of (6.49) must vanish when $s = \pm\bar{\beta}_2(p)$. This fact and (6.49) yield a matrix equation for $F_0(s)$, A_0 and C_0

$$\mathbf{D}(s,p)\cdot\begin{bmatrix} F_0(s) \\ A_0 \\ C_0 \end{bmatrix} = \begin{bmatrix} -i(s+\beta_1(p)) \\ -i[\bar{\beta}_2(p)+\beta_1(p)] \\ i[\bar{\beta}_2(p)-\beta_1(p)], \end{bmatrix}, \tag{6.54}$$

where $\mathbf{D}(s,p)$ is a 3×3 matrix

$$\mathbf{D}(s,p)=\begin{bmatrix}[s-\bar{\beta}_2(p)][s+\bar{\beta}_2(p)] & i(s-\beta_1(p)) & -i(s+\beta_3(p))e^{i[\beta_3(p)-s]l}\\ 0 & i[\bar{\beta}_2(p)-\beta_1(p)] & -i[\bar{\beta}_2(p)+\beta_3(p)]e^{i[\beta_3(p)-\bar{\beta}_2(p)]l}\\ 0 & -i[\bar{\beta}_2(p)+\beta_1(p)] & i[\bar{\beta}_2(p)-\beta_3(p)]e^{i[\beta_3(p)+\bar{\beta}_2(p)]l}\end{bmatrix}, \tag{6.55}$$

$$\det[\mathbf{D}(s,p)]=[s-\bar{\beta}_2(p)][s+\bar{\beta}_2(p)]\Delta(p)e^{i\beta_3(p)l}. \tag{6.56}$$

Here $\Delta(p)$ is the resonance factor due to the multiple reflection inside the thin film

$$\begin{aligned}\Delta(p) &= [\bar{\beta}_2(p)+\beta_1(p)][\bar{\beta}_2(p)+\beta_3(p)]e^{-i\bar{\beta}_2(p)l}\\ &\quad -[\bar{\beta}_2(p)-\beta_1(p)][\bar{\beta}_2(p)-\beta_3(p)]e^{i\bar{\beta}_2(p)l},\end{aligned} \tag{6.57}$$

which is shown in Fig.6.3. Solving (6.54), we obtain the zero order Wiener kernels $F_0(s)$, A_0 and C_0

$$A_0=-\frac{[\bar{\beta}_2(p)-\beta_1(p)][\bar{\beta}_2(p)+\beta_3(p)]e^{-i\bar{\beta}_2(p)l}-[\bar{\beta}_2(p)+\beta_1(p)][\bar{\beta}_2(p)-\beta_3(p)]e^{i\bar{\beta}_2(p)l}}{\Delta(p)}, \tag{6.58}$$

$$C_0=\frac{4\beta_1(p)\bar{\beta}_2(p)e^{-i\beta_3(p)l}}{\Delta(p)}, \tag{6.59}$$

$$F_0(s)=\frac{2i\beta_1(p)}{\Delta(p)}Q_0(s,p), \tag{6.60}$$

where

$$Q_0(s,p)=\left\{[\bar{\beta}_2(p)-\beta_3(p)]\frac{e^{-isl}-e^{i\bar{\beta}_2(p)l}}{s+\bar{\beta}_2(p)}+[\bar{\beta}_2(p)+\beta_3(p)]\frac{e^{-isl}-e^{-i\bar{\beta}_2(p)l}}{s-\bar{\beta}_2(p)}\right\}. \tag{6.61}$$

Clearly, $Q_0(s,p)$ and $F_0(s)$ are analytic in the complex s-plane. Since $Q_0(s,p)$ is a linear combination of finite Fourier transforms of $e^{\pm\bar{\beta}_2(p)(s-l)}$, $F_0(s)$ represents the coherent wave consisting of up and down going waves with 'dressed' propagation constant $\bar{\beta}_2(p)$.

Substituting (6.60) into (6.46) and using inverse Fourier transform, we determine the coherent wave within the thin film $(0<z<l)$,

$$\langle\Psi_2(\mathbf{r},\omega)\rangle=-\frac{2\beta_1(p)e^{ipx}}{\Delta(p)}\left\{[\bar{\beta}_2(p)-\beta_3(p)]e^{-i\bar{\beta}_2(p)(z-l)}+[\bar{\beta}_2(p)+\beta_3(p)]e^{i\bar{\beta}_2(p)(z-l)}\right\}, \tag{6.62}$$

where the first term of the right-hand side is a down going wave and the second term is an up going wave, due to the multiple reflections within the thin film. The coherent wave decreases exponentially because the imaginary part of the renormalized $\bar{\beta}_2(p)$ is positive.

Let us obtain the first order solution. Neglecting the integral term and the right-hand side in (6.47), we roughly obtain

$$F_2(\mathbf{\Lambda}_1,\mathbf{\Lambda}_2|s) \approx -\frac{k_2^2}{2}\frac{G(\mathbf{\Lambda}_1)F_1(\mathbf{\Lambda}_2|s)+G(\mathbf{\Lambda}_2)F_1(\mathbf{\Lambda}_1|s)}{k_2^2-(p+\Lambda_{x1}+\Lambda_{x2})^2-(s+\Lambda_{z1}+\Lambda_{z2})^2}. \tag{6.63}$$

Substituting this into (6.46) we have

$$\begin{aligned}
&\left[k_2^2-(p+\Lambda_x)^2-(s+\Lambda_z)^2+m\left(\sqrt{(p+\Lambda_x)^2+(s+\Lambda_z)^2}\right)\right]F_1(\mathbf{\Lambda}|s)\\
&+k_2^2G(\mathbf{\Lambda})F_0(s)\\
\approx\ & i[s+\Lambda_z-\beta_1(p+\Lambda_x)]A_1(\mathbf{\Lambda})\\
&-i[s+\Lambda_z+\beta_3(p+\Lambda_x)]e^{i(\beta_3(p+\Lambda_x)-\Lambda_z-s)l}C_1(\mathbf{\Lambda}).
\end{aligned} \tag{6.64}$$

From (6.64), we determine $F_1(\mathbf{\Lambda}|s)$, $A_1(\mathbf{\Lambda})$ and $C_1(\mathbf{\Lambda})$. The coefficient of $F_1(\mathbf{\Lambda}|s)$ in (6.64) has zeros,

$$s \approx -\Lambda_z \pm \bar{\beta}_2(p+\Lambda_x). \tag{6.65}$$

Since $F_1(\mathbf{\Lambda}|s)$ is an analytic function, the right-hand side of (6.64) must be zero when $s=\pm\bar{\beta}_2(p+\Lambda_x)$. This means that $F_1(\mathbf{\Lambda}|s)$, $A_1(\mathbf{\Lambda})$ and $C_1(\mathbf{\Lambda})$ satisfy a matrix equation

$$\mathbf{D}(s+\Lambda_z,p+\Lambda_x)\cdot\begin{bmatrix}F_1(\mathbf{\Lambda}|s)\\A_1(\mathbf{\Lambda})\\C_1(\mathbf{\Lambda})\end{bmatrix}=k_2^2G(\mathbf{\Lambda})\begin{bmatrix}F_0(s)\\F_0(-\Lambda_z+\bar{\beta}_2(p+\Lambda_x))\\F_0(-\Lambda_z-\bar{\beta}_2(p+\Lambda_x))\end{bmatrix}. \tag{6.66}$$

From (6.66), we have the first order Wiener kernels

$$\begin{aligned}
A_1(\mathbf{\Lambda}) =\ & \frac{ik_2^2G(\mathbf{\Lambda})}{\Delta(p+\Lambda_x)}\Big[[\bar{\beta}_2(p+\Lambda_x)-\beta_3(p+\Lambda_x)]e^{i\beta_2(p+\Lambda_x)l}F_0(-\Lambda_z+\bar{\beta}_2(p+\Lambda_x))\\
&+[\bar{\beta}_2(p+\Lambda_x)+\beta_3(p+\Lambda_x)]e^{-i\beta_2(p+\Lambda_x)l}F_0(-\Lambda_z-\bar{\beta}_2(p+\Lambda_x))\Big],
\end{aligned} \tag{6.67}$$

$$\begin{aligned}
C_1(\mathbf{\Lambda}) =\ & -e^{-i\beta_3(p+\Lambda_x)l}\frac{ik_2^2G(\mathbf{\Lambda})}{\Delta(p+\Lambda_x)}\Big[[\bar{\beta}_2(p+\Lambda_x)+\beta_1(p+\Lambda_x)]F_0(-\Lambda_z+\bar{\beta}_2(p+\Lambda_x))\\
&+[\bar{\beta}_2(p+\Lambda_x)-\beta_1(p+\Lambda_x)]F_0(-\Lambda_z-\bar{\beta}_2(p+\Lambda_x))\Big],
\end{aligned} \tag{6.68}$$

$$\begin{aligned}
F_1(\mathbf{\Lambda}|s) =\ & -\frac{k_2^2G(\mathbf{\Lambda})}{\Delta(p+\Lambda_x)}\Bigg[\frac{F_0(-\Lambda_z+\bar{\beta}_2(p+\Lambda_x))-F_0(s)}{s+\Lambda_z-\bar{\beta}_2(p+\Lambda_x)}Q^{(+)}(s+\Lambda_z,p+\Lambda_x)\\
&-\frac{F_0(-\Lambda_z-\bar{\beta}_2(p+\Lambda_x))-F_0(s)}{s+\Lambda_z+\bar{\beta}_2(p+\Lambda_x)}Q^{(-)}(s+\Lambda_z,p+\Lambda_x)\\
&+F_0(s)Q_0(s+\Lambda_z,p+\Lambda_x)\Bigg],
\end{aligned} \tag{6.69}$$

where

$$Q^{(\pm)}(s,p) = [\beta_1(p)+\beta_3(p)]e^{-isl} + [s-\beta_1(p)][\pm\bar{\beta}_2(p)-\beta_3(p)]\frac{e^{-isl}-e^{\pm i\bar{\beta}_2(p)l}}{s\pm\bar{\beta}_2(p)}, \tag{6.70}$$

$$Q^{(+)}(s,p) - Q^{(-)}(s,p) = [s-\beta_1(p)]Q_0(s,p). \tag{6.71}$$

Clearly, $Q^{(\pm)}(s,p)$ is an analytic function on the complex s-plane. Similarly, we can obtain equation of $F_2(\mathbf{\Lambda},\mathbf{\Lambda}'|s)$,

$$\begin{aligned}
&\left[k_2^2-(p+\Lambda_x+\Lambda_x')^2-(s+\Lambda_z+\Lambda_z')^2+m\left(\sqrt{(p+\Lambda_+\Lambda_x')^2+(s+\Lambda_z+\Lambda_z')^2}\right)\right]\\
&\times F_2(\mathbf{\Lambda},\mathbf{\Lambda}'|s)+\frac{k_2^2}{2}\left(G(\mathbf{\Lambda})F_1(\mathbf{\Lambda}'|s)+G(\mathbf{\Lambda}')F_1(\mathbf{\Lambda}|s)\right)\\
\approx\ & i[s+\Lambda_z+\Lambda_z'-\beta_1(p+\Lambda_x+\Lambda_x')]A_2(\mathbf{\Lambda},\mathbf{\Lambda}')\\
&-i[s+\Lambda_z+\Lambda_z'+\beta_3(p+\Lambda_x+\Lambda_x')]e^{i(\beta_3(p+\Lambda_x+\Lambda_x')-\Lambda_z-\Lambda_z'-s)l}C_2(\mathbf{\Lambda},\mathbf{\Lambda}').
\end{aligned} \tag{6.72}$$

Using a fact that $F_2(\mathbf{\Lambda},\mathbf{\Lambda}'|s)$ is an analytic function of s, we obtain an equation for $F_2(\mathbf{\Lambda},\mathbf{\Lambda}'|s)$, $A_2(\mathbf{\Lambda},\mathbf{\Lambda}')$ and $C_2(\mathbf{\Lambda},\mathbf{\Lambda}')$,

$$\begin{aligned}
&\mathbf{D}(s+\Lambda_z+\Lambda_z',p+\Lambda_x+\Lambda_x')\cdot\begin{bmatrix}F_2(\mathbf{\Lambda},\mathbf{\Lambda}'|s)\\A_2(\mathbf{\Lambda},\mathbf{\Lambda}')\\C_2(\mathbf{\Lambda},\mathbf{\Lambda}')\end{bmatrix}\\
=\ &\frac{k_2^2}{2}\begin{bmatrix}GF_1(\mathbf{\Lambda},\mathbf{\Lambda}'|s)\\GF_1(\mathbf{\Lambda},\mathbf{\Lambda}'|-\Lambda_z-\Lambda_z'+\bar{\beta}_2(p+\Lambda_x+\Lambda_x'))\\GF_1(\mathbf{\Lambda},\mathbf{\Lambda}'|-\Lambda_z-\Lambda_z'-\bar{\beta}_2(p+\Lambda_x+\Lambda_x'))\end{bmatrix},
\end{aligned} \tag{6.73}$$

where we put for simplicity,

$$GF_1(\mathbf{\Lambda},\mathbf{\Lambda}'|s) = G(\mathbf{\Lambda})F_1(\mathbf{\Lambda}'|s)+G(\mathbf{\Lambda}')F_1(\mathbf{\Lambda}|s). \tag{6.74}$$

Solving (6.73), we have the second order Wiener kernels

$$\begin{aligned}
A_2(\mathbf{\Lambda},\mathbf{\Lambda}') =\ & i\frac{k_2^2}{2\Delta(p+\Lambda_x+\Lambda_x')}\left[[\bar{\beta}_2(p+\Lambda_x+\Lambda_x')-\beta_3(p+\Lambda_x+\Lambda_x')]\right.\\
&\times GF_1\left(\mathbf{\Lambda},\mathbf{\Lambda}'|-\Lambda_z-\Lambda_z'+\bar{\beta}_2(p+\Lambda_x+\Lambda_x')\right)e^{i\beta_2(p+\Lambda_x+\Lambda_x')l}\\
&+[\bar{\beta}_2(p+\Lambda_x+\Lambda_x')+\beta_3(p+\Lambda_x+\Lambda_x')]\\
&\left.GF_1\left(\mathbf{\Lambda},\mathbf{\Lambda}'|-\Lambda_z-\Lambda_z'-\bar{\beta}_2(p+\Lambda_x+\Lambda_x')\right)e^{i\beta_3(p+\Lambda_x+\Lambda_x')l}\right],
\end{aligned} \tag{6.75}$$

$$\begin{aligned}
C_2(\mathbf{\Lambda},\mathbf{\Lambda}') = -ie^{-i\beta_3(p+\Lambda_x+\Lambda_x')l}&\frac{k_2^2}{2\Delta(p+\Lambda_x+\Lambda_x')}\left\{\left[\bar{\beta}_2(p+\Lambda_x+\Lambda_x')+\beta_1(p+\Lambda_x+\Lambda_x')\right]\right.\\
&\times GF_1\left(\mathbf{\Lambda},\mathbf{\Lambda}'|-\Lambda_z-\Lambda_z'+\bar{\beta}_2(p+\Lambda_x+\Lambda_x')\right)\\
&+\left[\bar{\beta}_2(p+\Lambda_x+\Lambda_x')-\beta_1(p+\Lambda_x+\Lambda_x')\right]\\
&\left.\times GF_1\left(\mathbf{\Lambda},\mathbf{\Lambda}'|-\Lambda_z-\Lambda_z'-\bar{\beta}_2(p+\Lambda_x+\Lambda_x')\right)\right\}.
\end{aligned} \tag{6.76}$$

Using these Wiener kernels, we will calculate statistical properties in the next section.

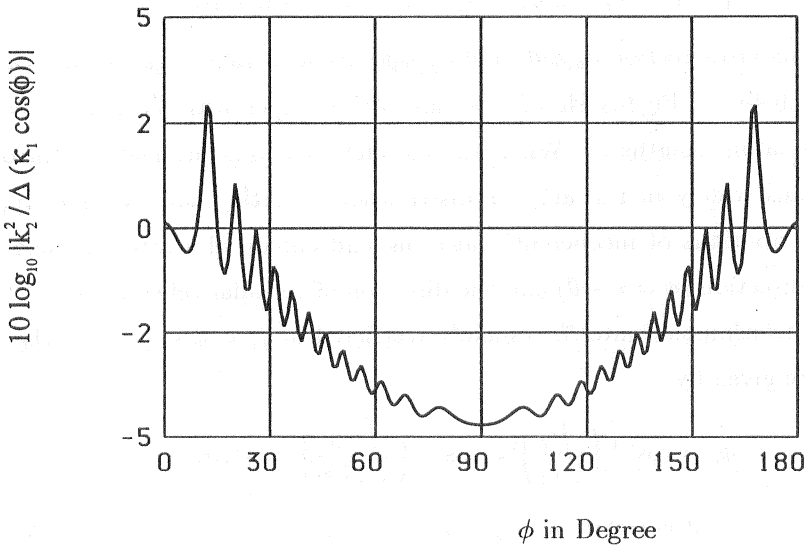

Figure 6.3: The resonance factor against ϕ a scattering angle for the parameters $\epsilon_1 = \epsilon_3 = 1, \bar{\epsilon}_2 = 2.25$, $l = 10\mu m$ and the incident wavelength $0.6328\mu m$. Ripples are caused by the multiple reflection in the film.

6.6 Numerical calculation and discussions

In the preceding section, we have obtained the zero order, first order and second order Wiener kernels, in terms of which we can calculate any statistical properties such as coherent scattering intensities and incoherent scattering cross section. To calculate the scattering cross section of the second order, however, we must calculate a triple integral. Here, we calculate the scattering cross section by only the first order Wiener kernels A_1 and C_1. We give two examples for the incident wave with wavelength $0.6328\mu m$. One is a case that SiC lies on Si substrate and these permittivities are given as

$$\epsilon_1 = 1, \quad \bar{\epsilon}_2 = 6.7, \quad \epsilon_3 = 11.8, \quad \sigma^2 = 1.0 \times 10^{-4}. \tag{6.77}$$

Another case is that a glass layer with disorders is placed in air and these permittivities are given as

$$\epsilon_1 = 1, \quad \bar{\epsilon}_2 = 2.25, \quad \epsilon_3 = 1, \quad \sigma^2 = 1.0 \times 10^{-4}. \tag{6.78}$$

The scattering cross section $\sigma_b(\phi|\theta)$ and $\sigma_f(\phi|\theta)$ are illustrated against the scattering angle ϕ in Figs.6.4-6.7. Fig.6.4 shows the case of S_iC layer with thickness $l = 10\mu m$ for several correlation lengths κ. When the correlation κ is shortened, the incoherent scattering spreads widely in the angular distribution. Furthermore, we see ripples in the angular distributions of incoherent scattering and enhanced scattering yield in the backscattering direction ($\phi = \pi + \theta$) and the direction of specular reflection ($\phi = 2\pi - \theta$). The incoherent transmission into S_i is mainly restricted in $\phi_c < \phi < \pi - \phi_c$, where ϕ_c is the critical angle given by

$$\phi_c = \cos^{-1}\left(\sqrt{\frac{\bar{\epsilon}_2}{\epsilon_3}}\right) = \cos^{-1}\left(\sqrt{\frac{6.7}{11.8}}\right) = 41.10°. \tag{6.79}$$

Fig.6.5 shows the case of correlation length $\kappa = 0.1\mu$ for several thickness l. When the thickness is thin ($l = 1\mu$), no ripples appear in the air side. However, when the thickness l is larger than 5μ, however, enhanced scattering appears in the backscattering direction ($\phi = \pi + \theta$) and the direction of specular reflection ($\phi = 2\pi - \theta$). Figs 6.6 and 6.7 show the case of glass layer, in which ripples and enhanced scattering exist in the incoherent scattering also.

Let us consider physical reasons for these ripples and enhanced scattering. In (6.67) and (6.68), $A_1(\mathbf{\Lambda})$ and $C_1(\mathbf{\Lambda})$ are given by a product of the spectrum function $G(\mathbf{\Lambda})$, the resonance factor $\Delta(p + \Lambda_x)$ and a factor involving $F_0(-\Lambda_z \pm \bar{\beta}_2(p + \Lambda_x))$, respectively. When the average permittivity $\bar{\epsilon}_2$ is quite different from ϵ_1 and ϵ_3 and when the thickness l is much larger than the wavelength, the thin film works as a resonator due to the multiple reflection. This effect is described by the resonance factor $k_2^2/\Delta(k_1\cos(\phi))$ that has ripples against a scattering angle ϕ as shown in Fig.6.3 and causes the ripples in the angular distribution. On the other hand, the factor involving $F_0(-\Lambda_z \pm \bar{\beta}_2(p+\Lambda_x))$ implies four processes of single-scattering, because $F_0(s)$ represents up and down going waves. For example, up and down going incoherent waves are generated by a single scatterer from up and down going coherent waves as illustrated in Fig.6.8, where four processes (a)(b)(c)(d) contribute to the backscattering and processes (e)(f)(g)(h) to the direction of specular reflection. Because processes (b) and (c) have equal propagation length, the enhanced backscattering takes place, specially in the case where $|G(0)|^2 \ll |G(2\beta_2(p))|^2$ holds and

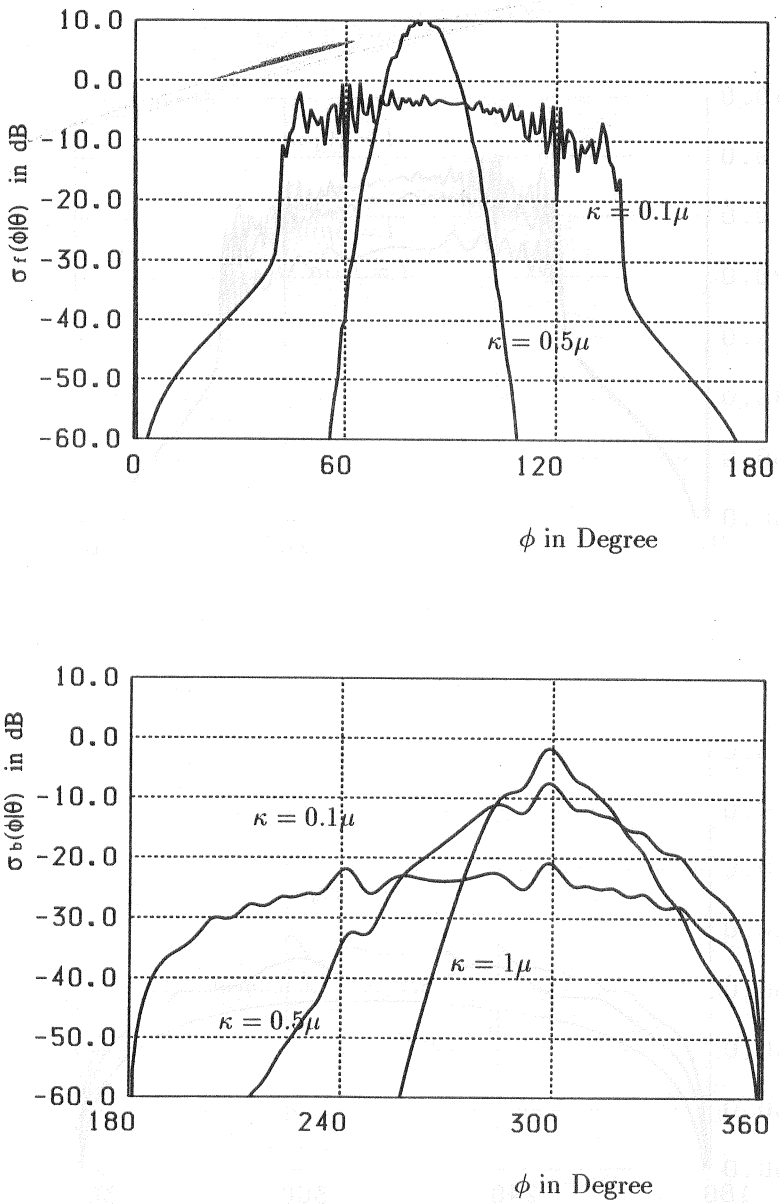

Figure 6.4: The scattering cross section with the parameters $l = 10\mu m$, $\epsilon_1 = 1$, $\bar{\epsilon}_2 = 6.7$(SiC), $\epsilon_3 = 11.8$ and $\theta = 60°$ for several correlation lengths κ. The incident wavelength is $0.6328\mu m$. When the correlation length κ is shortened, the incoherent scattering spreads in a wide angle area, ripples exist and enhanced scattering yields in the backscattering $\phi = \pi + \theta$ and the direction of specular reflection ($\phi = 2\pi - \theta$).

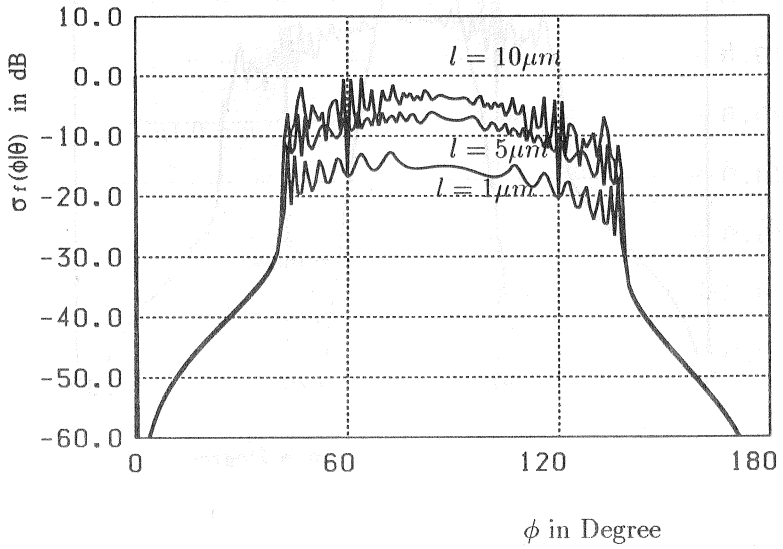

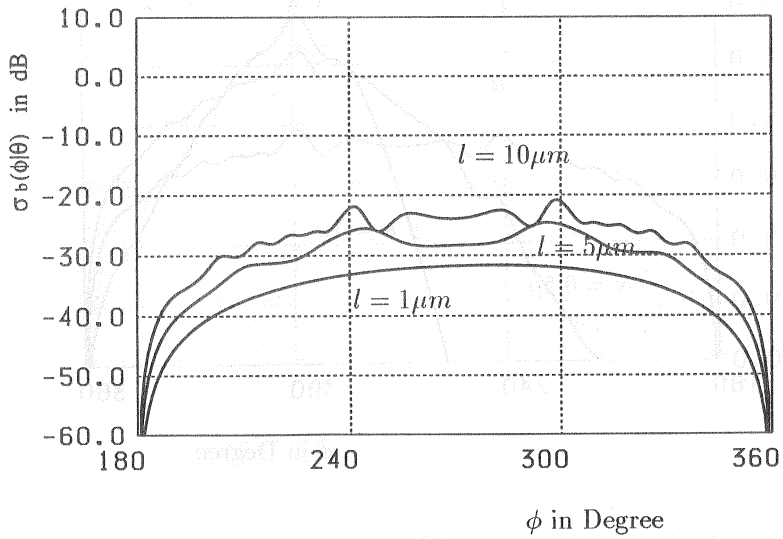

Figure 6.5: The scattering cross section (SiC) with parameters $\kappa = 0.1\mu$, $\bar{\epsilon}_2 = 6.7$, $\epsilon_1 = 1$, $\epsilon_3 = 11.8$ and $\theta = 60°$ for several different values of l.

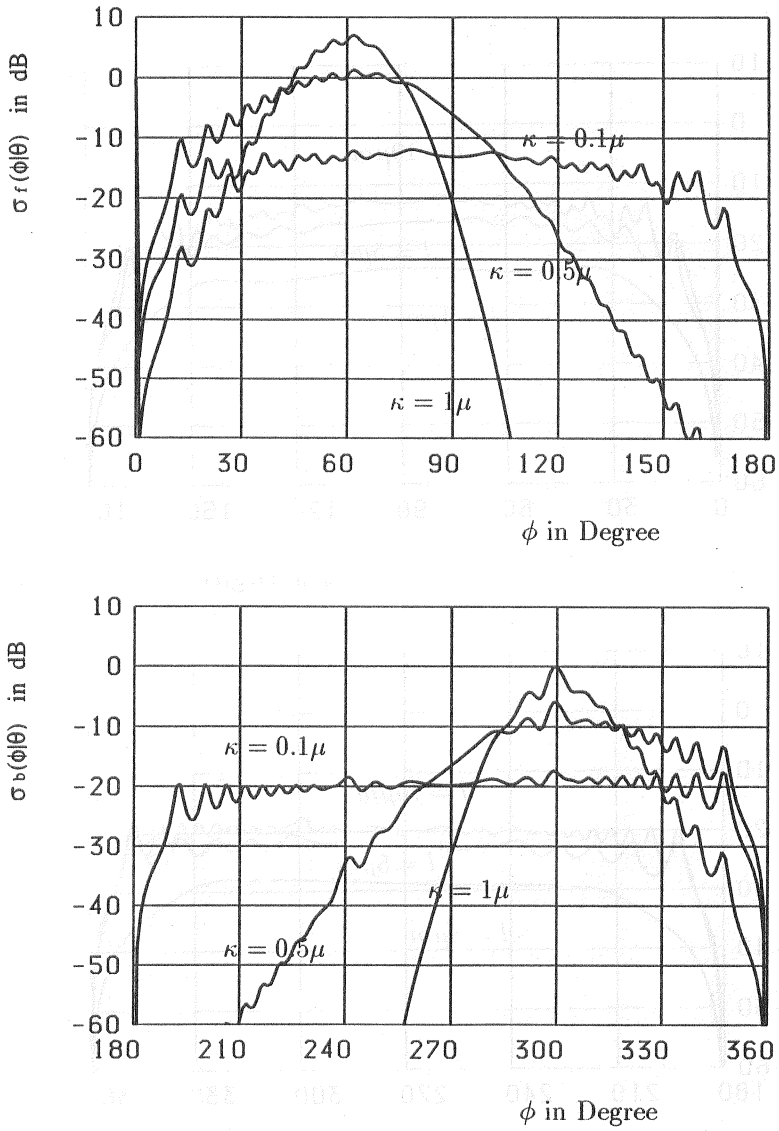

Figure 6.6: The scattering cross section with the parameters $l = 10\mu m$, $\epsilon_1 = \epsilon_3 = 1$, $\bar{\epsilon}_2 = 2.25$ and $\theta = 60°$ for several correlation lengths κ. The incident wavelength is $0.6328\mu m$. When the correlation length κ is shortened, the incoherent scattering spreads in a wide angle area, ripples exist and enhanced scattering yields in the backscattering $\phi = \pi + \theta$ and the direction of specular reflection ($\phi = 2\pi - \theta$).

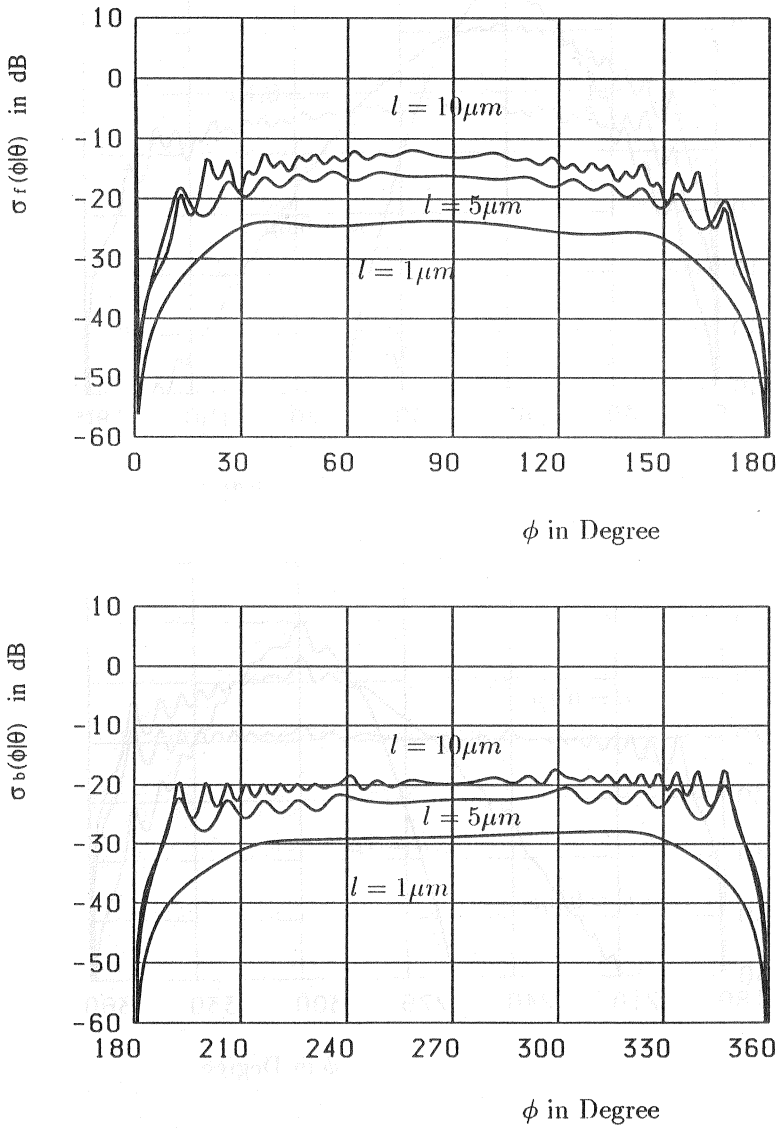

Figure 6.7: The scattering cross section with $\kappa = 0.1\mu$, $\bar{\epsilon}_2 = 2.25$, $\epsilon_1 = \epsilon_3 = 1$ and $\theta = 60°$ for several different values of l.

processes (a) and (d) become negligible. Similarly, the enhanced scattering in the direction of specular reflection yields because processes (f) and (g) are equal in the propagation length. This is a double path effect but differs from known double path effect [91], because an enhanced scattering appears not only in the backscattering direction but also in the direction of specular reflection. Fig.6.9 shows the optical theorem against the thickness l. The coherent power and the incoherent power fluctuate because of the multiple reflection by the top and bottom surfaces. The difference (energy error) of total scattered power and the incident power increases with the increase of thickness l.

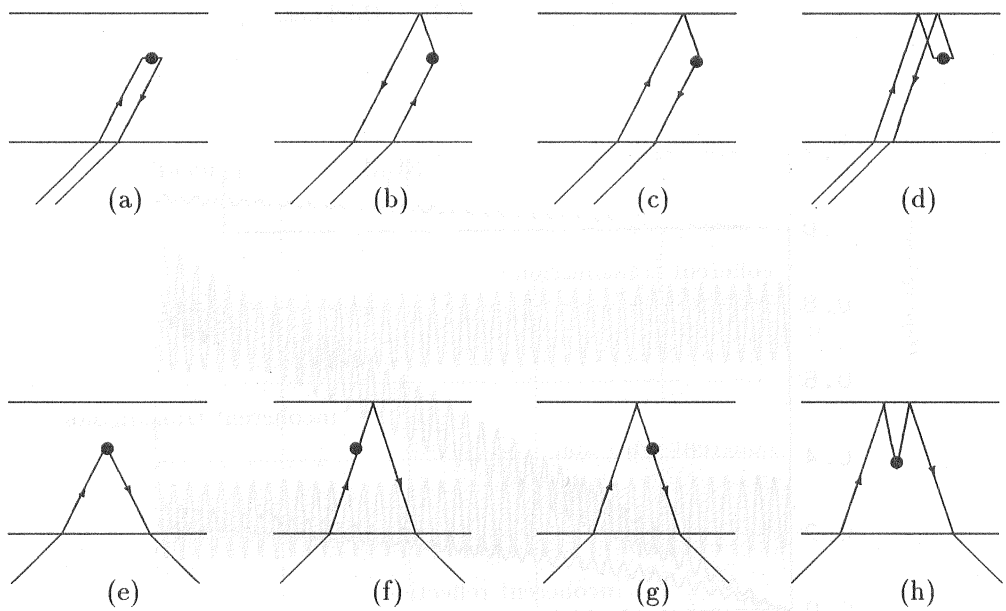

Figure 6.8: The backscattering processes (a)(b)(c)(d) and the scattering processes (e)(f)(g)(h) in the direction of specular reflection . Since (b) and (c) have equal propagation length, the backscattering enhancement may take place. Another enhanced scattering occurs in the direction of specular reflection, because (f) and (g) are equal in propagation length.

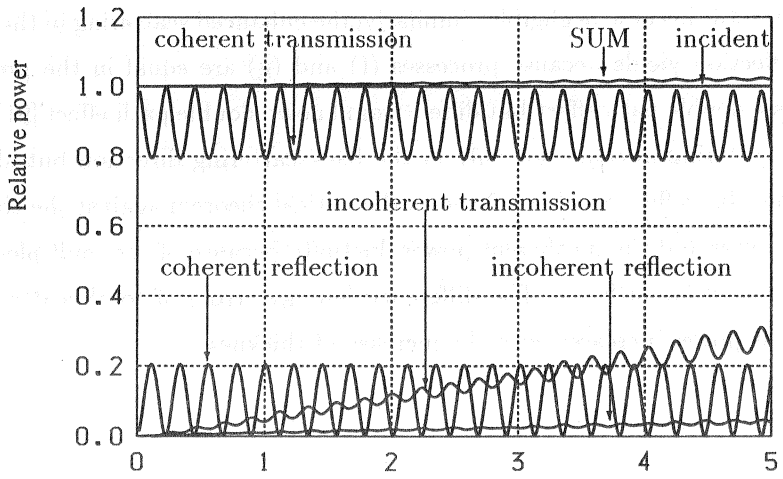

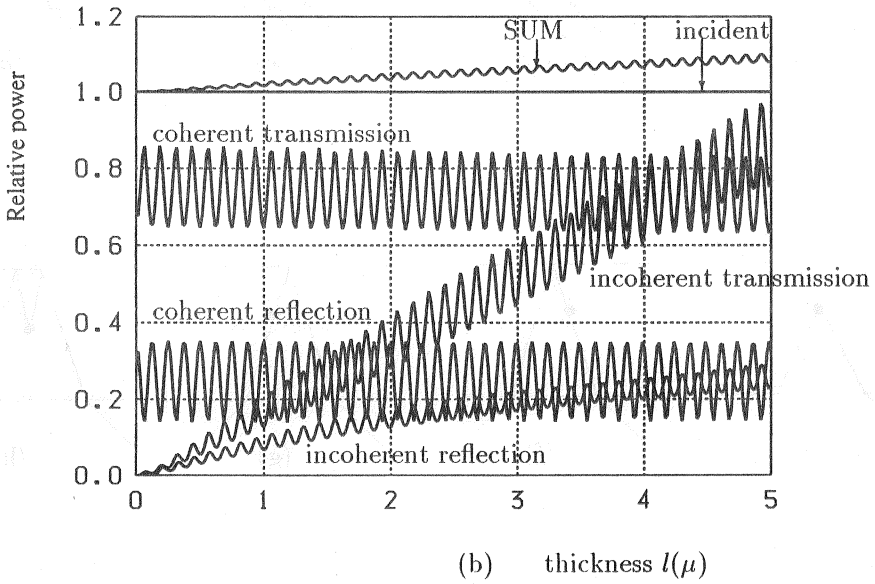

Figure 6.9: The optical theorem against thickness l for the parameters $\kappa = 0.2\mu$ and $\theta = 60°$. (a) glass, (b) S_iC. The incoherent scattering power is enlarged 10 times. The coherent scattering power and the incoherent scattering power fluctuate because of the multiple reflection by the top and bottom surface. The difference (energy error) of total scattered power and the incident power increases with the increase of thickness l.

6.7 Conclusion

This chapter deals with the scattering of a plane wave from a two-dimensional random thin film. For a Gaussian random disorder, an approximate solution up to the second order Wiener kernel is derived explicitly by a probabilistic method. We demonstrate that the ripples appear in angular distributions of the incoherent scattering. Moreover, the incoherent scattering is enhanced in the directions of backscattering and specular reflection. We clarify these phenomena can occur from a combination of 'single-scattering' by a random medium and multiple reflection between the top and bottle surfaces of the thin film. Furthermore, it is seen that fluctuation appears in coherent scattering and incoherent scattering. Such fluctuation is often used for measuring the film thickness [92].

There is a problem that the difference (energy error) between total scattered power and the incident power increases with the increase of the thickness l. To decrease such an error, methods of approximation for obtaining Wiener kernels should be studied. This is, however, left for the future study.

Chapter 7

Conclusion

In this thesis, we theoretically analyzed the scattering of plane waves from periodic random surfaces and random thin films as a random boundary problem of the wave equation. By means of a stochastic functional approach, we calculated many statistical properties of the scattering and discussed physical mechanisms of the scattering.

Periodic random surface

We find that periodic random surfaces with the periodic average and periodic correlation can be formulated mathematically by a periodic stationary process. Making use of the shift invariance property of a periodic random surface, we find that the scattered wave may have a stochastic Floquet's form: a product of a periodic stationary random function and an exponential phase factor. Then, we write such a periodic stationary random function as a harmonic series representation, where the harmonic coefficients are mutually correlated stationary processes. Next, we represent such stationary processes in terms of functional expansions with unknown kernel functions. Thus, the scattering problem is reduced to determining these kernel functions, which are represented in the form of vector. In the case of a slightly rough and small slope surface and a plane wave incidence, we obtain hierarchical matrix equations of the vector kernel functions from an approximate boundary condition. Solving the matrix equations, we calculate several statistical properties such as the coherent scattering, angular distributions of the incoherent scattering and optical theorem by the use of the kernel functions.

We find some common properties: the periodic random surface works as a periodic grating for the coherent wave, which is diffracted into discrete directions due to the periodic nature of the surface; incoherent scattering wave, generated from the coherently diffracted waves, is scattered into all directions due to the random nature of the surface.

In chapters 2 and 3, we considered the case that the periodic random surface is generated by a Gaussian sequence. For a TE plane wave incidence, we see there are ripples in angular distributions of the incoherent scattering, because of the inference between

incoherent waves generated from the coherently diffracted waves with different orders. For a TM plane wave incidence, we know that the guided surface waves propagate along the periodic random surface. When some coherently diffracted waves couple with the guided surface waves, the well-known Wood's anomaly is caused. Due to the random roughness, the guided surface waves are always excited and diffracted again. As a result, strong anomalous peaks appear in the angular distribution of incoherent scattering. The anomalous phenomenon which we call the incoherent Wood's anomalies is independent of the angle of incidence. But they take place at scattering angles determined by only period and wavelength. Further, as the guided surface waves are scattered and diffracted again, we find several enhanced scattering phenomena. They are the enhanced backscattering and diffracted backscattering enhancement.

In chapter 4, we obtained some new formulas concerning orthogonal functionals of stochastic binary sequence. These formulas can be used to solve binary random problems in physics and engineering.

In chapter 5, we applied those new formulas on binary functionals to scattering problems, where the periodic random surface is deformed by a binary sequence. We made the discussion on the scattering properties against roughness and height parameters.

Comparing the two cases of periodic random surfaces with binary sequence and with Gaussian sequence, we find that there are no difference, when statistical quantities are calculated by only the zero and first order kernel functions; difference may appear if the second order kernel functions are taken into consideration. However, there are many difficulties to get the second order kernels for the binary sequence case, because the equations for kernel functions become quite complex.

In addition, we have not yet considered the case of TM plane incidence; such a case can be solved by the same stochastic functional theory. In our studies on periodic random surfaces, we always assume that the surfaces have slight roughness and gentle slope. There are some open problems to be studied, to which we write some remarks:

(i) The case of relatively large rough surfaces.

To realize localization phenomenon, scattering theory should be perfected. In the present, however, the research for relatively large rough surfaces has not made progress in theory though has been studied by numerical calculations. Since Wiener expansion is essentially polynomial approximation, it seems that the Wiener expansion converges slowly for the large roughness. However, such convergence problem may disappear for the

binary functionals, because of its simplicity.

(ii) Approximate problems.

In the approximate calculation of the TM case, we neglected completely the action of the mass operator. The enhanced backscattering and the diffracted backscattering enhancements may become weak if the mass operator is considered. In case of the Gaussian sequence, the mass operator is possible to calculate but machine calculation needs quite time. In case of the binary sequence, however, it seems difficult to get the mathematical expression of the mass operator due to its special structure of the kernel equations. In addition, for the TM incidence, we studied only the case that the average surface is periodic. When the periodic random surface has a flat average, we have to consider the mass operator to solve the problem.

These problems will be considered as further study subjects.

Random media

In the case of the homogeneous Gaussian random thin film, we first transform the inhomogeneous random field in the film area into a homogeneous random field by use of translation invariance property. Then, we represent the homogeneous random fields in each area by Wiener expansion. Further, we determine these Wiener kernels by simultaneous equations which are obtained from the boundary condition.

In the chapter 6, we dealt with the scattering from the two-dimensional random thin film with volume disorder. We find the enhanced scattering in the directions of backscattering and specular reflection. Different from other researches, the enhanced scattering is caused by the combinations of 'single-scattering' and multiple reflection inside the film, rather than multiple-scattering.

The scattering from the random media which have random island structures is an interesting problem. We will consider such a problem by the use of the Poisson process.

Appendix A

Orthogonal functionals of stochastic Gaussian sequence

Here, we summarize several formulae on multi-variate Hermite polynomials and an orthogonal functional expansion called the Wiener expansion. For mathematical details, see references [60]-[62].

A.1 Multi-variate Hermite polynomials

We define the multi-variate Hermite polynomial $h^{(n)}$as

$$h^{(n)}[x_{i_1}, x_{i_2}, \cdots, x_{i_n}] = G\Big[\mathbf{x}; \mathbf{I}\Big]^{-1}(-1)^n \frac{\partial}{\partial x_{i_1}} \frac{\partial}{\partial x_{i_2}} \cdots \frac{\partial}{\partial x_{i_n}} G\Big[\mathbf{x}; \mathbf{I}\Big], \tag{A.1}$$

$$G\Big[\mathbf{x}; \mathbf{I}\Big] = \frac{1}{(2\pi)^{N/2}} \exp\left[-\frac{1}{2}\sum_{i=1}^{N} x_i^2\right], \tag{A.2}$$

$$1 \leq i_1, i_2, \cdots, i_n \leq N,$$

where $G\Big[\mathbf{x}; \mathbf{I}\Big]$ ($\mathbf{I}$ is unit matrix) is multi-variate N-dimensional standard normal distribution, and $\mathbf{x}$ is a large enough vector containing components $x_{i_1}, x_{i_2}, \cdots, x_{i_n}$. Here, N is a large enough number for the numbers $i_1, i_2, \cdots, i_n$. From (A.2), the lower order Hermite polynomials can be written by

$$h^{(0)} = 1, \tag{A.3}$$

$$h^{(1)}[x_i] = x_i, \tag{A.4}$$

$$h^{(2)}[x_m, x_n] = x_m \cdot x_n - \delta_{m,n}, \tag{A.5}$$

$$h^{(3)}[x_m, x_n, x_k] = x_m \cdot x_n \cdot x_k - \delta_{m,n}x_k - \delta_{n,k}x_m - \delta_{k,m}x_n. \tag{A.6}$$

A higher order polynomial may be obtained by the recurrence formula

$$h^{(n)}[x_{i_1}, x_{i_2}, \cdots, x_{i_n}] = h^{(n-1)}[x_{i_1}, x_{i_2}, \cdots, x_{i_{n-1}}]h^{(1)}[x_{i_n}]$$
$$-\sum_{l=1}^{n-1} h^{(n-2)}[x_{i_1}, x_{i_2}, \cdots, x_{i_{l-1}}, x_{i_{l+1}}, \cdots, x_{i_{n-1}}]\delta(i_l, i_n), \tag{A.7}$$
$$(n \geq 2).$$

Here, to obtain the recurrence formula (A.7), we have used the relations

$$\left(x_{i_n} - \frac{\partial}{\partial x_{i_n}}\right) h^{(n-1)}[x_{i_1}, x_{i_2}, \cdots, x_{i_{n-1}}] = h^{(n)}[x_{i_1}, x_{i_2}, \cdots, x_{i_n}], \tag{A.8}$$

and

$$\frac{\partial}{\partial x_i} x_j = \delta(i,j). \tag{A.9}$$

Now, we consider an independent Gaussian sequence $\{\epsilon_n(\omega), n = 0, \pm 1, \pm 2, \cdots\}$ with zero average and orthogonal correlation

$$\langle \epsilon_n(\omega) \rangle = 0, \quad \langle \epsilon_n(\omega)\epsilon_m(\omega) \rangle = \delta(n,m). \tag{A.10}$$

Then, the Hermite polynomials with the above Gaussian-variables for different orders are mutually uncorrelated

$$\left\langle h^{(n)}[\epsilon_{i_1}, \epsilon_{i_2}, \cdots, \epsilon_{i_n}] h^{(m)}[\epsilon_{j_1}, \epsilon_{j_2}, \cdots, \epsilon_{j_m}] \right\rangle = \delta(n,m)\delta^{(n)}(i,j), \tag{A.11}$$

which can be proved by the same way as the proof of (4.4). Here, we have dropped ω in (A.11), m and n are any integers, $\delta^{(n)}(i,j)$ is a sum of products of m deltas, of which concrete representation is given in (4.7). The relation (A.11) indicates that the Hermite polynomials with Gaussian-variate are orthogonal in the mean sense. Putting $n = 0$, the averages of the multi-variate Hermite polynomials satisfy

$$\left\langle h^{(n)}[\epsilon_{i_1}, \epsilon_{i_2}, \cdots, \epsilon_{i_n}] \right\rangle = \delta(n,0), \tag{A.12}$$

which are zero for $n \neq 0$.

A.2 Orthogonal functional expansion

We regard a sample point ω as an infinitely dimensional vector given by a sample sequence

$$\omega = (\cdots, \epsilon_{-2}, \epsilon_{-1}, \epsilon_0, \epsilon_1, \epsilon_2, \cdots), \quad \omega_i = \epsilon_i, \tag{A.13}$$

where ω_i is the i-th component of ω. Also, we assume that the sample space Ω is made up of all sample points. Now, we define a subset of Ω as

$$\Omega(j_1, j_2, \cdots, j_n) = \{\omega \in \Omega; \quad a_{j_i} < \omega_{j_i} = \epsilon_{j_i}(\omega) \leq b_{j_i}, \quad i = 1, 2, \cdots, n\}. \tag{A.14}$$

Then, the set of all such subsets becomes an additive class . Because subset $\Omega(j_1, j_2, \cdot, j_n)$ has the same probability as the n-dimensional interval

$$I = \{(\omega_{j_1}, \omega_{j_2}, \cdots, \omega_{j_n}) \in R^n; \quad a_{j_i} < \omega_{j_i} = \epsilon_{j_i}(\omega) \leq b_{j_i}, \quad i = 1, 2, \cdots, n\}, \tag{A.15}$$

these subsets will be measurable sets. By this mean, the sample space Ω is a measurable space. Let $\Phi(\omega)$ be a measurable functional on measurable space $L^2(\Omega)$ with a finite mean square

$$\left\langle |\Phi(\omega)|^2 \right\rangle < \infty. \tag{A.16}$$

Then, any a functional $\Phi(\omega)$ can be expanded as

$$\Phi(\omega) = \phi_0 + \sum_{m=-\infty}^{\infty} \phi_1(m) h^{(1)}[\epsilon_m] + \sum_{m,n=-\infty}^{\infty} \phi_2(m,n) h^{(2)}[\epsilon_m, \epsilon_n] + \cdots, \tag{A.17}$$

which holds in ensemble mean square sense and is often called the Wiener expansion or the Wiener-Itô expansion. Here, ϕ_0, $\phi_1(m)$, $\phi_2(m,n)$, $\cdots$ are expansion coefficients called Wiener kernels which are determined by the orthogonal relation (A.11) as

$$\phi_m(i_1, i_2, \cdots, i_m) = \frac{1}{m!} \left\langle \Phi(\omega) h^{(m)}[\epsilon_{i_1}, \epsilon_{i_2}, \cdots, \epsilon_{i_m}] \right\rangle, \quad m = 0, 1, 2, \cdots. \tag{A.18}$$

Here, $\phi_m(i_1, i_2, \cdots, i_m)$ has been assumed to be symmetrical with respect to its arguments. The Parseval relation is given by

$$\left\langle |\Phi(\omega)|^2 \right\rangle = \sum_{m=0}^{\infty} m! \sum_{i_1, i_2, \cdots, i_m = -\infty}^{\infty} |\phi_m(i_1, i_2, \cdots, i_m)|^2, \tag{A.19}$$

which is convergent by the condition (A.16). Thus, the right hand side of expansion (A.17) holds in ensemble mean square sense.

A.3 Stationary sequence

A stochastic functional $\Phi(\omega)$ is also a random variable. Applying the property (2.8), we obtain the translation property under shift T,

$$\begin{aligned} & T^q h^{(n)}\left[\epsilon_{i_1}(\omega), \epsilon_{i_2}(\omega), \cdots, \epsilon_{i_{n-1}}(\omega), \epsilon_{i_n}(\omega)\right] \\ &= h^{(n)}\left[\epsilon_{i_1}(T^q\omega), \epsilon_{i_2}(T^q\omega), \cdots, \epsilon_{i_{n-1}}(T^q\omega), \epsilon_{i_n}(T^q\omega)\right] \\ &= h^{(n)}\left[\epsilon_{i_1+q}(\omega), \epsilon_{i_2+q}(\omega), \cdots, \epsilon_{i_{n-1}+q}(\omega), \epsilon_{i_n+q}(\omega)\right], \end{aligned} \tag{A.20}$$

where the shift T is defined in Sec.2.2 and q is any integer. Using (A.17) and (A.20), we obtain the Wiener expansion for $g(T^\beta\omega)$

$$\Psi(T^q\omega) = \phi_0 + \sum_{k=\infty}^{\infty} \phi_1(k-q) h^{(1)}[\epsilon_k] + \sum_{k,l=\infty}^{\infty} \phi_2(k-q, l-q) h^{(2)}[\epsilon_k, \epsilon_l] + \cdots, \tag{A.21}$$

which is a stationary sequence generated from the Gaussian sequence $\{\epsilon_i\}$. The average and the correlation function may be easily calculated by the orthogonal relation (A.11) as

$$\langle \Phi(\omega) \rangle = \langle \Phi(T^q \omega) \rangle = \phi_0, \tag{A.22}$$

$$\langle \phi(T^\beta \omega) \phi^*(\omega) \rangle = |\phi_0|^2 + 1! \sum_{k=-\infty}^{\infty} \phi_1(k-\beta)\phi_1^*(k) + 2! \sum_{k,l=-\infty}^{\infty} \phi_2(k-\beta, l-\beta)\phi_2^*(k,l) + \cdots, \tag{A.23}$$

where asterisk means the complex conjugate.

Bibliography

[1] J. D. Jackson, *Classical Electrodynamics*, John Wiley & Sons, Inc., 1925.

[2] S.L Chuang and J. A. Kong, "Scattering of waves from periodic surfaces," IEEE, vol.69, no.9, Sep. 1981.

[3] E. Brookner, "Atmosphere propagation and communication channel model for laser wavelengths," IEEE Trans. COM-18, no.4, pp.396-416, Aug. 1970.

[4] R.S.Kennendy and E.V. Hoversten, " On the atmosphere as an optical communication channel," IEEE Trans. IT-14, no.5, pp.716-725, Sep. 1968.

[5] F.T.Ulaby and P.Batlivala, "Potimum radar parameters for mapping soil moisture," IEEE Trans. Geosci. Electro., vol.GE-14, no.2, pp.81-93, April 1976.

[6] R.W.Lee, and J.C.Harp, "Weak scattering in random media with applications to remote probing," Proc. IEEE, vol.57, no.4, pp.375-406, April 1969.

[7] R.S.Lawerence and J.W.Strohbehn, "A survey of clear-air propagation effects relevant to optical communications," Proc. IEEE, vol.58, no.10, pp.1523-1545, Oct. 1970.

[8] V.E. Derr and C.G. Little, "A comparison of remote sensing of the clear atmosphere by optical, radio and acoustic radar techniques," Appl. Opt., vol.9, no.9, pp.1976-1991, Sep. 1970.

[9] H.S. Hayre, "Radar scattering cross section–applied to Moon return," Proc. IRE, p. 1433, 1961.

[10] S. Ito, "Analysis of scalar wave scattering from slightly random rough surfaces: a multiple scattering theory," Radio. Sci., vol.20, pp.1-12, 1985.

[11] K. C. Chang, V. Shah, and T. Tamir, "Scattering and guiding of waves by dielectric gratings with arbitrary profiles," J. Opt. Soc. Am., vol.70, no.7, pp.804-813, July 1980.

[12] J. M. Soto-Crespo and M. Nieto-Vesperinas, "Electromagnetic scattering from very rough random surfaces and deep reflection gratings," *J. Opt. Soc. Am. A.*, vol.6, no.3, pp.367-384, Mar. 1989.

[13] M. L. Dakss, L. Kuhn, P. F. Heideich, and B. A. Scot, "A grating coupler for efficient excitation of optical guided waves in thin film," Appl. Phys. Lett., vol.16, p. 523, 1979.

[14] R. Petit, *Electromagnetic theory of gratings*, Springer-Verlag Berlin Heidelberg, New York, 1980.

[15] Y. V. Zamyatin and S. L. Prosvernin, " Diffraction of electromagnetic waves by an array with small random fluctuations of dimensions," Sov. J. Theh. Electron., vol.31, no.3, pp.43-50, 1986.

[16] D. P. Chrissoulidis, " EM wave scattering from statistically inhomogeneous and periodic random rough surfaces," *IEE Proc.*, vol.136, Pt.H, no.3, pp.209-214, Jun. 1989.

[17] H. A. Yueh, R. T. Shin, and J. A. Kong, "Scattering from randomly perturbed periodic surface," in *Process in Electromagnetic Research,* ed, J. A. Kong, Elsevier, New York, 1988.

[18] R. T. Shin and J. A. Kong, "Scattering of electromagnetic waves from a randomly perturbed quasiperiodic surface," *J. Appl. Phys.,* vol.56, no.1, pp.10-21, Jul. 1984.

[19] G. J. Dunning and M. L. Minden, "Scattering from high efficiency diffraction gratings, " Appl. Opt., vol.19, no.4, pp.2419-1425, July 1980.

[20] W. A. Gardner, *Cyclostationarity in Communications and Signal Processing*, IEEE PRESS, 1993.

[21] M. E. Knotts and K. A. O'Donnell, "Anomalous light scattering from a perturbed grating," Optics Letters, vol.15, no.24, pp.1485-1487, Dec. 1990.

[22] S. A. Masalov, Yu. K. Sirenko, and V. P. Shestopalov, "Anomalous wave scattering caused by jumps in the period of a diffraction grating," Sov. Tech. Phys. Lett., vol.4, no.3, pp. 117-118, Mar. 1978.

[23] C. Harvey Palmer, "Parallet diffraction grating anomalies," J. Opt. Soc. Amer., vol.42, no.4, pp.269-277, Apr. 1952.

[24] S. N. Vorob'ev, E. V. Zamyatin, and S. L. Prosvirnin, "Method for the solution of problems in wave diffraction by grating with random fluctuations of the parameters," Radio. Quan. Elec., vol. 32, no.9, pp.802-807, 1989.

[25] G. Hoffmann de Visme, *Binary Sequences*, Translated by M. Iri and U. Iri, Japan, 1977.

[26] N. Yasuda, "How to make CD-ROM," *Unix Magazine*, pp.26-35, Feb. 1993.

[27] H. H. Hopkins, "Diffraction theory of laser read-out systems for optical video discs," J. Opt. Soc. Am., vol.69, no.1, pp.4-24, Jan. 1979.

[28] V. I. Tatarski, *The effects of turbulent atmosphere on wave propagation,* IPST, Jerusalem, 1971.

[29] A. Ishimaru, *Wave propagation and scattering in random media*, vol.2, Academic Press, New York, 1978.

[30] S. Yoshida and H. Yajima, *Optical Thin Films and Devices*, University of Tokyo, 1994.

[31] P. Bussemer, K. Hehl, and S. Kassam, "Theory of light scattering from rough surfaces and interfaces and from volume inhomogeneities in an optical layer stack," *Waves in Random Media,* vol.1, pp.207-221, 1991.

[32] J. M. Elson, "Theory of light scattering from a rough surface with an inhomogeneous dielectric permittivity," *Phys. Rev. B.,* vol.30 pp.5460-5480, 1984.

[33] S. Kassam, A. Duparre, K. Hehl, P. Bussemer, and J. Meubert, "Light scattering from the volume of optical thin films: theory and experiment," *Appl. Optics,* vol.31, pp.1304-1331, 1992.

[34] R. W. Wood, "On a remarkable case of uneven distribution of light in a diffraction grating spectrum," Phil. Mag., vol.4, pp.396-402, 1902.

[35] R.F.Wallis and G.I.Stegeman, *Electromagnetic Surface Excitations,* Springer Series on Wave Phenomena, Springer-Verlag Berlin Heidelberg, New York, 1985.

[36] A. Hessel and A. A. Oliner, "A new theory of Wood's anomalies on optical gratings," Appl. Opt., vol.4, no.10, pp.1275-1297, Oct. 1965.

[37] R. H. Ritchie, E. T. Arakawa, J. J. Cowan, and R. N. Hamm, "Surface-plasmon resonance effect in grating diffraction," Phys. Rev. Lett., vol.21, no.22, pp.1530-1535, 1968.

[38] D. Maystre and R. Petit, "Brewster incidence for metallic gratings," Opt. Commun., vol.17, no.2, May 1976.

[39] L. Gao and J. Nakayama, "Scattering of a TM plane wave from randomly deformed periodic surface," EMT-97-21.

[40] A. D. Arsenieva and A. A. Maradudin, "Scattering of light from random surfaces that are periodic on average," Opt. Lett., vol.18, no.19, pp.1588-1590, Oct. 1993.

[41] P. Beckmann and A. Spizzichino, *The scattering of electromagnetic waves from rough surfaces,*" Artech House, 1987.

[42] E. R. Mendez and K. A. O'Donnell, "Observation of depolarization and backscattering enhancement in light scattering from Gaussian random surface," Optics Commu., vol.61, no.2, pp.91-95, Jan. 1987.

[43] H. Ogura, T. Kawanishi, N. Takahashi and Z. L. Wang, "Scattering of electromagnetic waves from a slightly random surface–reciprocal theorem, cross-polarization and backscattering enhancement," Wave in Random Media, vol.5, pp.461-495, 1995.

[44] V. Freilikher and I. Yurkevich, "Backscattering enhancement from surfaces with random impedance," Physics Letters A, pp.247-252, 183 (1993).

[45] Iwai, Okamoto and R. Asagura, "Development of scattering phenomena of lights," Appl. Phys., vol.63, no.1, 14(1994) (Japanese).

[46] G.H.Pettengill, "Measurements of lunar reflectivity using the millstone radar," Proc. IRE, pp.933-934, 1960.

[47] W.R.McCluney, "Multichannel forward scattering meter for oceanography," Appl. Opt., vol.13, no.3, pp.548-555, March 1974.

[48] A. Ishimaru, "Experimental and theoretical studies on enhanced backscattering from scatterers and rough surfaces", *Scattering in Volumes and Surfaces,*" M. Nieto-Vesperinas and J. C. Dainty (Editors), North-Holland, 1990.

[49] V. Freilikher, M. Kaveh and I. Yurkevich, "Backscattering indicatrix from surfaces with random impedance," Phys. A 200, pp. 452-461, 1993.

[50] R. C. Anderson and E. V. Browell, "First- and second-order backscattering from clouds illuminated by finite beams," Appl. Opt., vol.11, no.6, pp.1345-1351, June 1972.

[51] V. Freilikher, M. Pustilnik, I. Yurkevich and A. A. Maradudin, "Wave scattering from a thin film with volume disorder: reflection and transmission," *Opt. Comm.* 110, pp.263-268, 1994.

[52] V. Freilikher and I. Yurkevich, "Some aspects of electromagnetic wave scattering from a nonabsorbing rough surface," Physical Letters A, pp.253-256, 183 (1993).

[53] S. O. Rice, "Reflection of electromagnetic waves from slightly rough surfaces," Comm. Pure Appl. Math., vol.4, pp.351-378, 1951.

[54] R. T. Shin and J. A. Kong, "Scattering of electromagnetic wave from a Randomly Perturbed Quasiperiodic Surface," *J. Appl. Phys.*, vol.56, pp.10-21,1984.

[55] J. S. Chen and A. Ishimaru, "Numerical simulation of the second-order Kirchhoff approximation from very rough surfaces and a study of backscattering enhancement," J. Acoust. Soc. Am., vol.88, no.4 pp.1846-1850, Oct. 1990.

[56] G. G. Zipfil, and J. A. Desanto, "Scattering of a scalar wave from a random rough surface: A diagrammatic approach," J. Math. Phys., vol.13, no.12, pp.1903-1911, 1972.

[57] J.Nakayama,H.Ogura and S.Hasegawa, "Transmission and reflection by a three-dimensional random thin layer," *Tech.Rep.,IEE Japan,* EMT-81-57, pp.99-108, 1981.

[58] J.Nakayama,H.Ogura and M.Sakata,"Scattering of a scalar wave a slightly random surface," *J.Math Phys.,* vol.22, no.3, pp 471-477, March 1981.

[59] J.Nakayama,H.Ogura and B. Matsumoto, "A probabilistic theory of scattering from a rough surface," Radio Sinence, vol.15, no.6, pp.1049-1057, Nov.-Dec. 1980.

[60] H. Ogura, "Theory of waves in a homogeneous random medium," Phys. Rev. A, vol.11, no.3, pp.942-956, Mar. 1975.

[61] H. Ogura, *Theory of Random Process,* Corona, Tokyo, 1978.

[62] N. Wiener, "Nonlinear problems in random theory," MIT, Cambridge, MA, 1958.

[63] B. Kitagawa, *Probability and statistics*, Iwanami-shoten, 1953.

[64] K. Ito, *Theory of Probability*, Iwanami-shoten, 1952.

[65] H. Ogura, "On the orthogonal polynomials and functionals associated with a multi-valued random variable," (in Japanese), Tech. Rep. IECE, IT69-29, 1969.

[66] P. Z. Marmarelis and V. Z. Marmarelis, *Analysis of physiological systems,* Prenum, New York, 1978.

[67] J. Aracil, "Measurement of Wiener Kernels with binary random signals," IEEE Trans. Autom. Control, vol.15, pp.123-125, 1970.

[68] J. Nakayama, L. Gao, and Y. Tamura, "Scattering of a plane wave from a periodic random surface : a probabilistic approach," *Waves in Random Media,* vol.7, pp.65-78, 1997.

[69] J. Nakayama and L. Gao, "Stochastic processes derived from stationary binary sequence," Tech. Rep., IEE Japan, EMT-96-50, pp. 137-146, Oct. 1996.

[70] J. Nakayama and L. Gao, "Formulas on orthogonal functionals of stochastic binary sequence," IEICE Trans. Fundamentals, vol.E80-A, no.4, pp.782-785, Apr. 1997.

[71] L. Gao and J. Nakayama, "New formulas on orthogonal functionals of stochastic binary sequence with unequal probability," IEICE Trans. Fundamentals, vol.E81-A, no.2, pp.347-350, Feb. 1998.

[72] L. Gao and J. Nakayama, "Diffraction and scattering of a plane wave from randomly deformed periodic surface," IEICE Trans. Electron., vol.E80-C, no.11, pp.1374-1380, Nov. 1997.

[73] L. Gao and J. Nakayama, "Scattering of a plane wave from a periodic binary random surface," Tech. Rep., IEE Japan, EMT-96-33, pp.63-73, July 1996.

[74] L. Gao and J.Nakayama, "Scattering of a plane wave from a thin film with volume disorder", IEICE Trans. Electron., vol.E-79-C, no.10, pp. 1327-1333, Oct. 1996.

[75] J. Nakayama, K. Mizutani, and M. Tusneoka, "Scattering of electromagnetic waves from a perfectly conductive slightly random surface: Depolarization in backscatter," J. Math. Phys., vol.27, no.5, pp.1435-1448, 1996.

[76] J. Nakayama, "Scattering from a randomly rough surface: Linear equations for coefficients of the Wiener-Hermite expansion of the wave field," Radio Sci., 21 pp.707-712, 1986.

[77] F. G. Bass and I. M. Fuks, *Wave scattering from statistically rough surfaces,* Oxford: Hilger, 1991.

[78] J. G. Watson and J. B. Keller, "Rough surface scattering via the smoothing method," J. Acoust. Soc. Am., vol.75, pp.1705-1708, 1984.

[79] A. Imamura and J. S. Chen, "Scattering from very rough surfaces based on the modified second-order Kirchhoff approximation with angular and propagation shadowing," J. Acoust. Soc. Am. vol.88, no.4, pp. 1877-1883, Oct. 1990.

[80] Z. L. Wang, H. Ogura, and N. Takahashi, "Enhancement scattering from a planar waveguide structure with a slightly rough boundary," Phys. Rev. B, vol 52, no.8, pp.6027-6041, Aug. 1995.

[81] J.A.Ogilvy, *Theory of wave scattering from random rough surfaces,* Adam Hilger, Bristol, Philadelphia and New York, 1991.

[82] J. L. Doob, *Stochastic Processes*, John Wiely, 1953.

[83] T. Imamura, *Mathematics in random field theory*, Iwanami-shoten, Tokyo, 1976.

[84] M. Scheten, *The volterra and Wiener theories on nonlinear system*, Wiely, New York, 1980.

[85] E. Isobe and S. Sato, "Wiener-Hermite expansion of a process generated by an Ito stochastic differential equation," J. Appl. Prob., vol.20, pp.754-765, 1983.

[86] C. Eftimiu, "Modified Wiener-Hermite expansion in random-surface scattering," J. Opt. Soc. Am. A, Opt. Image Sci., pp.1584-1594, 1989.

[87] Z. L. Wang, H. Ogura, and N. Takahashi, "Radiation and coupling of guided modes in an optical fiber with a slightly rough boundary: stochastic functional approach," J. Opt. Soc. Am. A, Opt. Image Sci., pp.1489-1500, 1995.

[88] Mathematical dictionary, Iwanami-syoten, 1985.

[89] A. Ishimaru, *Wave propagation and scattering in random media*, Academic Press, 1978.

[90] P. Bruscaglioni and G. Zaccanti, "Multiple scattering in dense media," *Scattering in Volumes and Surfaces*", M. Nieto-Vesperinas and J. C. Dainty (Editors), North-Holland, 1990.

[91] M. Neito-Vesperinas and J. C. Dainty, *Scattering in Volumes and Surfaces,* North-Holland, 1990.

[92] T. J. Dalton, W.T. Conner, and H. H. Sawin, "Interferometric Real-Time measurement of uniformity for plasma etching," *J. Electrochem.,* vol.141, pp.1897-1900, 1994.

Related publications

1. Publication in Journal

(1) Lan Gao and Junich Nakayama, "Scattering of a plane wave from a thin film with volume disorder," IEICE Trans. Electron., vol.E-79, no.10, pp.1327-1333, Oct. 1996.

(2) Junich Nakayama, Lan Gao, and Yasuhiko Tamura, "Scattering of a plane wave from a periodic random surface: a probabilistic approach," Wave in Random Media, vol.7, no.1, pp.65-78, 1997.

(3) Junich Nakayama and Lan Gao, "Formulas on orthogonal functionals of stochastic binary sequence," IEICE Trans. Fundamentals, vol.E80-A, no.4, pp.782-785, Apr. 1997.

(4) Lan Gao and Junich Nakayama, "Diffraction and scattering of a plane wave from randomly deformed periodic surface," IEICE Trans. Electron., vol.E80-C, no.11, pp.1374-1380, Nov. 1997.

(5) Lan Gao and Junich Nakayama, "New formulas on orthogonal functionals of stochastic binary sequence with unequal probability," IEICE Trans. Fundamentals, vol.E81-A, no.2, pp.347-350, Feb. 1998.

2. Reference papers

(1) J. Nakayama, Gao Lan, and Y. Tamura, "Scattering of a plane wave from a random periodic grating," KJJC-EMTC Proceedings, pp.111-114, Aug. 1996 (Seoul).

(2) J. Nakayama, Gao Lan, and Y. Tamura, "A probabilistic theory of scattering from a random periodic surface," Proc. of 1997 Progress in Electromagnetics Research Symposium, p.923 (Hong Kong).

(3) Junich Nakayama and Gao Lan, "Scattering of plane waves from random media," Fukusha-kagaku-kenkyuukai, RS-95-11.

(4) Gao Lan and Junich Nakayama, "Enhanced scattering from a thin film with volume disorder," Technical report, IEE Japan, EMT-95-58, pp.121-136, 1995.

(5) Gao Lan and Junich Nakayama, "Wave scattering from a periodic random surface," Fukusha-kagaku-kenkyuukai, RS-96-2.

(6) Lan Gao and Junich Nakayama, "Scattering of a plane wave from a periodic binary random surface," Technical report, IEE Japan, EMT-96-33, pp.63-73, 1996.

(7) Junich Nakayama and Lan Gao, "Formulas on orthogonal functionals of stochastic binary sequence," Technical report, IEE Japan, EMT-96-32, pp.53-62, 1996.

(8) Lan Gao and Junich Nakayama, "Scattering of a plane wave from a periodic binary random surface: nonzero average case," Technical report, IEE Japan, EMT-96-51, pp.147-156, 1996.

(9) Junich Nakayama and Lan Gao, "Stochastic processes derived from stationary binary sequence," Technical report, IEE Japan, EMT-96-50, pp.137-146, 1996.

(10) Lan Gao and Junich Nakayama, "Scattering of a TM plane wave from a periodic random surface," Technical report, IEE Japan, EMT-97-21, pp.25-32, 1997.

(11) Lan Gao and Junich Nakayama, "Formulas on orthogonal functionals of stochastic binary sequence: the case of unequal probability, " Technical report, IEE Japan, EMT-97-85, pp.25-31, 1997.

(12) Lan Gao and Junich Nakayama, "Scattering of a TM plane wave from a periodic random surface — reciprocal theorem, backscattering enhancement and diffracted backscattering enhancement," Technical report, IEE Japan, EMT-97-81, pp.89-96, 1997.